Politecnico di Torino

Master's Degree in Automotive Engineering
A.A. 2025/2026
Graduation Session March 2026

Design and Development of a Pedal-Box-Integrated Emergency Brake System for a Formula Student Driverless Race Car

Supervisors:

Prof. Nicola Amati
Prof. Luis Miguel Castellanos Molina
Ing. Giorgio Bisciaio

Candidate:

Michel Hreiz

Abstract

This thesis focuses on the design and development of a pedal-box-integrated emergency brake system for the Squadra Corse Driverless team prototype, participating in various Formula Student competitions. In this context, autonomous vehicles must perceive the environment, process sensor data for path planning, and reproduce driver actions on the steering and pedals through dedicated actuators, with braking being a critical function both in normal manoeuvres and in emergency situations. In addition, all autonomous vehicles competing must enable complete control to the driver at any given moment, making the integration between autonomous and manual operation a vital part of the braking system. The work starts from the current SCD25 braking architecture, which combines a traditional dual-master-cylinder pedal box and separate autonomous actuators. The adoption of two separate systems significantly increases overall weight while showing an underperforming emergency braking system that causes tyre lockup. The first part of the thesis revisits the current setup of the entire braking system used by the team, in order to set benchmarks in terms of performance and weight. The following chapter introduces several proposed solutions for the new system development. Subsequently, an analysis of the vehicle's braking dynamics is conducted, considering different braking scenarios both in manual and autonomous modes while establishing key performance indicators and deceleration targets for various brake bias distributions. Design criteria are then established, allowing the development of the new integrated system, followed by structural and kinematic validation and comparison with the previous iteration in terms of performance and weight savings.

Acknowledgments

Firstly, I would like to express my gratitude to Professor Nicola Amati for giving me the opportunity to develop my idea and his guidance and trust as the team advisor. I would also like to thank my supervisors, Luis and Giorgio, who supported me in every step of my work, not only during this thesis but also during my time in SCD. A big thank you goes to all the members from the Power-train and Unsprung Mass divisions, who gave me the opportunity not only to teach, but also to learn every day. From team-members to close friends that I see everyday, I couldn't have asked for a better team. To my family, thank you for supporting me through my masters and always being there for me. To Giulia, my number one supporter, thank you for being next to me every step of the way and believing in me when I didn't, for pushing me when I wanted to give up. You will always be my biggest motivation.

Table of Contents

List of Tables

List of Figures

Nomenclature

α Driver thigh angle

β (Driver) Driver knee angle

β (Fluid) Isothermal bulk modulus of brake fluid

ΔP Design hydraulic pressure for compliance calculation

Δs Stopping distance penalty compared to ideal braking

ΔV_{fluid} Volume expansion due to fluid compressibility

ΔV_{lines} Volume expansion due to hose compliance

η_b Braking efficiency

η_{fric} Pneumatic actuator efficiency

κ_{lines} Brake hose volumetric compliance

λ_{loss} Pneumatic system loss factor

μ_x Longitudinal tire friction coefficient

μ_{pad} Brake pad friction coefficient

a Longitudinal distance from CG to front axle

a_x Longitudinal deceleration magnitude

a_{actual} Achieved vehicle deceleration with fixed bias

$A_{\text{cal,p}}$ Cross-sectional area of single caliper piston

$A_{\text{cal,tot}}$ Total caliper piston area per axle

$A_{\text{MC,f}}, A_{\text{MC,r}}$ Area of Front/Rear Master Cylinder

A_{piston} Pneumatic actuator bore area

A_{rod} Pneumatic actuator rod cross-sectional area

b Longitudinal distance from CG to rear axle

d Vehicle stopping distance

D_{bore} Pneumatic actuator bore diameter

$D_{\text{cal,p}}$ Diameter of caliper piston

D_{MC} Master cylinder bore diameter

D_{rod} Pneumatic actuator piston rod diameter

$F_{\text{act,ideal}}$ Theoretical force generated by pneumatic actuator

F_{act} Actual force generated by pneumatic actuator (with efficiency)

F_{clamp} Caliper clamping force

$F_{\text{leg,max}}$ Maximum driver leg push force (5th percentile)

$F_{\text{MC,max}}$ Maximum required master cylinder force at 2.2g deceleration

$F_{\text{MC,tot}}$ Total force applied to both master cylinders

F_{MC} Force applied to the master cylinder pushrod

$F_{x,f,\text{max}}$ Maximum front braking force at 2.2g deceleration

$F_{x,f}, F_{x,r}$ Longitudinal braking force on Front/Rear axle

$F_{z,f}, F_{z,r}$ Vertical load on Front/Rear axle

g Gravitational acceleration

h Center of gravity height

J_w Mass moment of inertia of one wheel

K_b Brake torque distribution ratio

L Wheelbase

l_f Balance bar lever arm to Front MC

l_r Balance bar lever arm to Rear MC

L_{bar} Total distance between balance bar pushrods

m Total vehicle mass

m_{act} Mass of air consumed per single actuation

m_{tank} Mass of air stored in the high-pressure tank

P_f, P_r Hydraulic line pressure (Front/Rear)

p_s Pneumatic supply pressure (regulated max)

P_{act} Pressure required at the actuator

P_{tank} Pressure of the high-pressure storage tank

PR_a Actuator pedal ratio

R Specific gas constant for air (287.05 $\mathrm{J/(kg \cdot K)}$)

r_i Inner radius of brake pad sweep

r_o Outer radius of brake pad sweep

r_w Effective tire rolling radius

R_{disk} Effective brake disc radius

s Usable master cylinder stroke (available)

s_{req} Master cylinder stroke required for fluid displacement

$s_{f,\text{cons}}$ Conservative front master cylinder stroke estimate

T Operating temperature

T_f, T_r Braking torque (Front/Rear)

V_0 Initial vehicle velocity

V_{liq} Total liquid volume in brake circuit

$V_{\text{MC,disp}}$ Fluid volume displaced by master cylinder

$V_{\text{req,f}}$ Total fluid volume required for front axle

$V_{\text{req,r}}$ Total fluid volume required for rear axle

V_{load} Total pneumatic load volume per actuation

w Band width of the pad sweep

$X_{\text{brake,f}}$ Front brake bias (share)

Chapter 1

Introduction

1.1 Road Safety

Since its invention in the late 1800s, the automobile has radically transformed human mobility. Over the last century, cars have evolved from being symbols of wealth to necessities for billions of people worldwide. People all around the world can now travel freely, crossing country borders within hours and no longer being limited to their immediate surroundings. According to the International Organization of Motor Vehicle Manufacturers (OICA), a total of 93,546,599 motor vehicles were produced in 2023 [12]. With the yearly increase in vehicles, traffic volumes and road utilization have dramatically risen. This has led to a higher number of accidents affecting both vehicle occupants and pedestrians, caused by distractions, congestion, and several additional factors. In 2021, approximately 1.19 million people died as a result of road traffic crashes globally, with between 20 and 50 million more suffering non-fatal injuries [13].

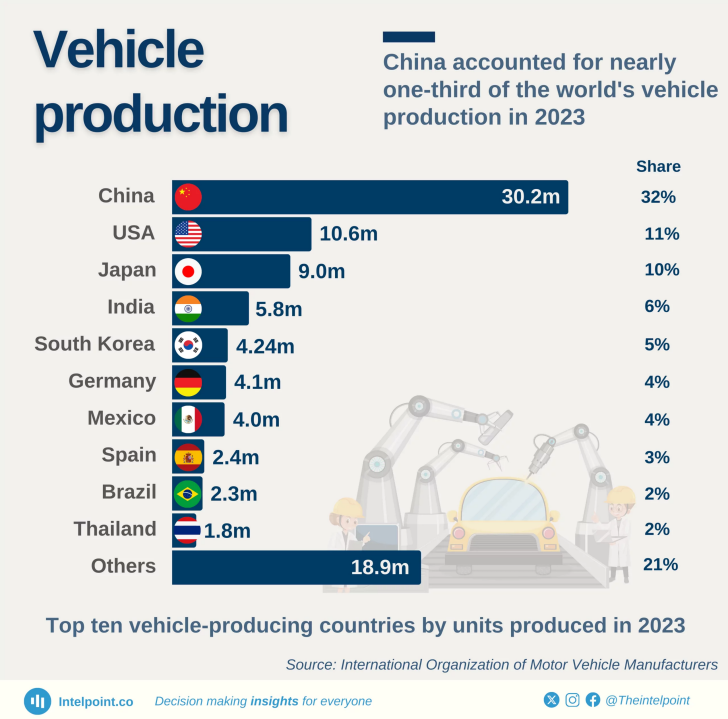

Figure 1.1: Vehicle production by country in 2023 [3]

Historically, moments of crisis have prompted significant safety improvements. For example, Ralph Nader's *Unsafe at Any Speed* (1965) revealed that car manufacturers had often prioritized style, comfort, or cost over safety [14]. This led to the introduction of mandatory seat belts, crash testing protocols, and safer vehicle designs, which gradually became standard. More recently, global policy efforts such as the United Nations' Second Decade of Action for Road Safety (2021–2030) have established clear targets: halving deaths and serious injuries from road crashes [15].

The most recent adoption of autonomous vehicles raises new safety concerns. If drivers rely excessively on automated systems, road safety may be compromised. The widespread adoption of autonomous vehicles without effective measures, protocols, or improved road conditions may potentially backfire, emphasizing the need for careful regulation and monitoring.

Vehicle safety today is mainly divided into two categories: **Passive safety** features aim to reduce the effects of a crash once it occurs; examples include crumple zones, airbags, and seat belts. **Active safety** refers to systems whose main role is the prevention of accidents through the use of systems such as Anti-lock Braking Systems (ABS) or Advanced Driver Assistance Systems (ADAS). Active safety is paving the way for autonomous driving, considering that, in a major U.S. crash causation survey, the driver was assigned the critical reason in about 94% of crashes [16]. Automation of vehicles shows great potential in reducing fatalities and injuries; however, with the technology still in development and refinement phase, its impact on real-world safety will only emerge over the next decade.

1.2 Autonomous Driving

The concept of autonomous driving can be traced back several decades. For example, the Carnegie Mellon University Navlab Project, which, in 1995, with the Navlab 5 minivan, was able to drive from Pittsburgh to San Diego. During the mission, throttle and brakes were handled by on-board researchers while the vehicle managed to steer itself about 98% of the journey [17]. Since then, advances in artificial intelligence, sensor technology, and vehicle-to-vehicle communication have started transforming the concept of autonomous driving into a rapidly developing industry.

To provide a common framework, the Society of Automotive Engineers (SAE) has defined six levels of driving automation, ranging from Level 0 (no automation) to Level 5 (full automation) [4]. These levels are summarized as follows:

- **Level 0 – No Automation:** The human driver performs all driving tasks, with systems only providing warnings or momentary assistance.
- **Level 1 – Driver Assistance:** The system can assist with either steering or acceleration/deceleration, but the driver remains fully responsible.
- **Level 2 – Partial Automation:** The system controls both steering and acceleration/deceleration under certain conditions, though the driver must monitor the environment and remain engaged.
- **Level 3 – Conditional Automation:** The system manages all driving tasks in specific scenarios, but the driver must be ready to intervene when requested.

- **Level 4 – High Automation:** The system performs all driving tasks in defined conditions or environments (e.g., urban areas, highways), with no driver intervention required in those situations.
- **Level 5 – Full Automation:** The vehicle is capable of performing all driving tasks under all conditions, eliminating the need for a human driver.

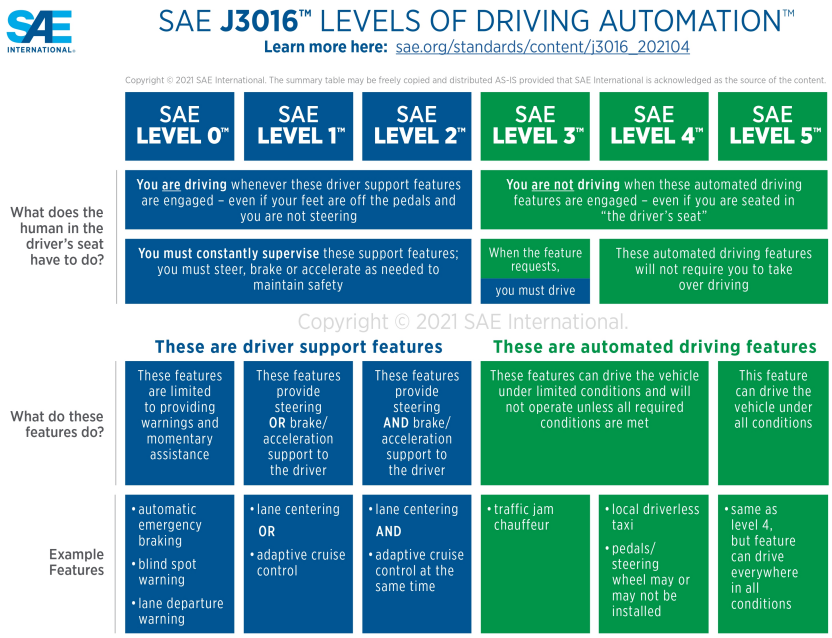

Figure 1.2: SAE J3016 levels of automation [4]

1.3 Formula Student Driverless

Formula Student (FS) is an international competition founded in 1981 by the Society of Automotive Engineers [18]. The competition challenges teams of university students to design, manufacture, and compete with small formula-style race cars. While Formula Student originated in the United States, it quickly spread to Europe, with Formula Student Germany (FSG) being the most prestigious event. The rules defined by FSG have been widely adopted across European competitions, with minor modifications introduced by other events.

Formula Student events are divided based on the propulsion system of the vehicles:Formula Student Combustion (FSC) for internal combustion prototypes, and Formula Student Electric (FSE) for electric vehicles.

In 2017, a new category was introduced to FSG: **Formula Student Driverless**, and in the subsequent year other competitions such as Formula SAE Italy, Formula Student UK and Formula East followed with the addition of the new category.

In this category, student-developed prototypes are equipped with autonomous systems comprising sensors such as LiDARs and cameras. These sensors allow the vehicle to

perceive the track, while onboard algorithms compute optimal trajectories and control the actuators for steering, acceleration, and braking, enabling fully autonomous navigation. Since the vehicles operate autonomously in a controlled environment (on closed competition tracks), they can be classified as SAE Level 4 automation [4].

The Driverless category permits the use of either combustion or electric powertrains, giving teams flexibility in designing their autonomous prototypes. It is worth mentioning that following FSG regulations, all driverless prototypes must also be capable of full manual operation by a human driver, making the development of the actuators slightly more complex as the vehicle must be able to provide full operation at any time during the competition.

According to Formula Student's most recent rule set, teams compete in three static and seven dynamic events with two of them dedicated to Driverless category. In addition, teams can choose to compete in the Driverless Cup (DC) dedicated to the autonomous prototypes.

Discipline	**FSC / FSE**	**DC**
Statics		
Business Plan	75 points	—
Cost and Manufacturing	100 points	—
Engineering Design	150 points	150 points
Dynamics		
Acceleration	50 points	—
Acceleration Driverless	75 points	75 points
Skidpad	50 points	—
Skidpad Driverless	75 points	75 points
Autocross	100 points	—
Autocross Driverless	—	100 points
Endurance	250 points	—
Efficiency	75 points	—
Trackdrive	—	200 points
Overall	1000 points	600 points

Table 1.1: Formula Student and Driverless Cup event points distribution

In the static events, teams compete by presenting different aspects prepared throughout the season:

- **Engineering Design:** Judges score the teams based on their designs and choices. They want proof that the best designs are implemented based on good practice and concrete evidence (e.g. simulation data, testing, etc.).
- **Cost and Manufacturing:** In this event, the teams present a detailed report of their total costs throughout the year considering their overall budget, production methods and manufacturing processes employed.
- **Business Plan:** Teams pitch a business plan for their prototypes to a fictitious company represented by the judges. The teams must show how their business model can be a successfully marketed product or service that could create a monetary profit.

On the other hand, teams that successfully pass the rigorous technical inspections will get to participate in the various Driverless dynamic events, described as follows:

- **Acceleration:** The prototypes compete for the fastest acceleration over a 75 m straight.
- **Skidpad:** In this event, the track is a figure-of-eight circuit with track cones as shown in Figure 1.3. The vehicle will perform two laps on each side with the second lap measured.
- **Autocross:** For the autocross, a handling track is presented at random built with various turns and straights following specific guidelines defined by the competition. The prototypes compete for the fastest lap time around that track.
- **Trackdrive:** Objectively the most difficult event awarding the highest number of points for the Driverless Cup. Vehicles are asked to complete ten laps around the track under fully autonomous conditions.

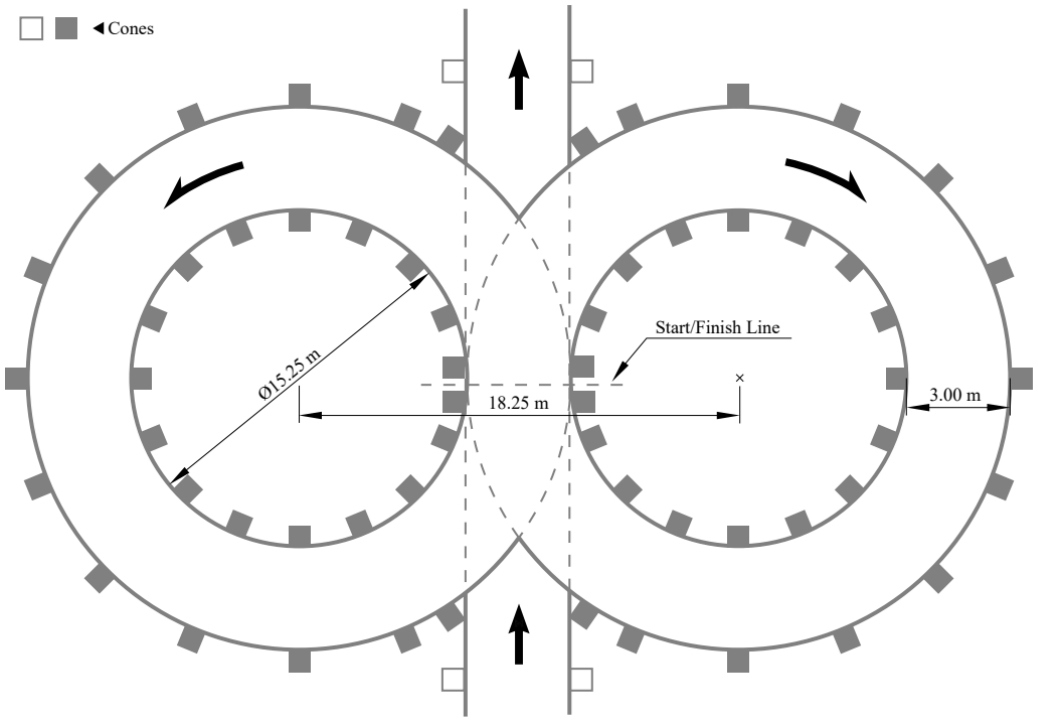

Figure 1.3: Skidpad track layout [5]

1.4 Squadra Corse Driverless

Squadra Corse Driverless (SCD) [19], established in 2021, is the main Formula Student Driverless team at Politecnico di Torino. The team originally started by adapting the SC19 vehicle from Squadra Corse [20] into a driverless prototype, fitting different sensors to detect the environment and enable path planning. The vehicle has a carbon fiber monocoque, with four in-wheel electric motors outputting a maximum power of 80 kW and 84 Nm of torque. During driver operation, the vehicle is capable of accelerating from 0-100 km/h in 2.6 s.

In 2022, the prototype was finally ready to participate in its first competition in Formula SAE Italy, where the team achieved third place overall. The next season proved to be a success, as Squadra Corse Driverless with the evolved prototype SCD23, managed to compete on an international level in FS East in Hungary. The SCD23 prototype was equipped with the latest upgrades on the perception side such as the addition of an Ouster OS1 LiDAR and two cameras, enabling sensor fusion algorithms to detect the cones that represent the track.

On the actuator side, the steering is composed of a ball screw mechanism driven by an electric motor. The autonomous steering is directly connected to the manual rack.

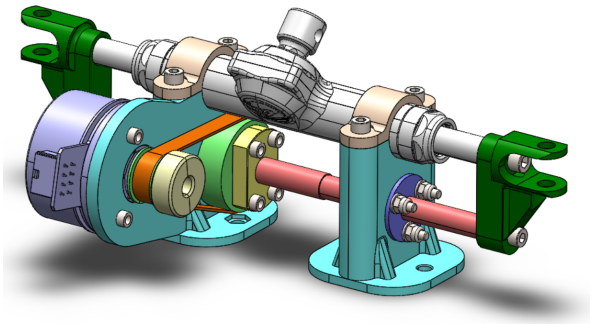

Figure 1.4: Steering system of Squadra Corse Driverless

Finally, the braking actuators, which are the topic of this thesis, will be covered in depth in the following section.

Unfortunately, the vehicle suffered a crash towards the end of 2023, preventing Squadra Corse Driverless from participating in the 2024 season. Consequently, most technical upgrades were frozen while the team focused on preparing for 2025. SCD25, nicknamed "Alba", was introduced in Formula ATA in Italy, where the team competed.

Figure 1.5: SCD25, "Alba" in Formula ATA 2025

1.5 Squadra Corse Driverless Braking Actuators

As an autonomous vehicle, it should be capable of braking according to the needs of the algorithm, which is achieved by a set of autonomous actuators directly linked to the rest of the braking system:

- Regarding braking under normal conditions, the braking is split between regenerative braking commanded by the algorithm and braking via a servomotor directly connected to the pedal whenever regenerative braking cannot be used.
- In case of emergency conditions, the vehicle should be able to shut down on its own by detecting critical faults or by a remote control device. This part is achieved through a dedicated emergency braking system.

According to Formula Student regulations, the vehicle should still be equipped with a fully functional braking system capable of being operated by a driver without any interference from the autonomous systems.

Due to the strict rules established mainly for safety reasons, teams are forced to find creative ways to combine the manual and autonomous systems without any interference between the two. The current systems equipped on SCD25 are outdated compared to top teams due to many issues:

- The vehicle, originally designed for manual driving only, lacks the necessary space for various autonomous systems, or at the very least the available volume has only been considered for the basic manual systems, not leaving additional room for autonomous hardware.

- Subsequently, the pedal, being completely carried over from the manual car, does not allow the option of combining the two systems into one.
- The current emergency braking system was over-dimensioned, leading to poor dynamics behavior and significant increase in weight.

Considering all the points mentioned above, the team finds it necessary to upgrade the system as they are falling behind in the competition. For that, the method will be shifted towards designing the autonomous systems properly and building around them instead of trying to incorporate the mechanisms into a normal vehicle.

Different solutions will be explored to better understand the performance needs and possible options.

1.6 Thesis Outline

This thesis is structured into six chapters, each addressing a specific phase of the design and development process for the system.

Chapter 2: Requirements & Baseline Analysis gives an insight into the Formula Student Germany 2025 rules relevant to braking systems. The current SCD25 braking architecture is examined in detail, covering brake layout, component specifications, master cylinder sizing, and current pedal box design. The next topic covered is the Autonomous System Brake and Emergency Brake System, where the different requirements are established. Weight and performance benchmarks are analyzed.

Chapter 3: Design Methodology evaluates three proposed solutions for integrating manual and autonomous braking, selecting the currently most feasible option. Before proceeding with the design, braking dynamics of the vehicle are analyzed in different conditions, in order to establish the optimal brake setups for various encountered scenarios in the competition. In addition, the emergency braking actuators are sized according to the analysis results, replicating as closely as possible ideal braking conditions. Finally, driver operation comfort is validated through an ergonomics analysis.

Chapter 4: Design and Validation details the component design process. Design constraints spanning functional, ergonomic, packaging, performance, weight, and structural requirements are defined. Each component is designed and validated through Finite Element Method (FEM) analysis under relevant load cases. The pedal ratio is calculated with an improved method. Lastly, the emergency shutdown mechanism is developed.

Chapter 5: System Assembly presents the complete integrated system. Weight analysis demonstrates significant reduction compared to previous subsystems. The compressed gas system is designed, improving upon the current design. Kinematic analysis validates mechanism motion throughout the operating range and identifies potential interferences.

Chapter 6: Conclusion summarizes the key achievements and provides recommendations for future development.

Chapter 2

Requirements & Baseline Analysis

This chapter will allow us to establish the baseline for developing the main concepts proposed for the pedal box and emergency braking system (EBS).

2.1 Formula Student Germany 2025 Rules

As previously stated, Formula Student Germany is the most prestigious competition and sets the baseline for all other competitions across Europe thus will be our guideline for the development of the 2026 system. It is worth noting that the majority of teams have trouble passing technical inspections, mainly due to insufficient adherence of their prototypes to the specified rules.

In order to create a robust and rule-compliant pedal box and emergency braking system, a list of all relevant rules has been extracted from the 2025 rule book [5]. This analysis of the rule book is fundamental before analyzing any of the manual and autonomous braking components mounted on the vehicle.

Brake System - General (T6)

T6.1.1 The vehicle must be equipped with a hydraulic brake system that acts on all four wheels and is operated by a single control.

T6.1.2 The brake system must have two independent hydraulic circuits such that in the case of a leak or failure at any point in the system, effective braking power is maintained on at least two wheels. Each hydraulic circuit must have its own fluid reserve, either by the use of separate reservoirs or by the use of a dammed reservoir.

T6.1.3 The brake system must be sealed to prevent leakage.

T6.1.4 A single brake acting on a limited-slip differential is acceptable.

T6.1.5 "Brake-by-wire" systems are prohibited in manual mode.

T6.1.6 Unarmored plastic brake lines are prohibited.

T6.1.9 The brake pedal and its mounting must be designed to withstand a force of 2 kN without any failure of the brake system or pedal box. This may be tested by pressing the pedal with the maximum force that can be exerted by any official when seated normally.

T6.1.10 The brake pedal, including pedal face, must be fabricated from steel or aluminium or machined from steel, aluminium or titanium.

T6.2.1 A BOTS must be installed on the vehicle as part of the Shutdown Circuit (SDC), as in EV6 or CV4.1. This switch must be installed that in the event of a failure in at least one of the brake circuits the brake pedal over-travel will result in the SDC being opened. This must function for all possible brake pedal and brake balance settings without damaging any part of the vehicle.

T6.2.2 Repeated actuation of the BOTS must not close the SDC, and the driver cannot reset it.

T6.2.3 The BOTS must be a push-pull, push-rotate or flip type mechanical switch. It may consist of a series connection of switches.

Critical Components (T9)

T9.1.1 Compressed Gas System (CGS): any system that uses a compressed gas as an actuating medium, except for gas springs.

T9.1.2 The working gas of any CGS must be non-flammable.

T9.1.3 The pressure inside any CGS must not exceed 10 bar. Gas cylinders/tanks may exceed 10 bar if a pressure regulator limiting the output pressure to a maximum of 10 bar is mounted directly onto them.

T9.1.4 All parts of any CGS must be designed for the maximum possible operating pressure.

T9.1.5 Gas cylinders/tanks and their pressure regulators must be of proprietary manufacture, certified and labeled as such.

T9.1.6 The pressure in the function critical part of any CGS required to ensure the functionality of the Autonomous System Brake (ASB), see T15, must be limited by means of an overpressure protection, if compressed gas cylinders/tanks exceed the pressure threshold as defined in T9.1.3.

Remote Emergency System (T14.3)

T14.3.1 Every vehicle must be equipped with a standard RES specified in the competition handbook. The system consists of two parts, the remote control and the vehicle module.

T14.3.2 The RES must be purchased by the team.

T14.3.3 The RES has two functions:

- When the remote emergency stop button is pressed, it must open the SDC defined in T14.4.
- When the "Go" button is pressed, the preselected autonomous mission is started.

T14.3.4 The RES vehicle module must be directly, see T1.3.1, integrated in the vehicle's SDC with one of its relays hard-wired in series to the shutdown buttons.

T14.3.5 The RES relay, which is integrated into the SDC, must be bypassed by a normally closed relay when driving manually. The relay must:

- Be directly supplied, see T1.3.1, by the ASMS, see T14.5.
- Have a safety-certified forcibly guided or a mirrored normally open contact which is directly connected, see T1.3.1, in series to the ASMS.

T14.3.6 The antenna of the RES must be mounted unobstructed and without interfering parts in proximity, e.g. other antennas, etc.

Autonomous System Brake (T15)

T15.1.1 To run in autonomous mode, the vehicle must be equipped with an ASB including an EBS.

T15.1.3 The TS is not considered a brake system.

T15.1.4 Manual braking must always be possible; if manual and autonomous braking occur simultaneously, the higher pressure must be applied.

T15.1.5 Master cylinders must not be connected in series.

T15.1.6 The ASB may be part of the hydraulic brake system. T6 applies to brake circuits; T9 applies to pneumatic/hydraulic components.

T15.1.7 The ASB must be designed so that it can be easily deactivated by a maximum of two deactivation points.

T15.1.8 Deactivation points must:

- work without the aid of electrical power
- be in proximity to each other
- either be mounted in proximity to the ASMS or on the top side of the vehicle between front bulkhead and front hoop close to the vehicles center line
- be protected against unintended actuation, e.g. by being hit by a cone, while driving
- be operable by maximum two simple push/pull and/or turning actions, the order and direction of these actions must be shown next to the deactivation points.
- be marked with "Brake release"
- have a red handle

T15.1.9 The use of push-in fittings is prohibited in function critical pneumatic circuits of the ASB and any other system which uses the same energy storage without proper decoupling.

T15.2.1 The EBS must only use passive systems with mechanical energy storage. Electrical powerloss at EBS must lead to a direct emergency brake maneuver with the performance specified in T15.4.

T15.4.1 The system reaction time, the time between opening of the SDC and the start of the deceleration, must not exceed 200 ms.

T15.4.2 The average deceleration must be greater than 10 m/s^2 under dry track conditions.

T15.4.3 In case of a single failure, the ASB should be designed to achieve at least half of the performance specified in T15.4.2.

T15.4.4 Whilst decelerating, the vehicle must remain in a stable driving condition.

Brake Test (IN11)

IN11.1.1 Lock all four wheels and stop the vehicle in a straight line at the end of an acceleration run specified by the officials.

IN11.1.3 [EV ONLY] After accelerating, the TS must be switched off by the driver, using the cockpit-mounted shutdown button, and the driver must brake using only the mechanical brakes.

IN11.1.4 After the brake test, the vehicle must be able to continue driving under its own power without external assistance.

IN11.2.1 The EBS performance will be tested dynamically and must demonstrate the performance described in T15.4.

IN11.2.2 The test will be performed in a straight line marked with cones similar to acceleration.

IN11.2.3 During the brake test, the vehicle must accelerate in autonomous mode up to at least 40 km/h within 20 m. From the point where the RES is triggered, the vehicle must come to a safe stop within a maximum distance of 8.5 m.

IN11.2.4 In case of wet track conditions, the stopping distance will be scaled by the officials dependent on the friction level of the track.

2.2 Braking System Architecture

Before delving into the current pedal box and emergency braking system of the SCD25 prototype, it is worth analyzing all the other components related to the braking system and relevant to this work. As previously mentioned, Squadra Corse Driverless inherited the SC19 prototype that was originally designed exclusively for manual operation without considering driverless operations. While most components needed to achieve autonomous driving were added later on, the unsprung mass including the braking system architecture, was not modified but rather maintained or renewed. In order to improve on the current autonomous braking actuators, a brief analysis of the entire braking system architecture is needed.

2.2.1 Brake Layout

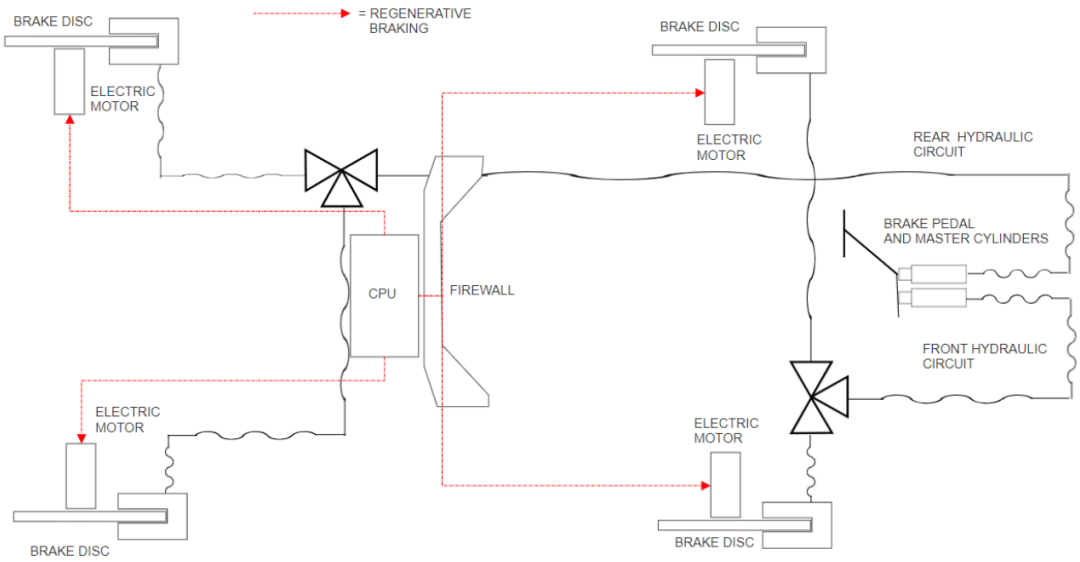

Figure 2.1: SCD25 manual braking layout

Considering a generic vehicle with four tires and a braking system acting on all four wheels, typical layouts of the brakes can be divided into:

- **Diagonal split (cross-split)**: In this configuration, two circuits are present with one of them controlling a front brake and its opposite rear brake, while the other circuit controls the other pair. This layout, most typically found in road cars, provides good redundancy as it ensures a level of stability and braking in case one circuit fails. The main disadvantage of using a diagonal split in motorsport is its lack of control and customization of front-rear brake balance.
- **Front-rear split:** This configuration is characterized by one hydraulic circuit operating both front calipers while the second one operates the rear calipers. With this split, a balance bar may be employed, allowing drivers to adjust their front and rear brake distribution even mid-race.

As discussed above, the front-rear split is the dominant layout for almost all motorsport applications and is currently employed on the SCD25 prototype as seen in figure 2.1, and while this configuration does not guarantee redundancy on its own, the use of two completely independent master cylinders and hydraulic circuits provides braking capacity even in case one of the circuit fails.

2.2.2 Brake Components

Brake Rotors

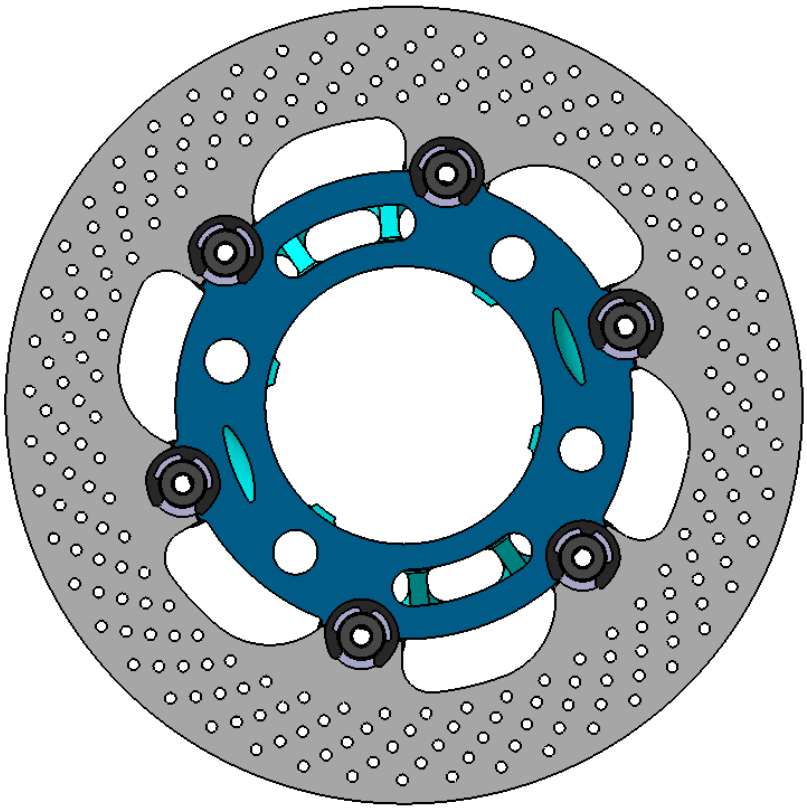

Figure 2.2: SCD25 front disc assembly

The brake rotors have been directly carried over from the last prototype along with the wheel hub: Custom designed heat treated AISI-410 discs. These discs have been developed in accordance with the provided Brembo components mentioned below to ensure no compatibility issues.

The most relevant information from the brake rotors for our development is the mean brake radius calculated as:

Given the pad sweeps from inner radius r_i to outer radius r_o (band width $w = r_o - r_i$), the disc effective radius R_{disk} can be computed as:

$$R_{disk} = \frac{r_i + r_o}{2}.$$

Rotor	Material	R_{disk} [mm]	r_i [mm]	r_o [mm]
Front	AISI 410 (SS)	94	79	109
Rear	AISI 410 (SS)	83	71	95

Table 2.1: Brake rotors materials and radii

While the current brake rotors might be subject to changes in next year's prototype, currently no data or development has taken place in terms of dimensional changes and thus, the mean effective radii used will be those of the current vehicle.

Calipers and Pads

As Formula Student vehicles are not subjected to a minimum weight requirement normally found in motorsport, it is easy to understand that teams often find themselves thriving to remove as much unnecessary weight as possible without compromising function or performance. By benchmarking a few competitor teams, quick research indicates most top teams are researching and developing in-house solutions for calipers and master cylinders as most of the commercial options are usually too heavy or oversized for Formula Student applications.

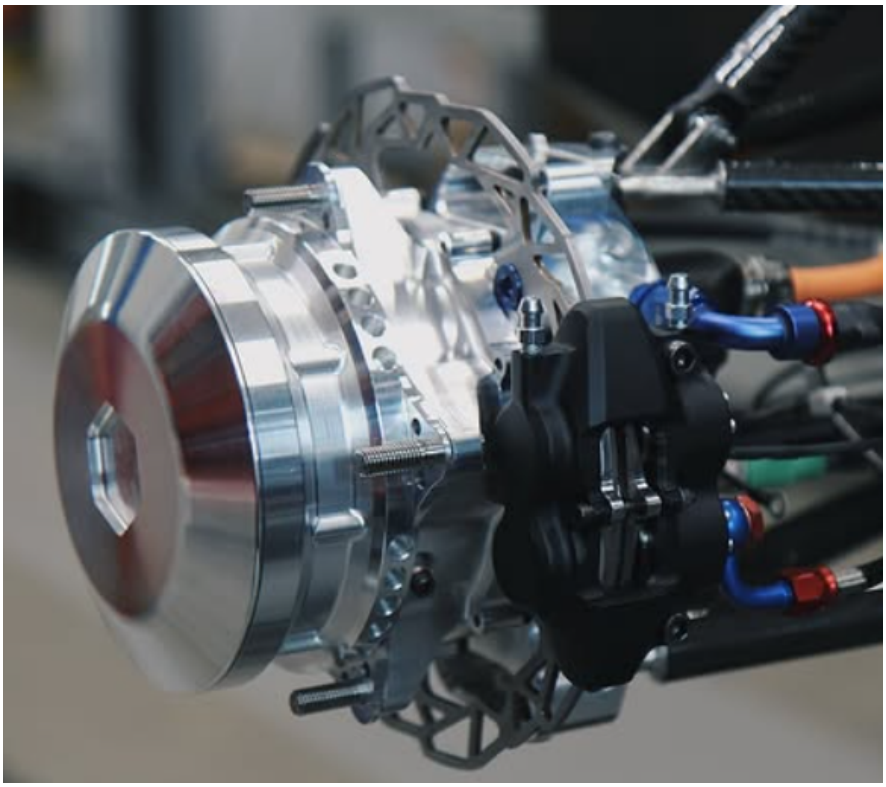

Figure 2.3: Custom wheel hubs, courtesy of Formula Student team Tallinn [6]

Unfortunately, the expertise and cost of developing custom braking components currently exceeds the team's budget and expertise. In addition, while weight saving would provide a significant advantage in terms of performance, reliability is currently a higher priority in this stage of development, and thus, for the time being, a custom in-house option provides too many drawbacks compared to the added benefits.

The prototype is currently equipped with commercially available parts from Brembo as part of a sponsorship agreement. Regarding the brake calipers, the most viable choices have been selected from Brembo's racing catalog [1] and the team has been using the Brembo P4 24, as seen in Figure 2.4, for the front and P2 24 for the rear for many years, with periodic maintenance offered by Brembo. While the front and the rear calipers belong to the same series, the main difference between them is the number of pistons on each side and thus the maximum clamping force.

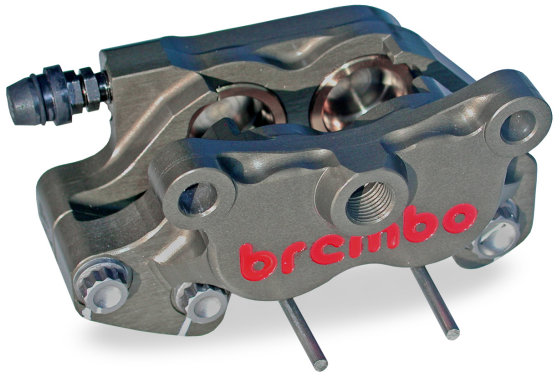

Figure 2.4: Brembo P4 24 [1]

Caliper	Pistons	Piston ⌀ [mm]	Body material	Piston material	Weight [g]
P4 24	4	24	Aluminum	Titanium	262
P2 24	2	24	Aluminum	Titanium	198

Table 2.2: Technical specifications of Brembo P4 24 and P2 24 calipers

As seen in Table 2.2, the calipers are made from CNC billet aluminum, while the pistons are made of titanium, which ensures high stiffness to weight as well as excellent thermal resistance in the sealing area. Regarding weight per axle, the front weighs 524 g and the rear 396 g, bringing the total to 920 g. Considering the reliability they have shown throughout many seasons, and the low cost thanks to the sponsorship, the team has decided to maintain using these calipers for the time being as their benefits in terms of reliability and availability outweigh the weight saving custom calipers may provide.

Figure 2.5: Pad compounds offered by Brembo [1]

Regarding pad choices, out of the available compounds for the calipers installed, the most viable choice tested was the H38 offering well-balanced attributes. Looking into the team's available documentation, telemetry data gathered indicated an average friction coefficient for the pads of $\mu_{\text{pad}} \approx 0.40$ during the last tests conducted.

Master Cylinders

A major part in developing the new pedal box with integrated emergency braking system is the correct sizing of the master cylinders, as they define pedal feel and achievable line pressure. Oversizing the master cylinders with a larger bore makes the pedal travel too short and stiff, not allowing drivers to correctly modulate their input and at the same time the required effort would greatly increase and potentially cause discomfort and fatigue. On the contrary, a small bore will create excessive travel which might cause the stroke to run out before building the necessary pressure.

From the available options provided in the racing catalog [1], the team runs the XB2.B5.11/15 - A1/A5 master cylinders. Considering that typically such components are used on larger vehicles such as GT or kit cars, any bore above 19 mm will be oversized for the Formula Student prototype.

MC Bore ⌀ [mm]	Pushrod thread	Part number
16.00	M10×1	`XB2.B5.11`
17.46	M10×1	`XB2.B5.12`
19.00	M10×1	`XB2.B5.13`
20.64	M10×1	`XB2.B5.14`
22.22	M10×1	`XB2.B5.15`

Table 2.3: Brembo forged master cylinders (XB2.B5 series) [1]

In the next section, an explanation is provided regarding the proper selection of master cylinders for each hydraulic circuit.

2.2.3 Master Cylinder Sizing

Caliper piston volumes

Both front and rear calipers use 24 mm pistons with a cross–sectional area of $A_{\text{cal,p}}$:

$$A_{\text{cal,p}} = \pi \left(\frac{D_{\text{cal,p}}}{2} \right)^2 = \pi (12\,\text{mm})^2 \approx 452\,\text{mm}^2.$$

Thus, moving one piston by 0.8 *mm* (accounting for pad wear) requires a volume: $0.8A_{\text{cal,p}} \approx 361.6\,\text{mm}^3$ of fluid.

For the *front* axle (two P4 24 calipers, 4 pistons per caliper, 8 pistons total):

$$V_{\text{req,f}}(0.8\,\text{mm}) \approx 2{,}892.8\,\text{mm}^3.$$

For the *rear* axle (two P2 24 calipers, 2 pistons per caliper, 4 pistons total):

$$V_{\text{req,r}}(0.8\,\text{mm}) \approx 1{,}446.4\,\text{mm}^3.$$

Axle	Caliper	Total pistons	$A_{\text{cal,p}}$ (mm^2)	Required volume (mm^3)
Front	P4 24	8	452	2,892.8
Rear	P2 24	4	452	1,446.4

Table 2.4: Caliper geometry and volume demand per axle

Master cylinder displacement

According to the Brembo Catalog [1], the employed master cylinders are characterized by a stroke of 23 mm, but considering a safety mechanism has to be implemented in case of total brake failure which will be covered in a later section, the actual usable stroke should be slightly shorter.

Assuming a usable stroke of $s = 20\,\text{mm}$, the fluid volume delivered by a master cylinder of bore D_{MC} is

$$V_{\text{MC,disp}} = \pi \left(\frac{D_{\text{MC}}}{2} \right)^2 s$$

Bore D_{MC} (mm)	Area A_{MC} (mm^2)	Displaced Volume $V_{\text{MC,disp}}$ (mm^3)
16.00	201.0	4,020
17.46	239.4	4,788
19.00	283.4	5,668

Table 2.5: Master cylinder displacement for 20 mm stroke

Matching volumes and travel

Having calculated the required volume for each axle as well as the fluid displaced by each master cylinder throughout its usable stroke, we can move on to matching the master cylinders to the axles with the following requirements:

1. Supply the required caliper volume with comfortable margin.
2. Keep circuit strokes in a target window for pedal feel/modulation.
3. Yield a sensible front-rear torque repartition [21].

In lightweight Formula Student cars, weight transfer under deceleration increases normal load on the front axle, and, to maintain stability and avoid spin risk during hard braking, it is desirable that the *front* axle reaches lock before the rear. Therefore, according to empirical/analytical studies on vehicles and general braking-stability analyses indicate a front-biased target in the ∼60–70% range as a safe starting point for setup and design [22, 23].

Balance Bar

It is worth noting that the vehicle is equipped with the CP5520-25 Trunnion type balance bar from AP Racing seen in Figure 2.6 [7].

Figure 2.6: AP Racing CP5520-25 [7]

While the balance bar itself allows fine-tuning the brake repartition, it is preferable to start in the target range, as stated in the manual [7], since the more adjustment is employed, the lower the efficiency of the balance bar becomes.

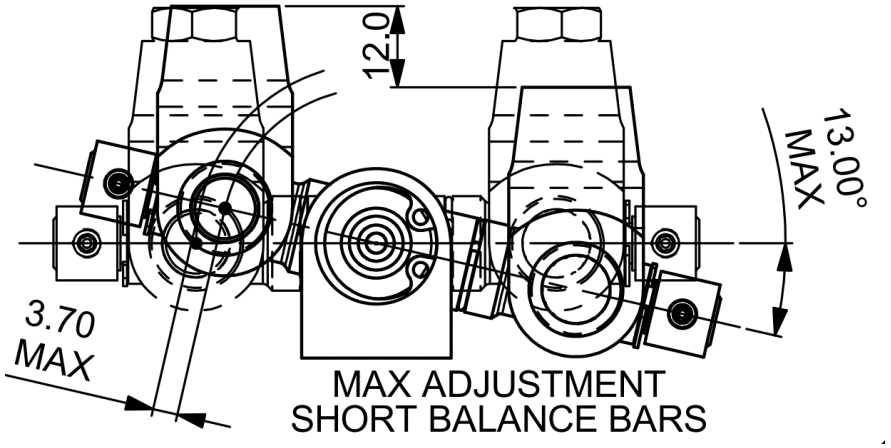

Figure 2.7: Balance bar maximum recommended adjustment

Considering what has been discussed above, the optimum range of brake repartition with a neutral balance bar should fall within 60–70% with 65% being the target. This initial choice will allow for most efficient adjustment on brake bias using the balance bar during testing and will establish the base in choosing the correct master cylinders.

Brake repartition

We estimate front/rear brake share considering: (i) a *neutral balance bar* so the pedal force is split equally into the front and rear master cylinders (MCs); (ii) identical pad friction coefficients and similar pad/disc materials front vs. rear; (iii) the same number of pads per caliper, so only total piston area and disc effective radius differ.

With a neutral balance bar, each circuit sees the same mechanical input force F_{MC}. Line pressure in a hydraulic circuit is $P = F_{\mathrm{MC}}/A_{\mathrm{MC}}$, hence the front/rear pressure ratio depends only on MC areas:

$$\frac{P_f}{P_r} = \frac{F_{\mathrm{MC}}/A_{\mathrm{MC,f}}}{F_{\mathrm{MC}}/A_{\mathrm{MC,r}}} = \frac{A_{\mathrm{MC,r}}}{A_{\mathrm{MC,f}}}.$$

Caliper *clamp* force scales with line pressure and total piston area on that axle ($A_{\mathrm{cal,tot}}$):

$$F_{\mathrm{clamp}} \propto P \cdot A_{\mathrm{cal,tot}}.$$

Brake torque on each axle is the clamp force times the disc effective radius (R_{disk}):

$$T \propto F_{\mathrm{clamp}} \cdot R_{\mathrm{disk}} \quad \Rightarrow \quad \frac{T_f}{T_r} = \frac{P_f}{P_r} \cdot \frac{A_{\mathrm{cal,tot,f}}}{A_{\mathrm{cal,tot,r}}} \cdot \frac{R_{\mathrm{disk,f}}}{R_{\mathrm{disk,r}}}.$$

Each front/rear bore choice ($D_{\mathrm{MC,f}}, D_{\mathrm{MC,r}}$) gives a pressure ratio $P_f/P_r = A_{\mathrm{MC,r}}/A_{\mathrm{MC,f}}$ and therefore a torque ratio via the relation above. Finally, the front brake *share* ($X_{\mathrm{brake,f}}$) is:

$$X_{\mathrm{brake,f}} = \frac{T_f}{T_f + T_r} = \frac{T_f/T_r}{1 + T_f/T_r}.$$

Front MC (mm)	Rear MC (mm)	P_f/P_r	T_f/T_r	Bias ($X_{\text{brake,f}}$)
16.00	16.00	1.000	2.265	69.4
16.00	17.46	1.191	2.697	73.0
16.00	19.00	1.410	3.194	76.2
17.46	16.00	0.840	1.902	65.5
17.46	17.46	1.000	2.265	69.4
17.46	19.00	1.184	2.682	72.8
19.00	16.00	0.709	1.606	61.6
19.00	17.46	0.844	1.913	65.7
19.00	19.00	1.000	2.265	69.4

Table 2.6: Calculated brake repartition for all MC-bore pairs.

Final Selection

Two combinations fall at the 65% front target:

- (i) $D_{\text{MC,f}} = 17.46\,\text{mm},\ D_{\text{MC,r}} = 16.00\,\text{mm} \Rightarrow 65.5\%$
- (ii) $D_{\text{MC,f}} = 19.00\,\text{mm},\ D_{\text{MC,r}} = 17.46\,\text{mm} \Rightarrow 65.7\%$

We now compare the *required circuit strokes* each pair needs to deliver the axle volume demands $V_{\text{req,f}} = 2{,}892.8\,\text{mm}^3$ and $V_{\text{req,r}} = 1{,}446.4\,\text{mm}^3$:

Front MC (mm)	Rear MC (mm)	Front stroke $s_{req,f}$ (mm)	Rear stroke $s_{req,r}$ (mm)
17.46	16.00	12.08	7.19
19.00	17.46	10.20	6.04

Table 2.7: Stroke comparison for the two pair candidates

Both pairs meet the **60–70%** target. However, (17.46/16.00) yields longer front and rear strokes (12.08 mm / 7.19 mm) versus (10.2 mm / 6.04 mm) with the (19/17.46) pair, the longer stroke will improve pedal modulation. Therefore, the best possible combination for the master cylinders is **17.46 mm** at the front and **16 mm** at the rear.

2.2.4 Pedal Box

The SCD25 pedal box is completely carried over from the original prototype with no changes done as the pedal box managed to pass all the technical requirements and provided reliability. For what concerns the analysis of the pedal box, in order to develop a new and updated model, the most critical aspects to look into are the pedal ratio and weight.

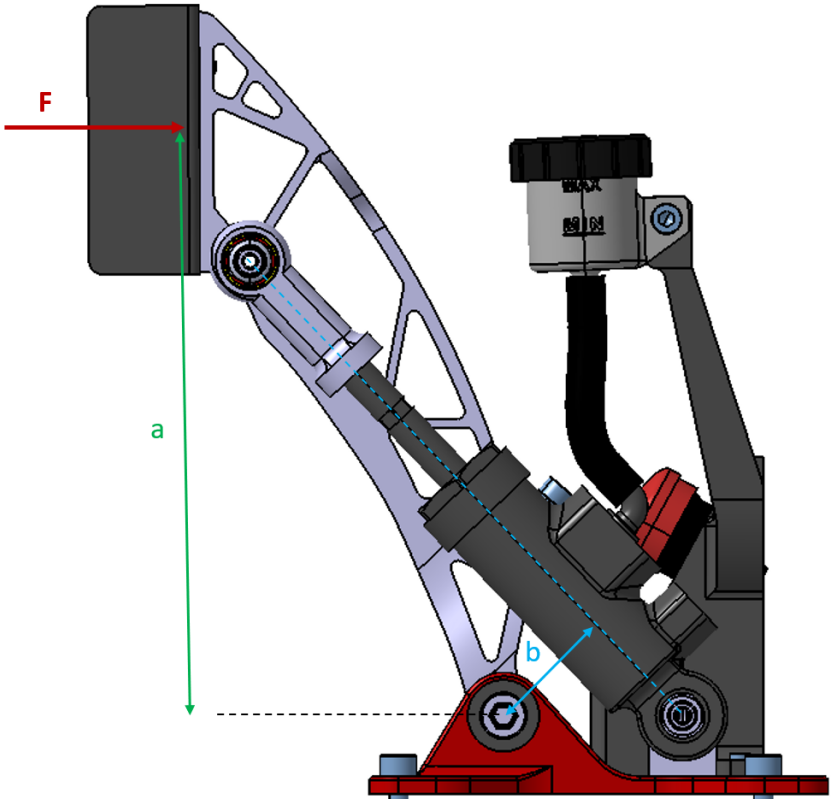

Figure 2.8: SCD25 pedal ratio

According to the documentation found from the designers of Squadra Corse, their pedal ratio can be defined as $PR = \frac{a}{b}$ with a defined as the pedal arm from the pedal face to pivot point and b the push rod arm defined as the perpendicular from the master cylinder axis to the pivot. By extracting the dimensions straight from CAD:

Quantity	**Symbol**	**Value**
Pedal arm	a	180 mm
Pushrod arm	b	36.2 mm
Pedal ratio	$PR = \frac{a}{b}$	4.9

Table 2.8: SCD25 pedal ratio geometry

While the pedal ratio will be covered in depth when dimensioning the new system, the value currently used does not properly estimate the effort needed from the driver or the master cylinder push force, so a new method will be developed. Nevertheless, to briefly summarize the effect of pedal ratio [24], it can be stated that:

- **High pedal ratio:** Reduces required driver force and increases available modulation at the expense of longer pedal travel. It will allow for easier control for the driver.
- **Low pedal ratio:** Increases required driver force and shortens pedal travel, giving a firmer feel. The main advantage provided is the shorter pedal travel.

Pedal Box Weight

With regard to the pedal box weight, a bill of materials and a Pareto analysis have been conducted below. When calculating the weight, certain components such as the shut down button, mounting fasteners and low pressure reservoir have been omitted so that the analysis can be more accurate when comparing to the new system. In other words, the components considered are strictly that of the pedal box.

Component	**Qty**	**Material**	**Mass [g]**
Pedal Base	1	Al 2024	113
Pedal	1	Al 7075-T6	287
Master Cylinder	2	–	320
Balance Bar	1	–	225
BOTS Support	1	PA12	61
Teflon Washer	2	PTFE	2
Rod end	2	Al 7075-T6	38
Radial bearing GE8C	2	–	13.2
Rod-end pin	1	39NiCrMo3	38
Rod-end spacer	4	Al 2024	4
Locknut M8 (ISO 7040)	2	Steel	5.2
Locknut M6 (ISO 7040)	1	Steel	1.5
CSK screw M4×10	4	Steel	3.2
SHCS M3×8	3	Steel	1.2
Pedal face	1	CFRP	64
CSK screw M3×10	4	Steel	1.6
Pedal-base bushing	2	Bronze	18
Shoulder screw 8×55	1	Steel	28
SHCS M5×20	1	Steel	3
Total System			**1226.9**

Table 2.9: SCD25 pedal box bill of materials.

The total weight of the SCD25 pedal box comes out as **1226.9 g** and will be used as a benchmark to evaluate the new designed system. Since the aim of this thesis is to incorporate the emergency braking system directly into the pedal box, the weight of the new system will be compared to that of the 2025 pedal box and EBS combined.

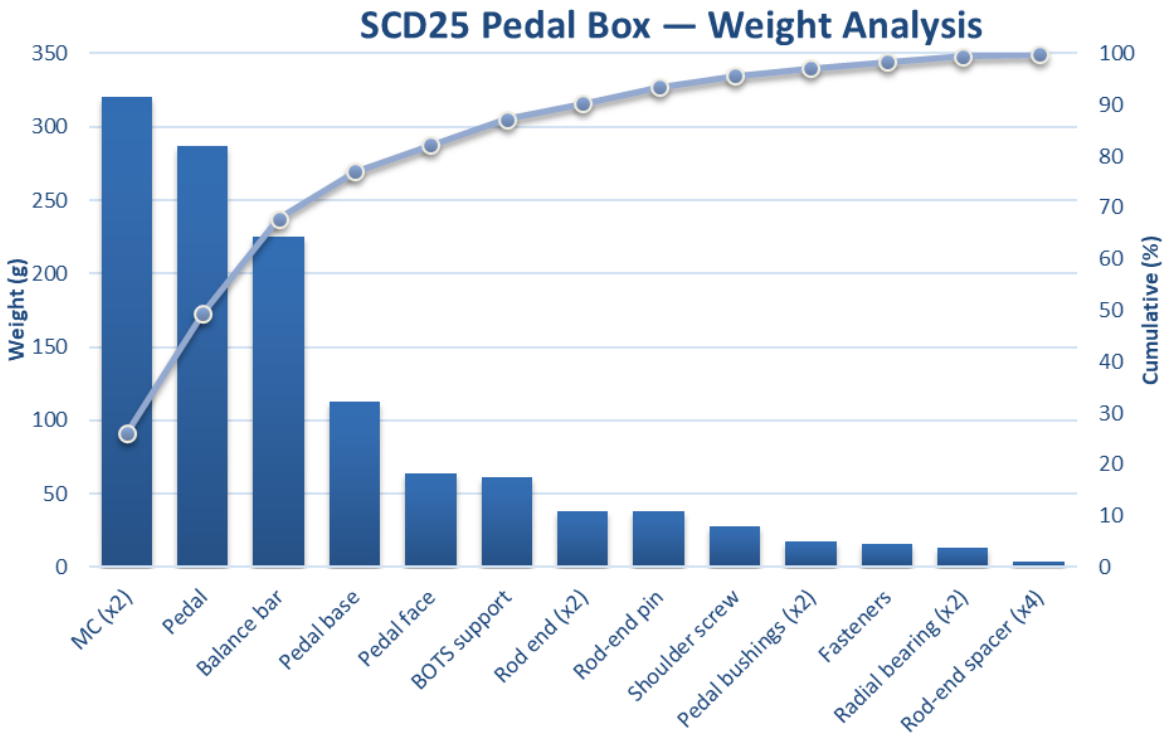

Figure 2.9: Pareto weight analysis SCD25 pedal box

The graph in Figure 2.9 gives us an insight into where most of the weight is concentrated. It can be observed that four components alone constitute about 70% of the weight. Out of those four parts, two of them will be carried over (master cylinders and balance bar) leaving little room for adjustment in terms of weight on the pedal and pedal base. Nevertheless, most of the weight reduction will be coming on the emergency system side seen below.

2.3 Autonomous & Emergency Braking Systems

2.3.1 Description

The Autonomous System Brake (ASB) is the brake actuator needed to run in autonomous as stated in T15. The Emergency Brake System (EBS), is the part of the ASB that takes care of emergency braking. In practical words, the ASB's main role is the normal braking while the EBS is the safety component in case of failure. T15.1.3 states that the traction system is not considered a brake system, this does not imply that techniques such as regenerative braking may not be used but rather that a secondary braking system must be present at all times. As a safety feature, the EBS is subjected to various requirements on the control and electrical side to dictate how and when the EBS is activated. While Figure 2.10 shows that the EBS is a subsystem of the ASB, in order to avoid confusion, from now on the ASB will refer to the actuator responsible for normal braking and EBS for emergency braking.

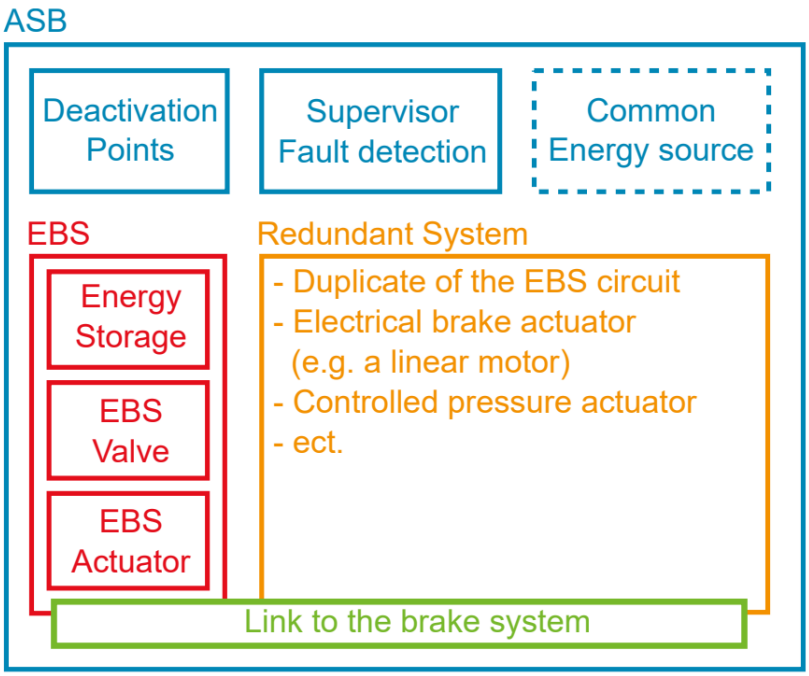

Figure 2.10: Hierarchical overview of the ASB [8]

2.3.2 Shutdown Circuit & Remote Emergency System

Following the autonomous systems guide [8], the Remote Emergency System (RES) seen in figure 2.11, consists of a remote control and a receiver unit wired into the shutdown circuit (SDC) (Figure 2.12) define in rule T14.4.4. Once the shutdown button on the RES is activated or a signal loss occurs, the tractive system (TS) is disabled and the EBS is activated. In addition, the RES enables the signal to activate the ready-to-drive (R2D), which enables the autonomous system (AS).

Figure 2.11: RES remote control (left) and receiver unit (right) by Grossfunk [9]

The SDC is the main control line for the TS of the vehicle. It is subjected to numerous checks that make sure the closed SDC is safe before activating the TS. Out of the various checks established in figure 2.12, the most critical for the design of the new pedal box and EBS are the RES previously mentioned and the Brake Over-Travel Switch (BOTS) of rule T6.2.1. The BOTS opens the SDC in case of failure of at least one of the brake circuits.

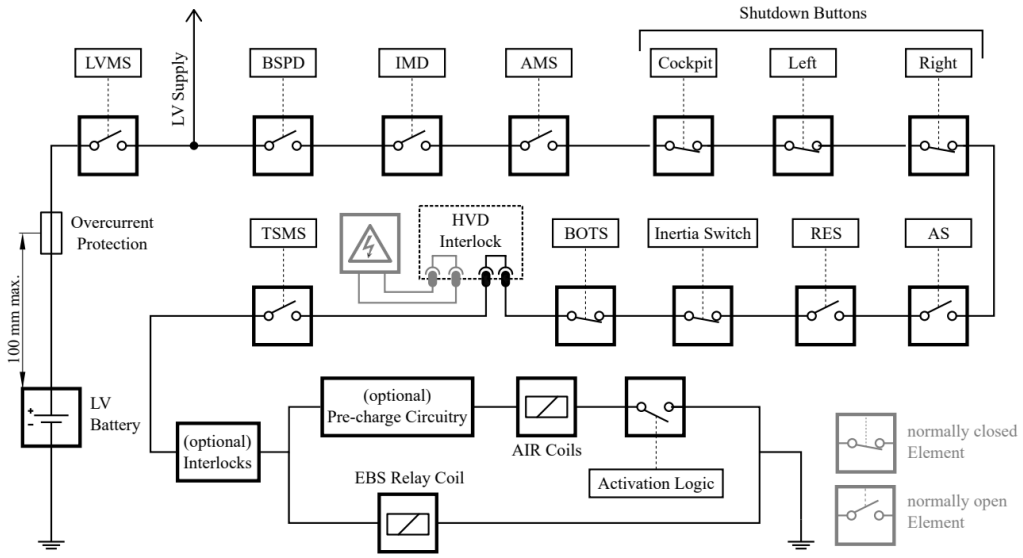

Figure 2.12: Shut Down Circuit [5]

2.3.3 Mechanical Part

With the shutdown circuit covered, we can move on to the mechanical requirements of the EBS. The mechanical part of the EBS is required to function without the aid of electrical power (T15.2.1) by the release of stored brake energy. Energy storage is generally achieved by the use of springs, pneumatic or hydraulic pressure. The first EBS featured in Squadra Corse Driverless seen in figure 2.13 employed a pneumatic-hydraulic system with pressure intensifiers that used stored pneumatic energy to increase the hydraulic pressure of the braking system, thus compressing the master cylinders. A big flaw of the original EBS was the leakage of oil from the oil to air chamber which resulted in damaged seals that lead to low brake fluid pressure. The system has since then been replaced with a complete separation of the pneumatic and hydraulic systems, as covered in section 2.4 featuring pneumatic actuators connected in series directly to an extra pair of master cylinders dedicated to the emergency braking.

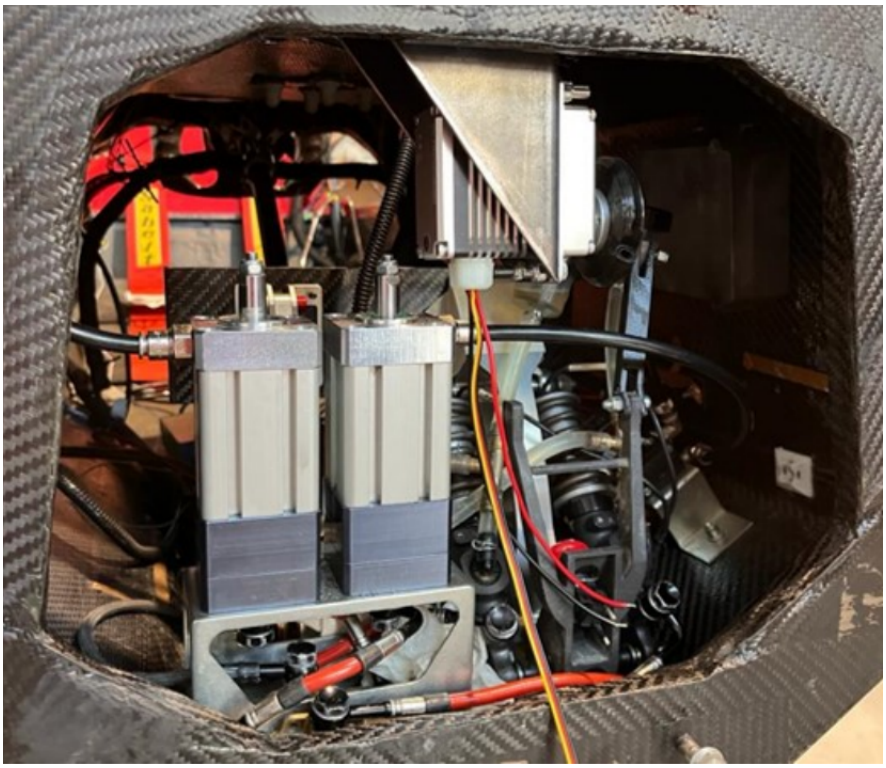

Figure 2.13: SCD22 EBS with pressure intensifier

2.3.4 Redundancy

Another important requirement for developing the EBS is the redundancy. The Formula Student guide [8] defines redundancy as having independent systems fulfilling the EBS requirements in parallel. In the event of a single failure (T15.3.4) the system should still be able to come to a safe state. On the mechanical side, two examples are presented on what can be considered as fully redundant systems according to the student guide.

Actively Applied Braking Energy:

In Figure 2.14, the redundancy is achieved with two independent, identical pneumatic systems: Braking energy is stored in the form of pressurized air inside a tank connected to a normally open valve. The brakes are only released if electrical power is applied to the valve. With this configuration the only way to switch to manual driving mode is to release the pressure and subsequently release the brakes, or disconnect completely the tanks. In case power loss occurs due to any failure, the air is automatically released bringing the vehicle to full stop. The use of two independent identical systems ensures the redundancy since any failure or loss of pressure in one side would still allow braking capability guaranteeing at least half the necessary deceleration or more, depending on the sizing of the actuators (T15.4.3).

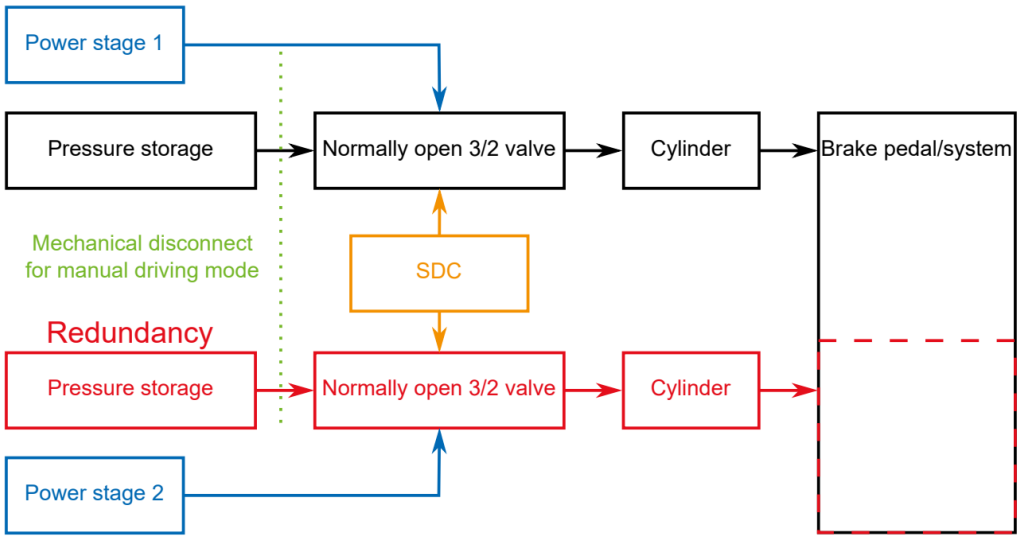

Figure 2.14: Actively applied braking energy model

Removal of Counterforce:

In Figure 2.15, two independent springs are constantly clamping the pedal or system in the default state. This ensures both redundancy with the two springs and eliminates the need for energy storage to activate the brakes. On the other hand, a pressure source would still be required to release the springs with a counteracting force (cylinder) against the springs. A normally closed 3/2 valve supplied with electrical power is connected to the pressure source that will counteract the spring force. Any power loss will release the counter force and the spring can re-apply the brakes bringing the vehicle to a stop. While this option seems simpler as it eliminates the need for two identical pressure storage systems and cylinders, complexity arises in the decoupling for the manual driving mode. The springs must be mechanically detachable so as not to impede driver action, or in case of gas-springs, the pressure must be releasable (attention to T14.9).

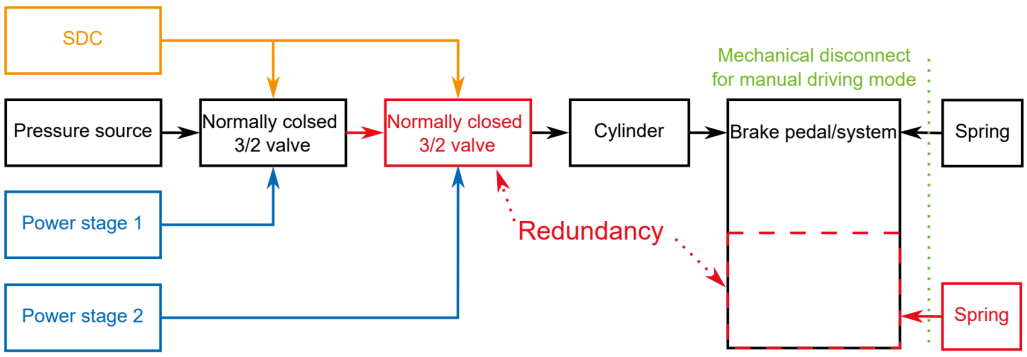

Figure 2.15: Removal of counterforce model

Out of the two proposed options, the use of actively applied braking energy is generally more adopted as the decoupling mechanism generally comes with additional weight gain and complexity, giving it more drawbacks than advantages.

2.4 SCD25 Current Systems

In this section, an analysis of the current ASB and EBS equipped on the vehicle will be conducted, with the purpose of identifying potential areas of improvement for the development of the new system.

2.4.1 Autonomous System Brake

As previously stated, in this context the ASB refers to the actuator in charge of normal braking. During the 2025 season, the Powertrain & Unsprung Mass division worked on developing an autonomous actuator pictured in figure 2.16. As the SCD25 is a fully electric prototype, most of the braking during dynamic events was set to be achieved utilizing regenerative braking. Nonetheless, several concerns were raised regarding the efficiency and capability of the regenerative system. In order to guarantee braking in all possible scenarios (for example regenerative braking would not be possible at very low speeds or high SoC of the battery), a servo motor was coupled to a crank-link mechanism behind the pedal to provide braking force in such scenarios.

Figure 2.16: ASB initial prototype

The development of the ASB prototype relied on the use of an already available servo motor pictured in figure 2.17, as it was one of the most powerful servomotors in its weight range, making it ideal for the ASB application. The design featured a crank that defined the lever arm and linkage system connecting to the pedal. In order to guarantee separation between manual driving and servo motor, a slot was added in the linkage such as any actuation on the pedal would not be met with loads coming from the servo. The parts were realized using 3D printing during the prototyping phase as it allowed for fast prototyping when testing different geometries while still withstanding the loads.

Specification	Value
Voltage Range	11.1V - 14.8V
No-Load Speed (11.1V)	0.26 sec/60°
No-Load Speed (14.8V)	0.19 sec/60°
Peak Current	6.5 A
Stall Torque (11.1V)	8.24 Nm
Stall Torque (14.8V)	10.79 Nm
Weight	310 g
Max Rotation Angle	139°
Travel per µs	0.099°/µs
Max PWM Signal Range	800-2200 µs

Figure 2.17: HS-1005SGT servomotor [10]

Servo Dimensioning:

The major issue with the servo motor was the trade-off between the maximum force F that the servomotor can exert and the total travel the servo may allow the pedal to achieve. A longer arm would reduce the maximum force while simultaneously increasing the pedal travel.

Given the stall torques at different voltages, we can calculate the achievable force for various lever arm lengths:

At 11.1V with $T_{stall} = 8.24\,\text{Nm}$; At 14.8V with $T_{stall} = 10.79\,\text{Nm}$

Using different arm lengths:

1. For Arm Length $k = 0.025\,\text{m}$:

$$F_{11.1V} = \frac{8.24\,\text{Nm}}{0.025\,\text{m}} = 329.6\,\text{N}$$
$$F_{14.8V} = \frac{10.79\,\text{Nm}}{0.025\,\text{m}} = 431.6\,\text{N}$$

2. For Arm Length $k = 0.03\,\text{m}$:

$$F_{11.1V} = \frac{8.24\,\text{Nm}}{0.03\,\text{m}} = 274.67\,\text{N}$$
$$F_{14.8V} = \frac{10.79\,\text{Nm}}{0.03\,\text{m}} = 359.67\,\text{N}$$

These calculations illustrate that as the arm length increases, the maximum force decreases. Unfortunately, during the 2025 season, due to major technical issues on the car no testing occurred. As a result, the prototype was mostly abandoned and never made it outside development phase. In addition, it was decided that the prototype would switch to employing a 100% regenerative braking strategy, eliminating the need for an ASB actuator, keeping only the emergency mechanical actuator as it is mandatory by regulation. Since the feasibility of only regenerative braking has not been tested properly, it was requested to finish the development and dimensioning of the ASB prototype as a backup plan in case of necessity using the calculations done in chapter 3.

2.4.2 Emergency Brake System

For the most fundamental analysis of this chapter, the current emergency braking system will constitute the foundation for the development of the new solution. As previously described in subsection 2.3.3, the original EBS suffered from issues such as pressure loss and oil leaks which led to the development of the system:

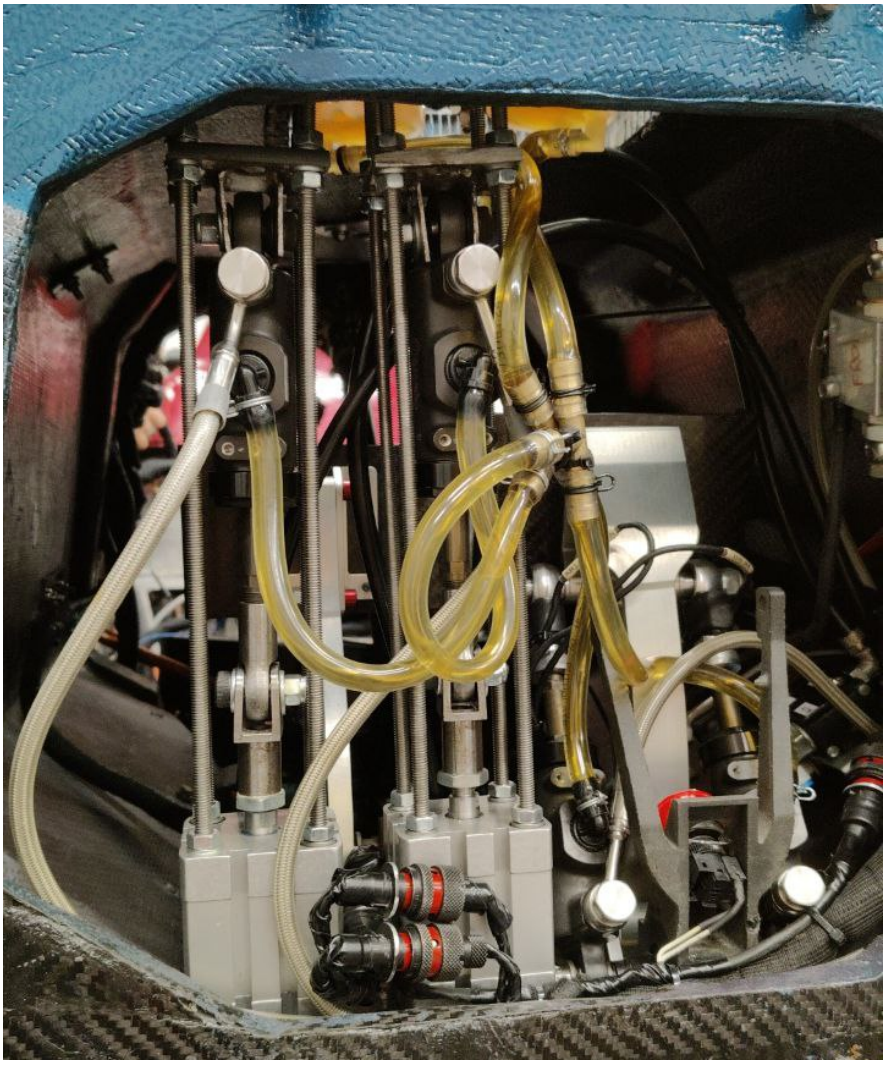

Figure 2.18: EBS mounted inside vehicle during the 2025 season

The main feature of the 2023 EBS was the addition of two master cylinders coupled directly to pneumatic actuators from Festo [25], once the RES was activated or any power loss occurs, 3/2 normally open solenoid valves would direct high pressure air from the canisters straight to the pneumatic actuators, fully compressing the master cylinders.

Considering this, the EBS can be divided into:

1. Compressed Gas System: Featuring the compressed air canisters, manual valves and solenoid valves.

2. Actuator Assembly: Contains the pneumatic actuators, master cylinders, shuttle valves and additional high pressure lines.

Actuator Assembly

Since the Compressed gas system will be covered in detail in another chapter, as it will still be required for the new system, the main analysis here will focus solely on the actuator assembly. The actuator seen in figure 2.18 supplied by high pressure compressed air is directly connected to the master cylinder through a clevis and rod end. As master cylinders must only be subjected to axial loads, both ends have been equipped with radial bearings to reduce any bending loads that may occur. The chosen pneumatic cylinder manages to deliver 1273 N of force at 10 bars of pressure, achieving an estimated $12.20\,\mathrm{m\,s^{-2}}$ deceleration, verifying rule T15.4.2.

In order to guarantee rule T15.1.4, the system utilizes a shuttle valve from Rexroth [26], which allows to output the highest pressure coming from either the EBS or manual braking system. In this configuration, manual operation is always feasible and, in case emergency braking system gets activated, the much higher pressures the system outputs will overcome manual operation and bring the vehicle to a full stop.

Weight analysis

Component	**Qty**	**Mass [g]**
Top Bracket	2	250
Pneumatic Cylinder	2	896
Master Cylinder	2	320
MC Rodend	2	38
Radial Bearing GE10E	2	22
Piston Nut	2	16
Fork	2	206
Bottom Bracket top	1	126
Bottom Bracket bottom	1	138
Banjo bolts	6	84
Shuttle valves	2	340
Brake Lines 1.4 m	1	84
Banjo Straight Fitting	4	64
Banjo fitting 45°	4	68
Threaded Rods M6	8	352
Shoulder Screw 8×20	2	28
Total System		**3032**

Table 2.10: Actuation system bill of material.

Weighing about 3 kg, the system is very heavy for Formula Student applications, adding a lot of necessary weight to the prototype which could affect performance.

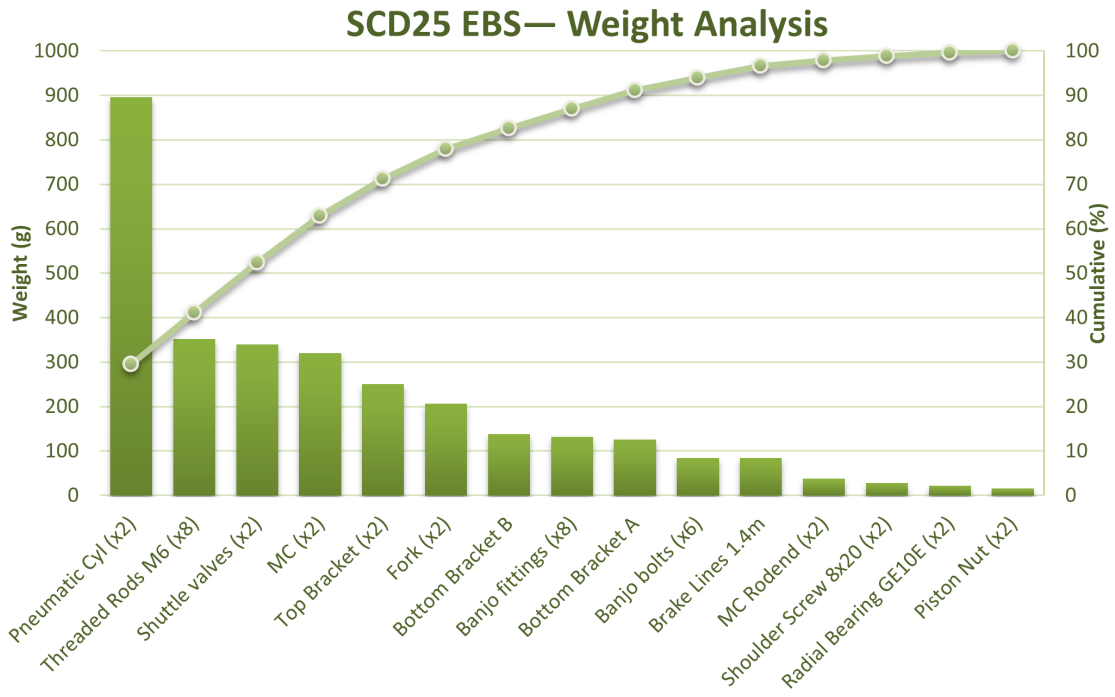

Figure 2.19: Pareto weight analysis SCD25 EBS

- About 30% of the weight comes from the pneumatic cylinders. Without the use of a lever arm, the actuators require large bores to address the high load.
- The use of long threaded rods around all corners of the assembly to stabilize it adds around 10% of the total weight.
- Shuttle valves used for the pressure distribution add another 10%.
- Finally, the extra pair of master cylinders constitutes an additional 10%.

4 components constitute about 60% of the total assembly weight. In addition, the need for redundancy forces us to double every component in this assembly to remain rule compliant and thus effectively doubling the total weight.

Drawbacks

While the upgraded EBS managed to solve the oil leakage issues and complied with the redundancy criteria and regulations, several issues were noted during operation:

1. Due to the addition of several hydraulic high pressure lines and many inlets at the OR valves, proper bleeding of the system was difficult to achieve.
2. The chosen Pneumatic Actuators were oversized, resulting in excessive force directly acting on the master cylinders.
3. The axial force generated from the system caused damage to the carbon fiber monocoque, which was addressed with heavy support to address this issue.
4. The overall length of the assembly made it very difficult to conduct maintenance from the front of the vehicle and hindered the ASB servo motor mounting.

Chapter 3

Design Methodology

The previous chapter established the baseline with regard to rule book requirements and benchmarked the current systems, showcasing the need for improvement. In this chapter, different proposed solutions will be analyzed in order to determine the most viable option to develop.

3.1 Proposed Solutions

The Autonomous System Beginners Guide 2021-2022 [8] helps autonomous teams by presenting three reliable solutions for integrating the ASB into their vehicles. While the guide doesn't provide complete instructions or cover all possible solutions, the listed ones are enough to establish a baseline to work from.

3.1.1 Secondary Master Cylinder Actuation

The proposed option is fundamentally identical to the current EBS. The guide describes the use of a pneumatic cylinder acting on an additional master cylinder. As already seen, to handle redundancy two master cylinders need to be used. To properly integrate into the brake system, the guide recommends the use of an OR-Valve or connecting the master cylinders in series to the manual ones. Figure 3.1 uses a lever arm system to reduce the actuation force, potentially reducing the size and weight of the pneumatic cylinder. This idea would require additional volume inside the monocoque, which may not be available.

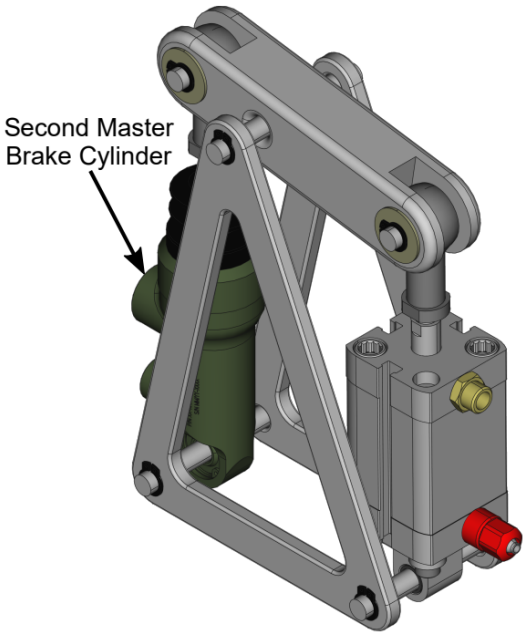

Figure 3.1: Secondary Master Cylinder

3.1.2 Brake Pedal Actuation

In this second proposed option, the ASB actuators are directly connected to the back of the brake pedal. This solution will help reduce the actuator dimensions as the pedal ratio will greatly reduce the forces needed. On the other hand, attention must be given to the decoupling mechanism, which by design must make it impossible for the actuators to block each other or the movement of the pedal, this can be achieved through the use of anti-locking mechanism as shown in Figure 3.2.

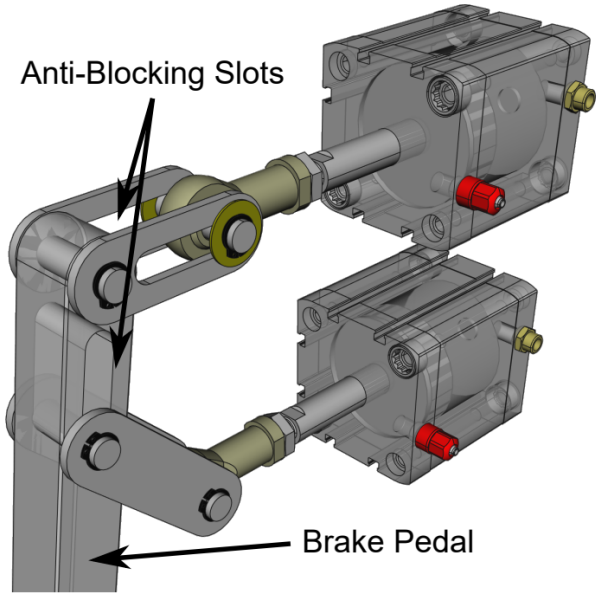

Figure 3.2: Brake Pedal Actuation

3.1.3 Direct Pressure Transducer

The final proposed solution involves the combination of the pneumatic and hydraulic cylinders into a single transducer. While this option seems to be the most compact, it is also the most complex in terms of production. The entire part has to be completely self-built with great attention to tolerances and materials since brake fluid is a very corrosive material. In addition, this would require high technical knowledge from the team otherwise reliability might be compromised due to the sealing and construction. This option should be reserved only when the team manages to achieve excellent reliability in all other areas, as it would require long development times, high manufacturing costs, and room for trial and error.

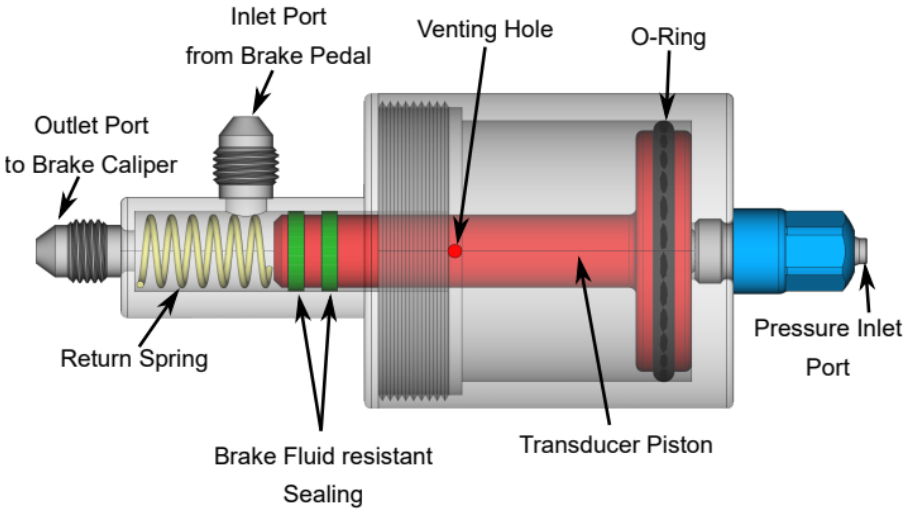

Figure 3.3: Pressure Transducer

3.1.4 Comparison and Selection

In order to rank the different solutions, a Pugh matrix (Figure 3.1) has been devised to evaluate the advantages and disadvantages of each system.

Criteria	**Secondary MC**	**Pedal Actuation**	**Transducer**
Mass	–	++	++++
Volume	–	+	+++
Complexity	+++	+	—
Reliability	+	+	–
Cost	++	+	—
Integration	–	–	+++
Maintenance	–	+	–
Total	**+2**	**+6**	**+4**

Table 3.1: Pugh matrix for EBS selection

By considering different aspects, it is clear that the current system is the most simple in terms of complexity and cost, making it ideal as a first system for newly founded teams. The pedal actuation is the most balanced choice considering the different criteria as it falls in the middle between effort needed and performance. Finally, the direct transducer, while showing great performance, is a very costly and complex project that may not yield good reliability on the first tries.

Having said that, it has been decided to move forward with a pedal actuation system as the next evolution as reliability and cost are listed as higher priorities for the team in its current plan. Evolving directly from the current system to a direct transducer system may backfire as the skill set and knowledge currently present may not suffice and so an intermediate balanced system can greatly help members working to further improve their skills and create useful documentation for the future of the team.

3.2 Braking Dynamics

Having chosen to develop the **Brake Pedal Actuation System**, some calculations are required to properly dimension the actuators. Below is a table containing all the relevant vehicle data based on the SCD25 as a reference.

Parameter	Symbol	Value	Unit
Total mass	m	200	kg
Wheelbase	L	1.525	m
CG height	h	0.241	m
CG distance to front axle	a	0.838	m
CG distance to rear axle	b	0.687	m
Effective wheel radius	r_w	0.237	m
Front disc effective radius	$R_{\text{disk,f}}$	0.094	m
Rear disc effective radius	$R_{\text{disk,r}}$	0.083	m
Pad/disc friction	μ_{pad}	0.40	–
Caliper piston bore (all)	$D_{\text{cal,p}}$	24	mm
Front pistons (both wheels)	$n_{\text{p,f}}$	8	–
Rear pistons (both wheels)	$n_{\text{p,r}}$	4	–
Front MC bore	$D_{\text{MC,f}}$	17.46	mm
Rear MC bore	$D_{\text{MC,r}}$	16.00	mm
Gravitational acceleration	g	9.81	m/s^2

Table 3.2: Vehicle parameters

In the following passages, aerodynamic loads will not be considered when sizing the braking system and autonomous actuators. This assumption is justified since, although top speeds can reach 90–120 km/h, the average speed is typically around 40–50 km/h and even lower in autonomous competitions. Secondly, sizing the braking system without accounting for aerodynamic loads which tend to contribute to the braking force will ensure the system is adequate even in the worse-case scenario.

3.2.1 Ideal Braking

As a first approximation, Ideal Braking will be considered to estimate vehicle stopping distances as required by IN11.2.3. The autonomous brake test requires the vehicle to achieve a complete stop within a maximum of 8.5 m from when the RES is triggered and while the vehicle is driving at least 40 km/h. As the autonomous system may overshoot the 40 km/h target, it is safer to consider different scenarios at different friction coefficients. Ideal Braking can be defined as the condition in which all wheels brake with the same longitudinal force coefficient μ_x [22]. As the brake test is conducted on a level road, the maximum deceleration in ideal conditions can be calculated as:

$$a_x = \mu_x \, g \tag{3.1}$$

By using the maximum μ_x, the maximum deceleration can be obtained for an ideal case where the braking torques applied are proportional to the forces F_z. For constant μ_x during the deceleration, the distance to stop the vehicle from speed V_0 can be calculated as:

$$d = \frac{V_0^2}{2\,\mu_x \, g}. \tag{3.2}$$

The formula clearly shows that the stopping distance increases quadratically with speed, making any overshoot dramatically increase the chances of missing the required stopping distance.

The tire friction coefficient μ_x is hard to replicate in all conditions since it not only depends on tire factors such as compound, construction, temperature and pressure but also on road conditions. The best found solution was to establish a maximum bound for the stopping distance of **7.5 m**, 1 meter less than the required as a conservative value and then find the maximum permissible speed overshoot of the vehicle for different friction coefficients.

Typical values achieved during testing were recorded somewhere between $\mu_x = 1.2{-}1.6$. By using what was discussed above, the following plot was done on MATLAB.

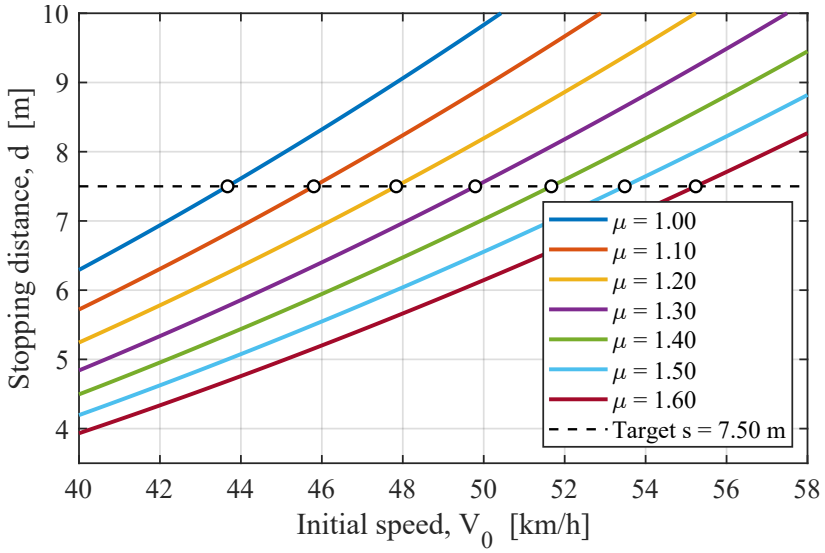

Figure 3.4: Initial velocities V_0 & corresponding stopping distance for different μ_x

μ_x	V_0 [m/s]	V_0 [km/h]
1.00	12.13	43.67
1.10	12.72	45.80
1.20	13.29	47.84
1.30	13.83	49.79
1.40	14.35	51.67
1.50	14.86	53.48
1.60	15.34	55.24

Table 3.3: Initial velocities V_0 for different μ_x to reach target stopping distance

By analyzing the graph and the table, the heavy penalty of speed overshoot can be seen, as the required friction coefficient increases sharply. Since values above 1.4 are generally hard to replicate outside ideal track conditions, the maximum allowable overshoot target should be limited to 49 km/h. In fact, for an average $\mu_x = 1.3$ with a 10% overshoot (44 km/h), the vehicle would still be able to brake in:

$$d = \frac{V_0^2}{2\,\mu_x\,g} \approx 5.85 \text{ m}.$$

To compute the longitudinal forces F_x each wheel must exert in ideal braking, normal forces F_z must be computed.

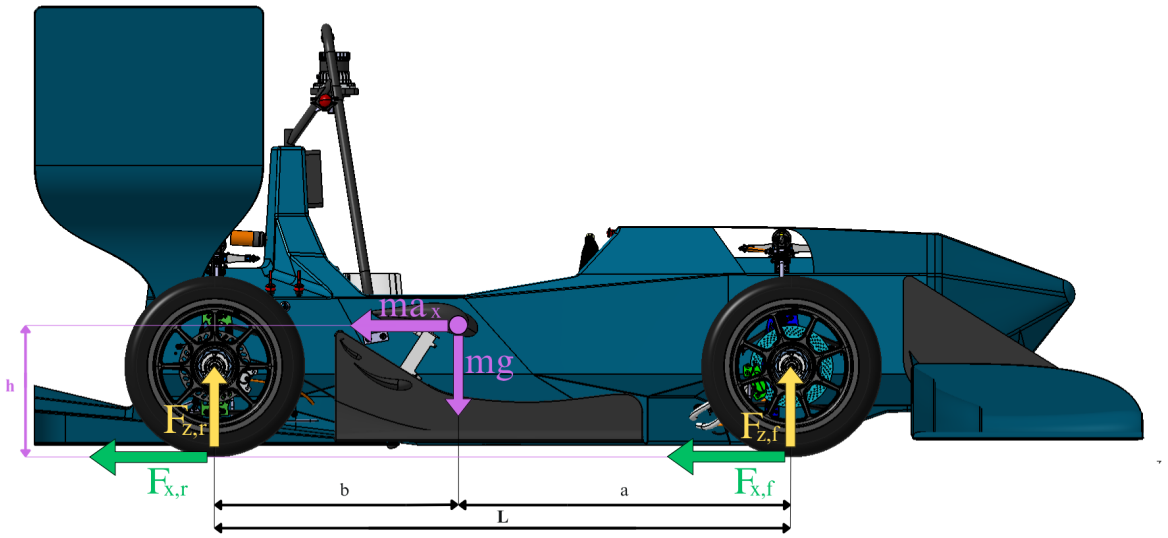

Figure 3.5: Vehicle loads during braking

Taking as reference figure 3.5, the normal forces under a braking deceleration are:

$$F_{z,f} = \frac{mg\,b - ma_x\,h}{L}, \qquad F_{z,r} = \frac{mg\,a + ma_x\,h}{L}. \tag{3.3}$$

Since the values of μ_x are all equal in ideal braking, the longitudinal forces F_x are:

$$F_{x,f} = \mu_x F_{z,f} = \mu_x \frac{m}{L} (g\, b - a_x\, h)\,, \tag{3.4}$$

$$F_{x,r} = \mu_x F_{z,r} = \mu_x \frac{m}{L} (g\, a + a_x\, h)\,. \tag{3.5}$$

By eliminating μ_x from the above expressions, the relationship between $F_{x,f}$ and $F_{x,r}$ is obtained as:

$$(F_{x,f} + F_{x,r})^2 + mg \left(\frac{F_{x,f} a - F_{x,r} b}{h} \right) = 0. \tag{3.6}$$

The plot of Figure 3.6 for the previous equation in the $F_{x,f}$–$F_{x,r}$ plane represents the *ideal braking locus*, showing all combinations of front and rear longitudinal forces that satisfy ideal braking conditions.

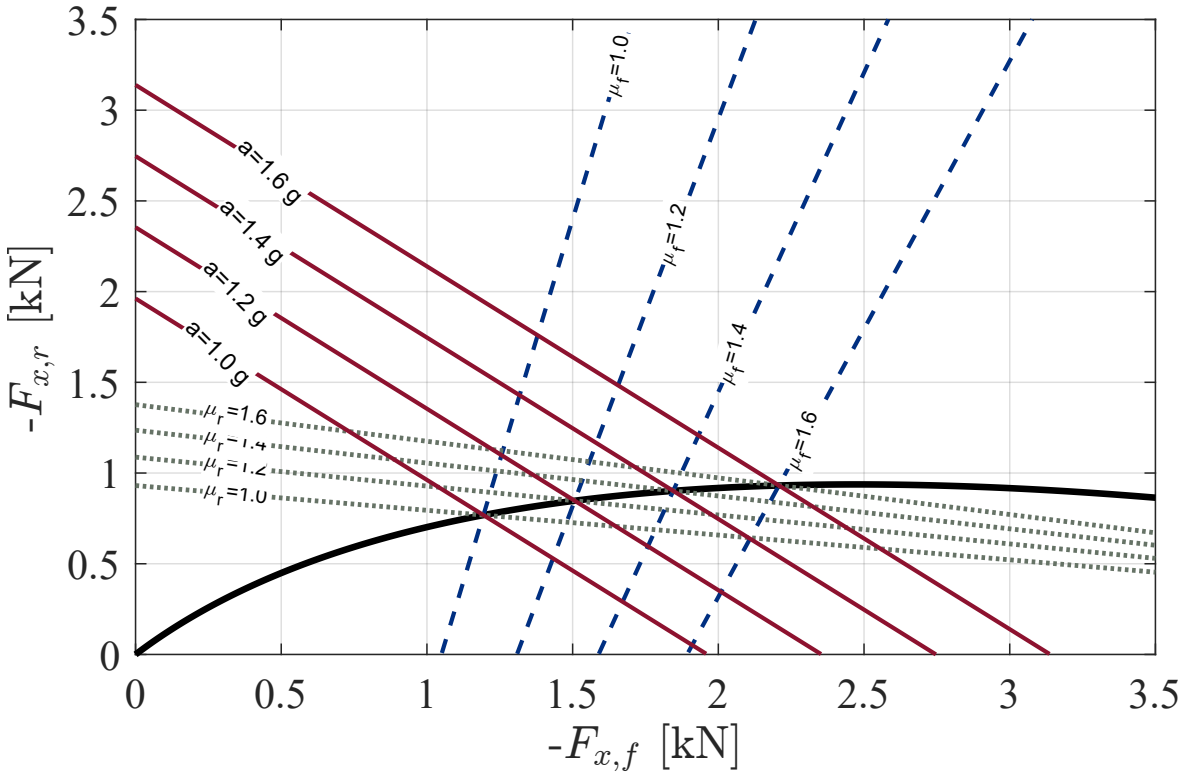

Figure 3.6: Ideal braking conditions

3.2.2 Braking in Actual Conditions

In order to properly size the braking system, adjust the balance bar, and choose the autonomous actuators, braking in actual conditions must be considered where the relationship between braking moments of the front and the rear are dictated by the components of the actual braking system and is generally considered fixed by the hardware contrary to the ideal braking case where force distribution adjusts dynamically with load transfer. As a result, the effective friction coefficients of the front and rear wheels, $\mu_{x,f}$ and $\mu_{x,r}$, are not identical during braking. To avoid loss of stability, the system should be designed to have the front wheels lock first under maximum braking due to the dynamic load transfer effect.

Brake Ratio

Knowing the hydraulic characteristics of the braking system, the distribution of braking moments between the two axles can be expressed as a ratio:

$$K_b = \frac{T_f}{T_r} = \frac{\dfrac{F_{\text{pedal}}}{A_{\text{MC},f}} \dfrac{l_r}{L_{bar}} R_{\text{disk},f} A_{\text{cal,tot},f} \mu_{\text{pad,f}}}{\dfrac{F_{\text{pedal}}}{A_{\text{MC},r}} \dfrac{l_f}{L_{bar}} R_{\text{disk},r} A_{\text{cal,tot},r} \mu_{\text{pad,r}}}, \tag{3.7}$$

where $A_{\text{MC},f}$ and $A_{\text{MC},r}$ are the master–cylinder areas for the front and rear circuits, l_f and l_r are the lever–arm distances from the balance-bar pivot to each master cylinder, R_{disk} is the effective radius of the brake pad contact, A_C is the total caliper piston area per axle, and μ_{pad} is the pad–disc friction coefficient.

If both circuits use the same brake–pad compound (i.e. $\mu_{pad,f} = \mu_{pad,r}$), Eq. (3.7) simplifies to:

$$K_b = \left(\frac{l_r}{l_f}\right) \left(\frac{A_{\text{MC},r}\, R_{\text{disk},f} A_{cal,tot,f}}{A_{\text{MC},f}\, R_{\text{disk},r} A_{cal,tot,r}}\right). \tag{3.8}$$

Equation (3.8) shows that the total brake bias ratio K_b can be interpreted as the product of two independent contributions. The first term,

$$\left(\frac{l_r}{l_f}\right),$$

represents the **mechanical leverage** imposed by the balance bar, which distributes the pedal force between the front and rear master cylinders. The second term,

$$\left(\frac{A_{\text{MC},r}\, R_{\text{disk},f} A_{cal,tot,f}}{A_{\text{MC},f}\, R_{\text{disk},r} A_{cal,tot,r}}\right),$$

represents the **hydraulic ratio** determined by the fixed hardware parameters which was already covered in Section 2.2.3 .

Nominally, the brake bias is about **65.5% front and 34.5% rear**, which can be further adjust using the ratio of lever arms l_r/l_f of the balance bar (Figure 3.7).

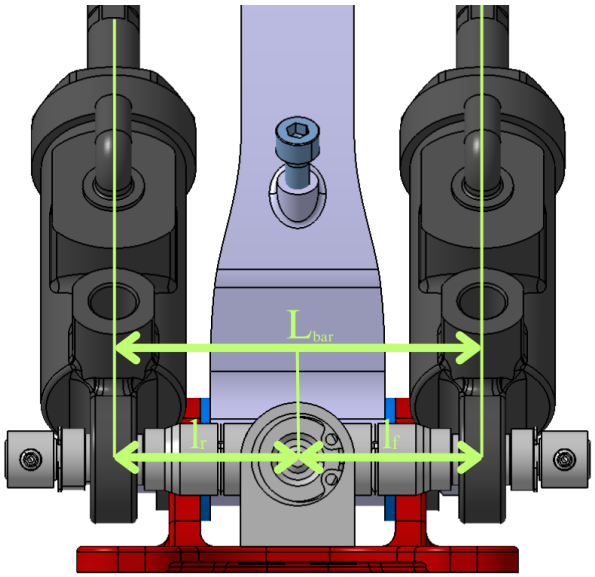

Figure 3.7: Balance bar geometry

As opposed to the ideal braking relationship characterized by a parabolic behavior, the actual braking is a straight line with slope K_b and by changing the bias, the steepness can therefore be adjusted.

To better understand the behavior of the system, by considering an actual case where track conditions are suboptimal and the maximum achievable friction coefficient is $\mu_{lim} = 1.3$ with a target deceleration of $a_x = 1.3g$ magnitude, and a neutral balance bar with a brake bias of 65.5%. In this case, the following curve can be analyzed.

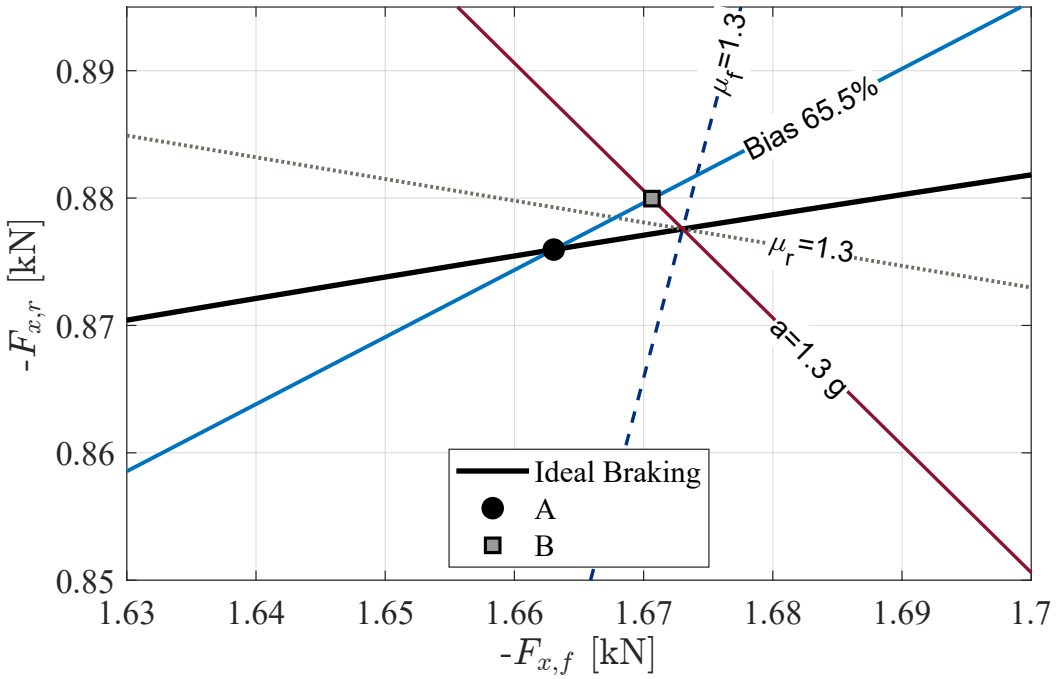

Figure 3.8: Actual braking conditions

The friction coefficient iso-lines at the front and rear create four different quadrants,

each indicating a different tire operating condition:

1. **Top-left, rear tire slip zone:** The Rear tires saturate and lock first, braking more than required. This condition under exploits the front wheel's braking capacity and may lead to instability as described in the beginning of the section, making this zone unfavorable.

2. **Top-right, both tire slip zone:** Both tires are saturated and locked, making the vehicle very unstable. This condition will tend to occur while attempting high deceleration when the tires are not able to achieve the required friction coefficient.

3. **Bottom-left, no slip:** All tires are under exploited, while no slip occurs, the braking performance is suboptimal.

4. **Bottom-right, front tire slip zone:** The front tires are locked, opposite to the top-left zone, since $\mu_f > \mu_r$, this condition is the most favorable when an axle is forced to lock in terms of stability.

As seen in Figure 3.8, attempting to decelerate with the current brake bias setup will coincide with the deceleration curve in the top-left quadrant (point A), causing the rear tires to lock up first and thus limiting the maximum deceleration to point B without locking any tires.

3.2.3 Braking Setup

As ideal braking is hard to achieve without risking rear lock, a system that prioritizes front locking is generally used, giving more room for the front to saturate before the rear gets close to locking conditions. Having said that, to properly dimension the system and test its performance, three different scenarios will be analyzed in order to evaluate the outcome. A MATLAB script has been prepared to output the ideal braking bias by ensuring front lock condition is met through the different proposed friction coefficient ranges. Vertical and longitudinal forces will be recorded, as they will serve to dimension the systems in the next section.

Wet Track Conditions:

In this first scenario, damp and wet track conditions are characterized by very low friction coefficients between tire and ground. While rain tires can be fitted with tread patterns that may improve water evacuation and increase the contact patch, the friction coefficient will still be relatively low. Taking as ranges of $\mu = 0.4 - 0.9$, the best brake bias that can be considered has to ensure no rear lock in any condition, thus favoring front saturation.

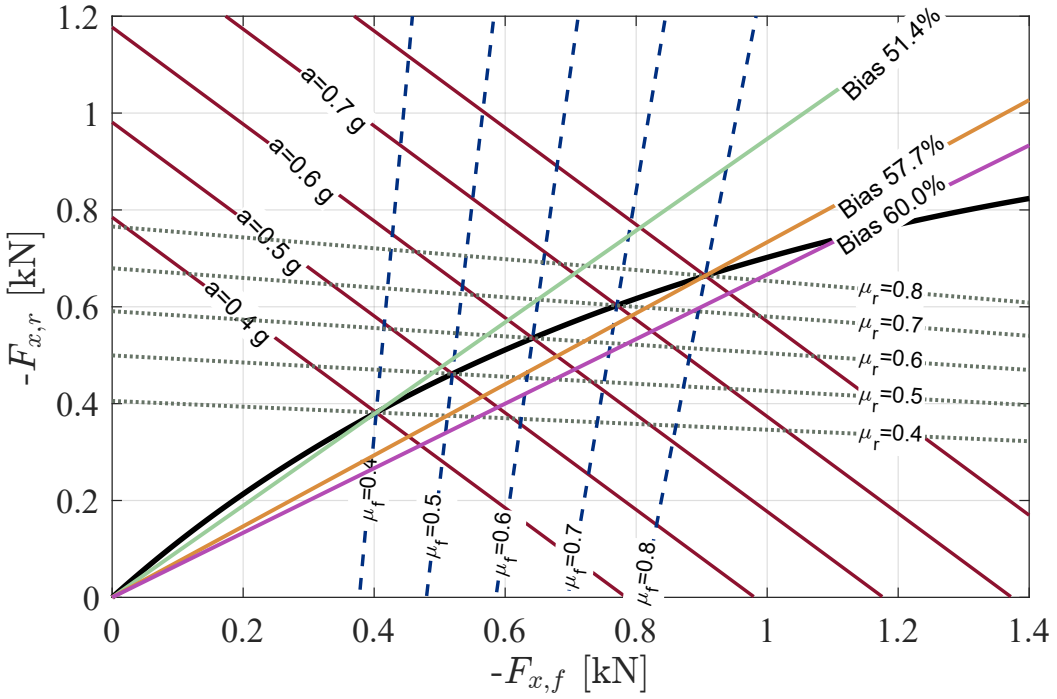

Figure 3.9: Wet braking Conditions

The optimal bias for the lowest and highest friction coefficients in these conditions are respectively 51.4% and 57.7%. As seen in Figure 3.9, the lower brake bias would only ensure good conditions for its own friction coefficient but resulting in rear locking for all other conditions. In contrast, the higher brake bias would ensure front locking for all other scenarios without straying too far from the ideal parabola. An intermediate solution can be employed that would approximate the curve more accurately but as safety is prioritized, rear locking will strictly be avoided in any possible case, sacrificing efficiency and performance for safety.

A brake bias of 60% is finally chosen in order to guarantee the front locking even with the highest friction coefficient.

To better understand its performance, two KPIs are considered:

1. **Braking Efficiency η_b**:

$$\eta_b(\mu) = \frac{a_{\text{actual}}}{\mu_x\, g} \tag{3.9}$$

   the fraction of the tire-limited deceleration μg that is actually achieved with a fixed bias.

2. **Stopping–distance penalty Δs**:

$$\Delta s(\mu) = \frac{V_0^2}{2\, a_{\text{actual}}} - \frac{V_0^2}{2\, \mu_x\, g} \tag{3.10}$$

   Indicates the extra meters for stopping required with the fixed bias setup, allowing us to ensure the prototype passes technical brake inspections.

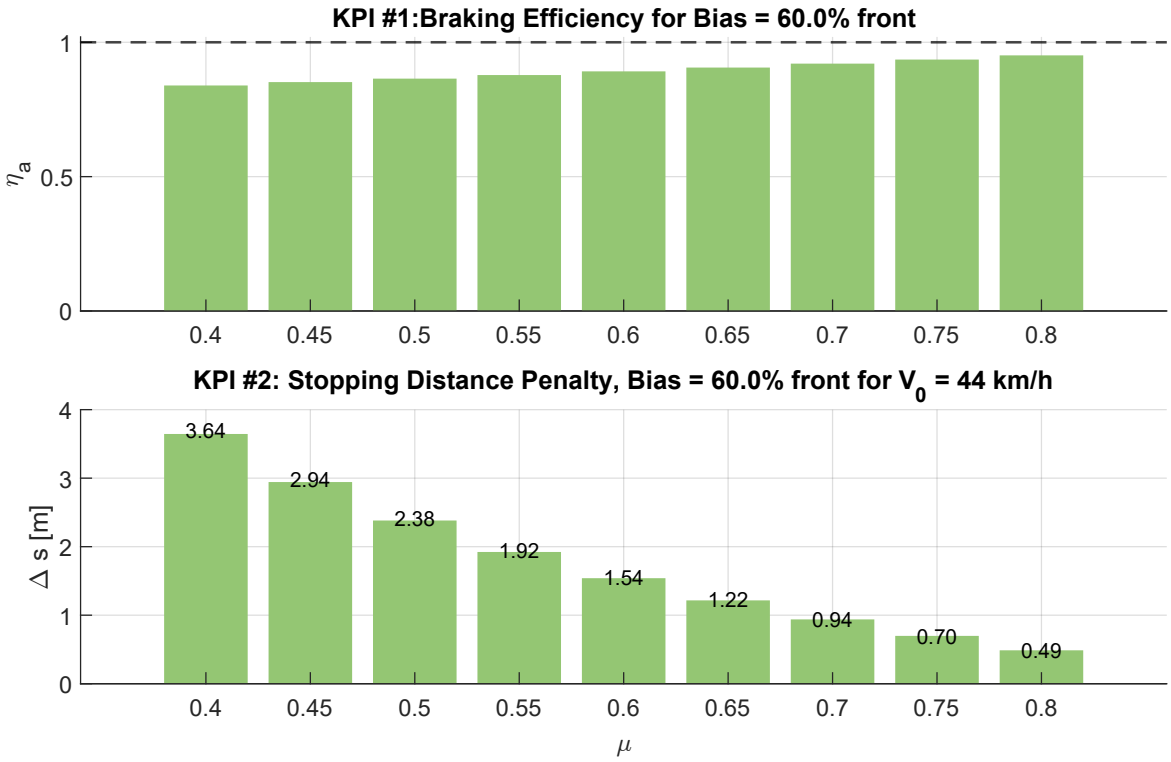

Figure 3.10: KPI values for wet braking, setup 1

Starting with the braking efficiency, the mean efficiency is 89.3% with a minimum of 83.9%, at $\mu_x = 0.4$. This performance can be acceptable in wet conditions, as the setup prioritizes stability over efficiency. Regarding stopping distance, as rule IN11.2.4 indicates that the stopping distance will be evaluated by judges depending on track conditions and thus, for this specific scenario the KPI cannot be properly judged, as no data on distance have been found, but starting from $V_0 = 44km/h$, the maximum experienced brake penalty is 3.64 m at the lowest friction coefficient, resulting in a total stopping distance of 19.3 m.

In order to better understand the losses caused by prioritizing safety in those conditions, a brake bias of 54.5% can be considered which would theoretically better approximate the ideal braking curve and thus reduce efficiency losses or braking distance penalty as seen in the following KPI values.

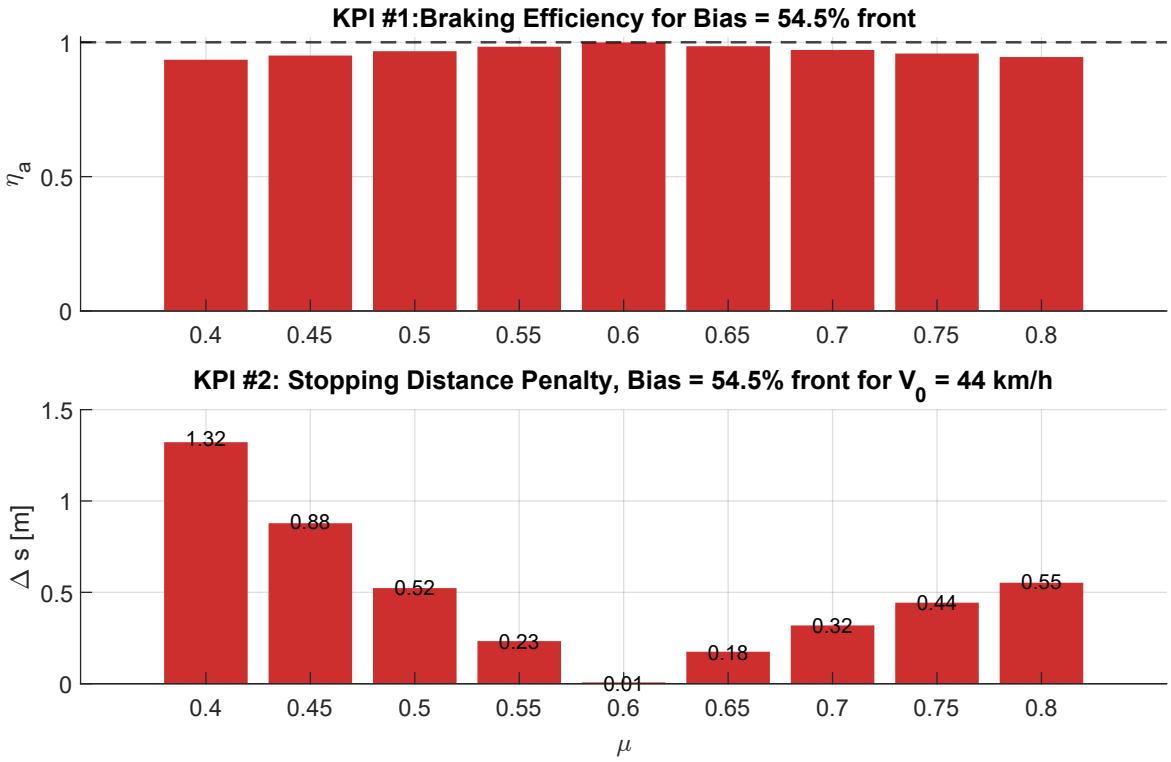

Figure 3.11: KPI values under wet braking, setup 2

The second setup shows a much higher efficiency all over the range, with a much smaller stopping distance in comparison to the first setup. While this may seem like the better option, the risk of rear lock likelihood is not shown in these plots and thus to properly compare the two setups, it is better to refer to the plot of Figure 3.12.

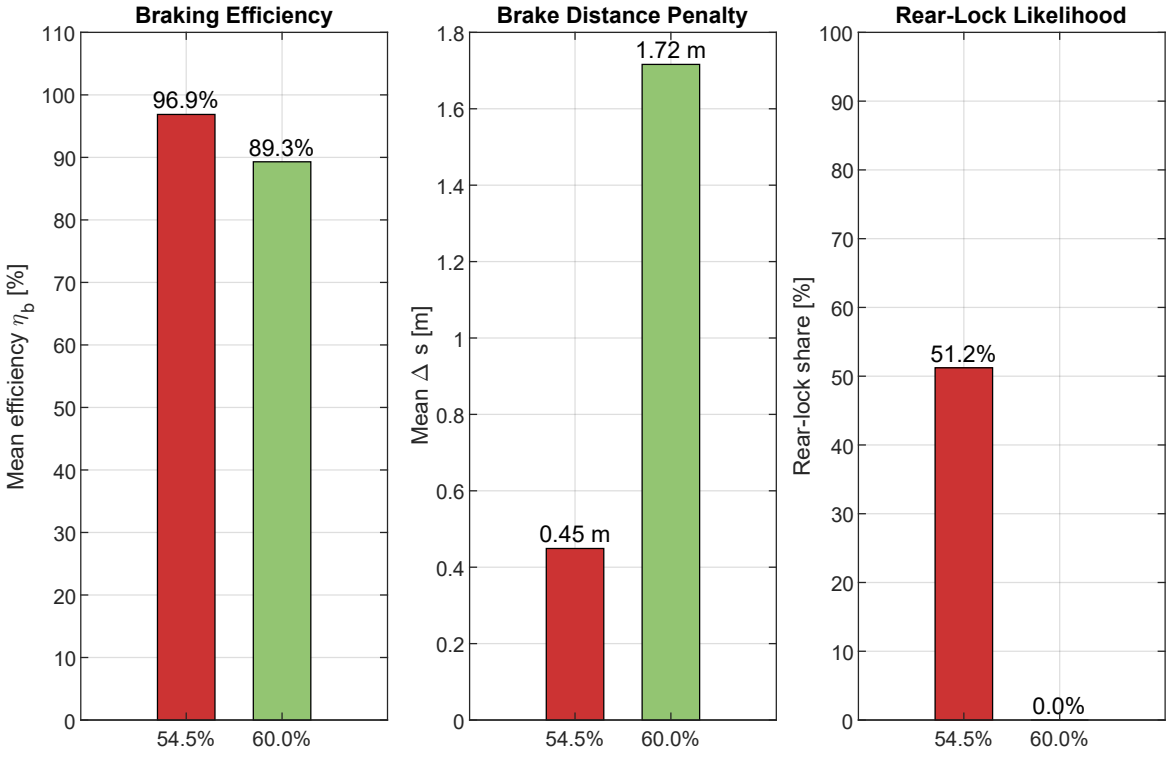

Figure 3.12: KPI comparison for wet braking setups

As seen above, the main benefit of reducing the brake bias comes with a much shorter mean stopping distance, about 3.8 times lower over the entire friction range. While this benefit may compel us to use the second setup, it is worth remembering that in wet conditions the most important aspect is going to be safety, where the increase of rear-lock likelihood to more than 50% for the second setup makes it unsafe as the vehicle may end up locking the rear and increase the risk of losing stability, especially in autonomous mode.

Considering all the above, it has been decided to adopt a front bias setup of 60%, prioritizing safety over performance in wet conditions with the main parameters reported in Table 3.4.

Parameter	**Symbol**	**Value**	**Unit**
Mean Front Braking Load	$F_{x,f}$	706	N
Mean Rear Braking Load	$F_{x,r}$	471	N
Mean braking efficiency	$\bar{\eta}_b$	0.893	–
Lowest braking efficiency	$\eta_{b,\min}$	0.839	–
Mean stopping distance penalty	$\overline{\Delta s}$	1.76	m
Maximum stopping distance penalty	$\Delta s_{\max}$	3.64	m

Table 3.4: Braking performance under wet conditions, front bias ($X_{\text{brake,f}} = 60\%$).

Normal Braking Conditions:

By considering the range of $\mu_x = 1 - 1.8$, we can analyze the behavior of the system for different brake bias settings.

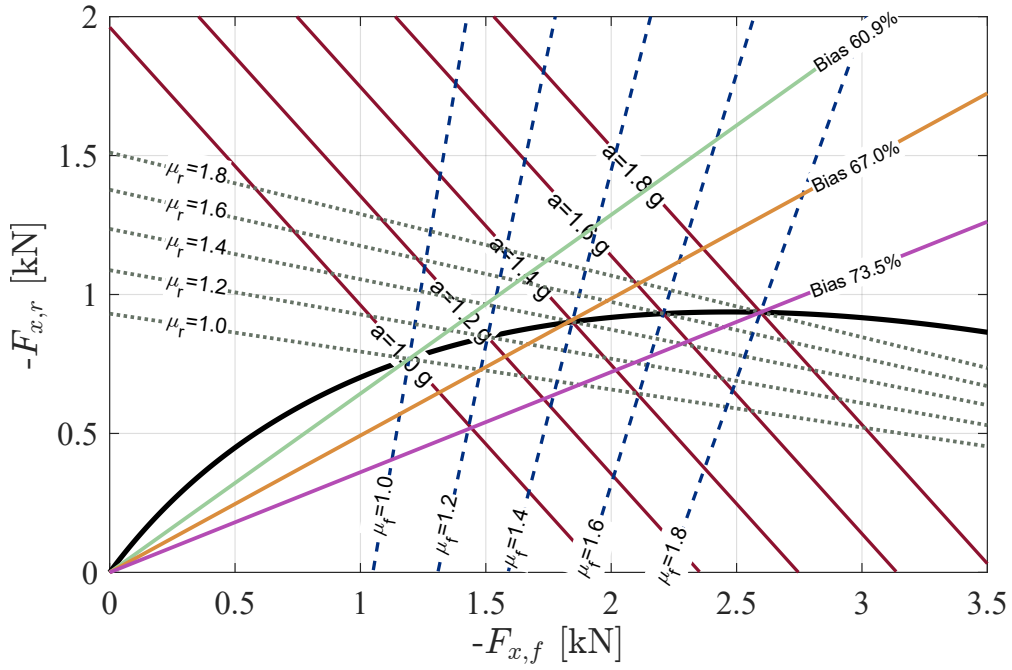

Figure 3.13: Braking in Normal Conditions

As the range here is much bigger, approximating with a too high front bias will result in low efficiency especially at low friction coefficients. By using a bias of 73.5% corresponding to no rear-lock condition even for the highest friction coefficient:

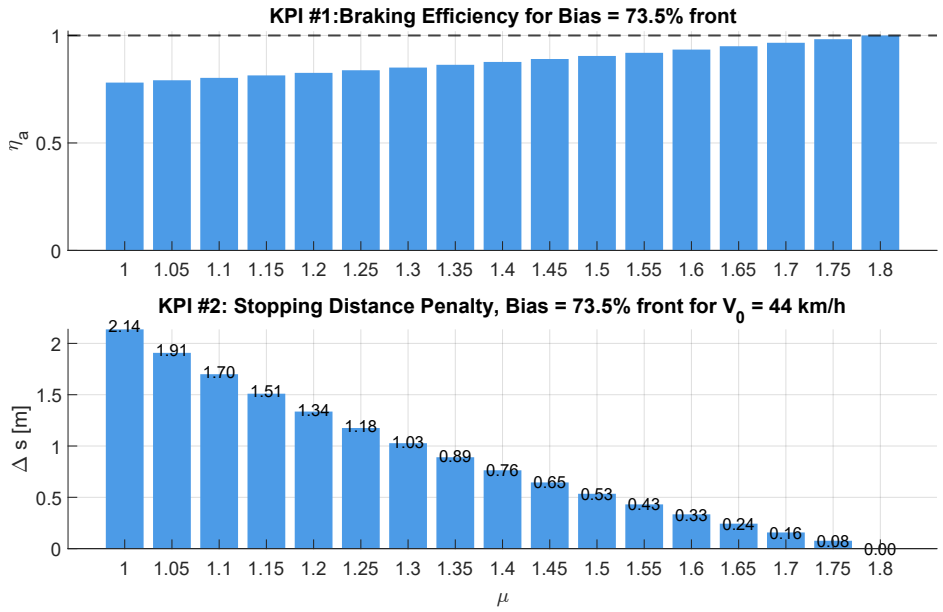

Figure 3.14: KPI values under normal braking, setup 1

While this option ensures no rear wheel lock, from a performance point of view the mean efficiency suffers a drop with $\eta_b = 0.881$ and a maximum stopping distance penalty of 2.137 m for the lowest friction coefficient. Instead, a secondary setup may be considered where performance can be increased even if rear lock braking may occur by approximating closely the optimal braking line with a brake bias of 67%:

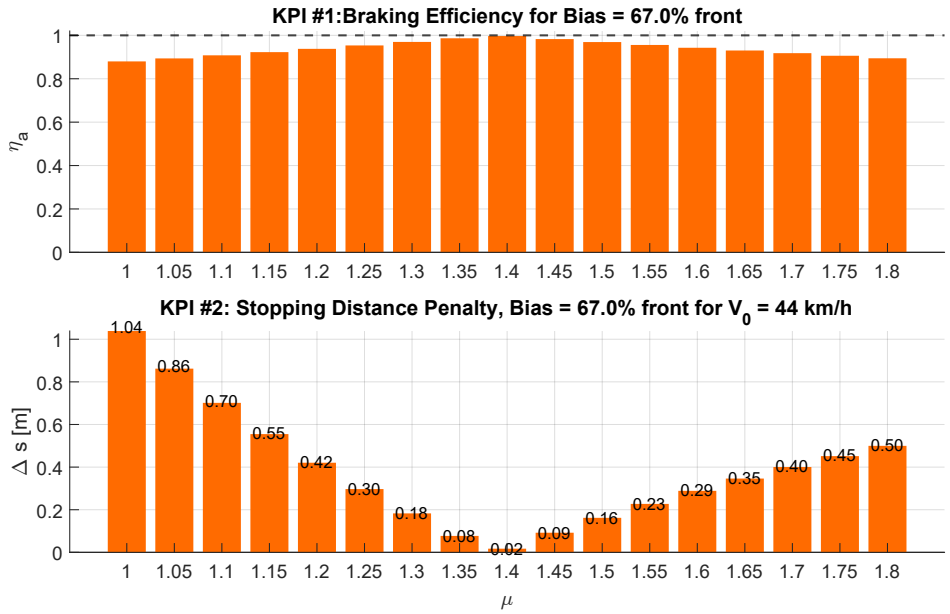

Figure 3.15: KPI values under normal braking, setup 2

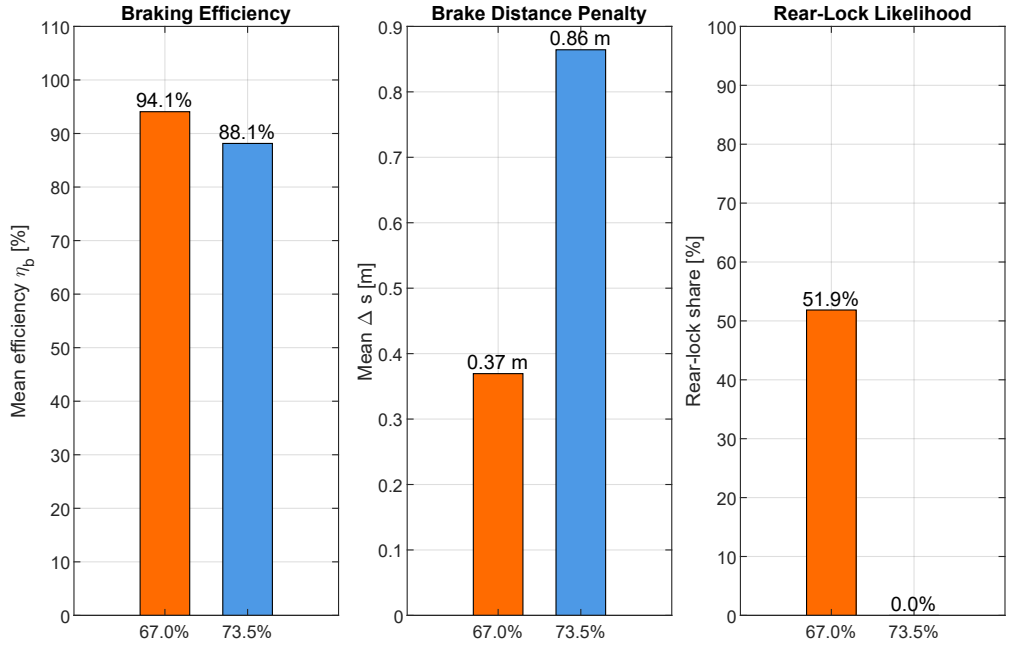

Figure 3.16: KPI comparison for normal braking setups

The second setup would decrease the mean brake distance penalty by about 57%, and considering most of rear locking phenomena would occur only at high deceleration targets, the risk of locking should be accepted considering the performance gain.

Parameter	**Symbol**	**Value**	**Unit**
Mean Front Braking Load	$F_{x,f}$	1840.4	N
Mean Rear Braking Load	$F_{x,r}$	906.4	N
Mean braking efficiency	$\bar{\eta}_b$	0.941	–
Lowest braking efficiency	$\eta_{b,\min}$	0.880	–
Mean stopping distance penalty	$\overline{\Delta s}$	0.369	m
Maximum stopping distance penalty	$\Delta s_{\max}$	1.039	m

Table 3.5: Braking performance under normal conditions ($X_{\text{brake,f}} = 69\%$).

3.3 Emergency Braking System

In this section, using the values of the different setups, dimensions for the autonomous systems' actuators will be estimated, taking into consideration the mean required forces in each braking condition in order to guarantee no wheel locking under most conditions.

3.3.1 Force Estimation

As described in Section 3.1, the pedal box actuation requires pneumatic pistons, similar to the ones used in the SCD25 solution. The current actuators will be oversized for this application and need to be reduced. To properly choose the dimension of the piston,

it is best to start dimensioning from the required braking load taken from normal conditions. Setting the ideal deceleration target of $a = 1.4\ g$ and the corresponding ideal brake bias of 67%.

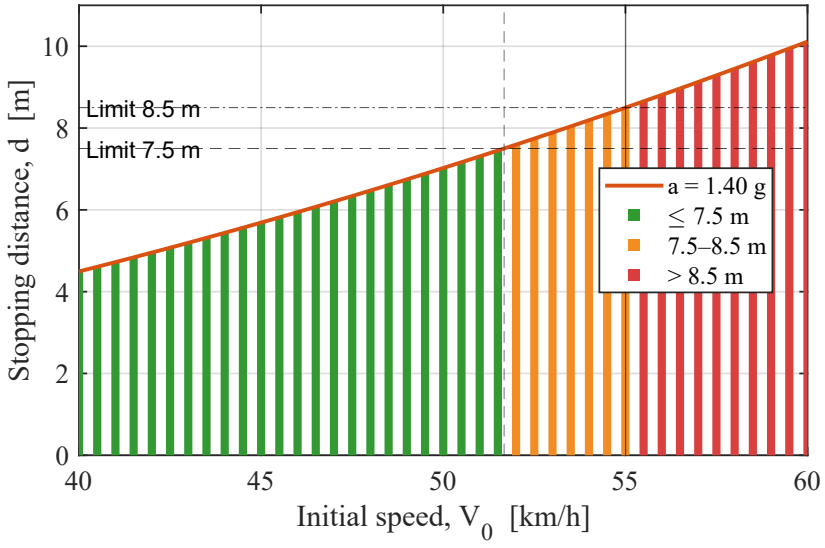

Figure 3.17: Speed Overshoots and Stopping Distance for constant deceleration

As seem in Figure 3.17, with the set deceleration target, the vehicle is allowed to overshoot the minimum velocity requirement up to about 55 km/h but as mentioned earlier, the relationship between stopping distance and speed is quadratic, and so the maximum permissible overshoot should stay below 50 km/h in order to guarantee meeting the brake test requirements. Having established that the set load transfer guarantees a good performance, the actuator dimensioning will be conducted as follows:

Starting from the longitudinal brake forces obtained for each axle in table 3.5 that correspond to the chosen friction coefficient and by considering the wheel's moment of inertia $J_w = 0.27\ kgm^2$ as provided by the unsprung mass division, the torque demand per axle can be calculated as:

$$T_f = F_{x,f}\, r_w + \frac{2J_w\, a_x}{r_w} = 468 \text{ Nm} \qquad T_r = F_{x,r}\, r_w + \frac{2J_w\, a_x}{r_w} = 244 \text{ Nm} \quad (3.11)$$

Subsequently, by using the torque demand on each axle, the average friction between pads and disk $\mu_{pad} = 0.4$ seen in Section 2.2.2 and the define disc effective radii R_{disc} the required clamping force for each axle is:

$$\begin{aligned} T_f &= \mu_{\text{pad}}\, F_{\text{clamp},f}\, R_{\text{disk},f} \quad \Rightarrow \quad F_{\text{clamp},f} = \frac{T_f}{\mu_{\text{pad}}\, R_{\text{disk},f}} = 12462.5 \text{ N} \\ T_r &= \mu_{\text{pad}}\, F_{\text{clamp},r}\, R_{\text{disk},r} \quad \Rightarrow \quad F_{\text{clamp},r} = \frac{T_r}{\mu_{\text{pad}}\, R_{\text{disk},r}} = 7379.2 \text{ N} \end{aligned} \quad (3.12)$$

Using the clamping force and the total piston area per axle ($A_{\text{cal,tot}}$), the hydraulic line pressure needed on each axle is obtained:

$$A_{\text{cal,p}} = \pi\left(\frac{D_{\text{cal,p}}}{2}\right)^2, \qquad A_{\text{cal,tot,f}} = n_{\text{p,f}}\, A_{\text{cal,p}}, \qquad A_{\text{cal,tot,r}} = n_{\text{p,r}}\, A_{\text{cal,p}}$$

$$P_f \;=\; \frac{F_{\text{clamp},f}}{A_{\text{cal,tot,f}}} = 34.44 \text{ bar} \qquad P_r \;=\; \frac{F_{\text{clamp},r}}{A_{\text{cal,tot,r}}} = 40.78 \text{ bar} \tag{3.13}$$

$$F_{\text{MC},f} \;=\; P_f\, A_{\text{MC,f}} \;=\; 824.5 \text{ N} \qquad F_{\text{MC},r} \;=\; P_r\, A_{\text{MC,r}} \;=\; 819.9 \text{ N} \tag{3.14}$$

$$\boxed{F_{\text{MC,tot}} = F_{\text{MC},f} + F_{\text{MC},r} = 1644.4 \text{ N}}$$

3.3.2 Stroke Estimation

Now that the required total force on the master cylinders has been defined, the pneumatic actuators can be chosen from the Festo catalog of the ADN-S series [2]. Considering the values from Table 2.7, the maximum expected stroke of the front master cylinder is expected to be around $s_{req,f} = 12.08\ mm$, but in order to remain conservative when choosing the actuator stroke, we account for additional pad wear, trapped air in the brake lines or possible knock back, the model can be better approximated by including a compliance volume that includes brake-fluid compressibility (DOT 4) and a lumped hose compliance term.

Let β be the isothermal bulk modulus of the fluid and ΔP the design hydraulic pressure. For a circuit with total liquid volume V_{liq} the fluid compressibility adds

$$\Delta V_{\text{fluid}} \;=\; V_{\text{liq}}\, \frac{\Delta P}{\beta}\,,$$

while hose expansion can be represented by a linear compliance κ_{lines}, giving

$$\Delta V_{\text{lines}} \;=\; \kappa_{\text{lines}}\, \Delta P\,.$$

Thus the conservative stroke estimate for the front master cylinder becomes

$$s_{f,\text{cons}} \;=\; \left(\underbrace{s_{req,f}}_{\text{expected stroke}} + \underbrace{\frac{\Delta V_{\text{fluid}} + \Delta V_{\text{lines}}}{A_{\text{MC},f}}}_{\text{compliance}} \right)$$

For DOT 4 brake fluid, the isothermal modulus is listed near $\beta \simeq 2.179\,\text{GPa}$ at atmospheric conditions [27]. On the other hand, hose volumetric expansion is regulated and measured under FMVSS 106 (cc/ft at specified pressures) [28].

Taking $\Delta P = 50$ bar, as the upper limit for the system, $V_{\text{liq}} = 25{,}000$ mm^3, and a lumped hose/caliper compliance $\kappa_{\text{lines}} = 1.5$ mm^3/bar:

$$\Delta V_{\text{fluid}} \approx 57.4 \text{ mm}^3, \qquad \Delta V_{\text{lines}} \approx 75 \text{ mm}^3.$$

Therefore,

$$s_{f,\text{cons}} = 12.63 \text{ mm}$$

which will be used as the maximum master cylinder stroke for the EBS calculation.

By introducing a pedal ratio for the actuator similar to the pedal ratio for the driver, the force requirement to compress the master cylinders $F_{\text{MC,tot}} = 1644.4\ N$ can be

greatly reduced and thus reducing the dimensions and most importantly the weight of the actuators. This reduction in force comes at the cost of a longer stroke for the actuator, which can be determined by multiplying $s_{\text{f,cons}}$ by the actuator pedal ratio PR_a. To determine the force generated by the actuators, the supplied pressure from the compressed gas system of section 2.4 must be established, based on Section T9 of the rule book, the maximum output pressure from the compressed gas system may not exceed 10 bar, and in order to keep some additional force in reserve which may be needed when high deceleration is required or simply the vehicle overcomes the set weight, the supplied pressure that will be used will be lowered to $p_s = 9$ bar.

Figure 3.18: ADN-S-25-35-I-P

Based on the available bore and stroke sizes of the different actuators from the ADN-S series [2], which allows the actuator to work in retraction as needed, we can estimate the theoretical force generated using:

$$F_{\text{actuator,ideal}} = p_s \left(A_{\text{piston}} - A_{\text{rod}}\right) = p_s \left(\frac{\pi D_{\text{bore}}^2}{4} - \frac{\pi D_{\text{rod}}^2}{4}\right) \tag{3.15}$$

where rod refers to the rod of the piston which essentially reduces the effective area during extension. While Festo indicates the theoretical force on their website which corresponds to Equation 3.15, additional force is required to overcome friction losses inside the master cylinder which are generally about $5 - 10\%$ for an actuator of this size from different sources [29]. Assuming worst case value of $\eta_{\text{fric}} = 0.9$ the delivered force is then:

$$F_{\text{act}} = \eta_{\text{fric}} F_{\text{actuator,ideal}} \tag{3.16}$$

3.3.3 Actuator Selection

Using the gathered data, the best solution to dimension the actuator is by finding the optimal trade-off between force and stroke requirements for the different actuator bores available. As $F_{\text{MC,tot}}$ is shared among two actuators in parallel, the following plot allows us to see the required force and stroke in function of the pedal ratio:

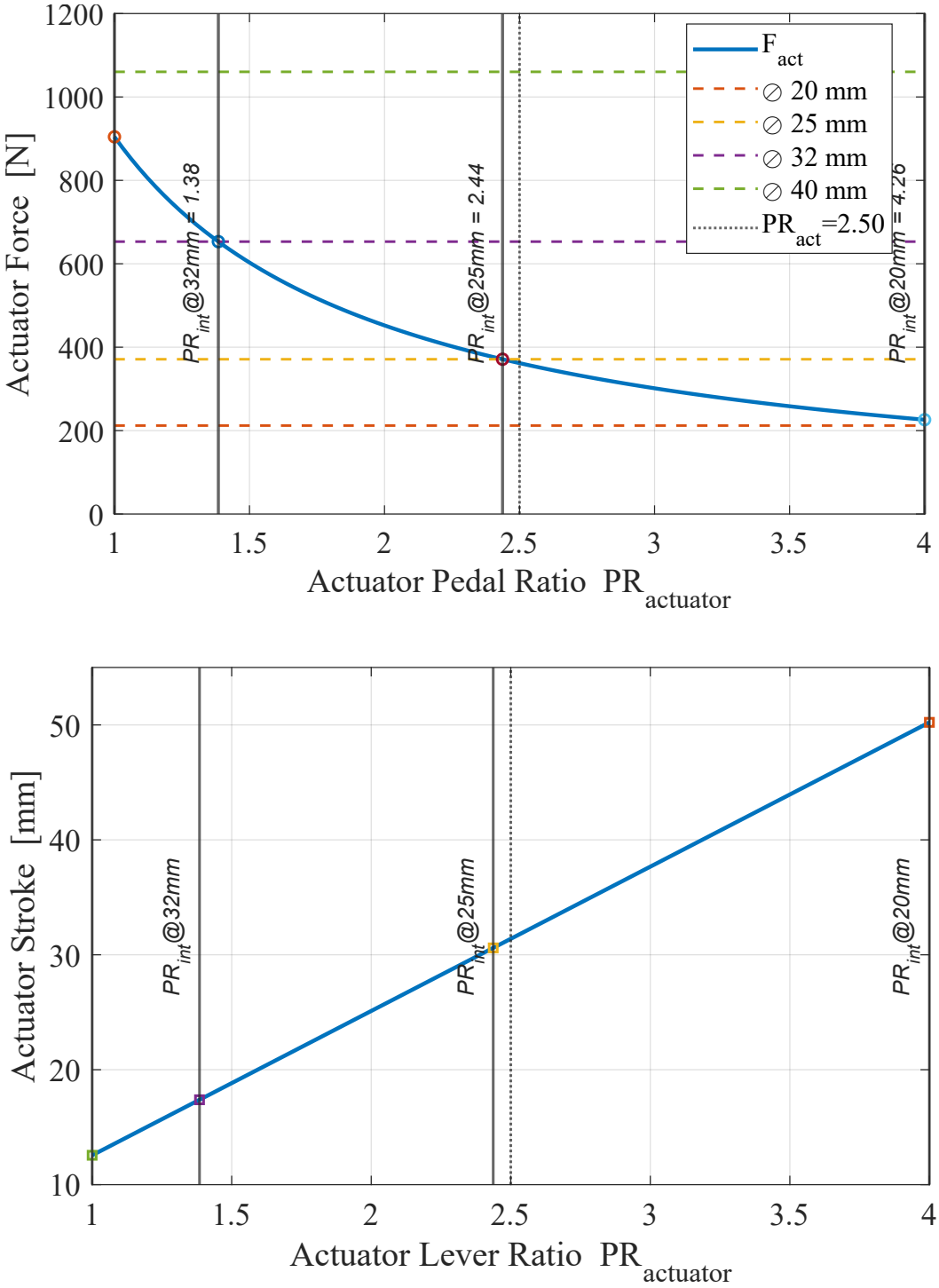

Figure 3.19: Required force (top) and stroke (bottom) in function of actuator ratio

The best compromise between force and stroke found was found at **the actuator ratio of 2.5**, where the force delivered by the actuator is very close to the maximum provided one but still leaves some room for safety. In contrast, the actuator stroke has to be longer than 31.6 mm, making the closest choice a stroke of 35 mm, still leaving some additional room for safety.

The newly introduced ADN-S series are characterized by much smaller dimensions compared to the current ones used, as well as lighter weight. After comparing the two series, there proved to be no downsides to opting for the new smaller series.

Another important feature of the EBS actuator should be the possibility to operate with different forces in order to accommodate different deceleration requirements in different conditions. The delivered piston force can be adjusted by adjusting the delivered pressure. The recommended operating pressure for the ADN-S chosen series is $0.6 - 10$ *bar* [2], but at very low pressures, the cylinder may stall or stick due to seal friction—especially after idle. In addition, very low operating pressure are outside the needed range for such application. In order to avoid any malfunction, the minimum operating pressure is going to be set to 2.5 *bar*.

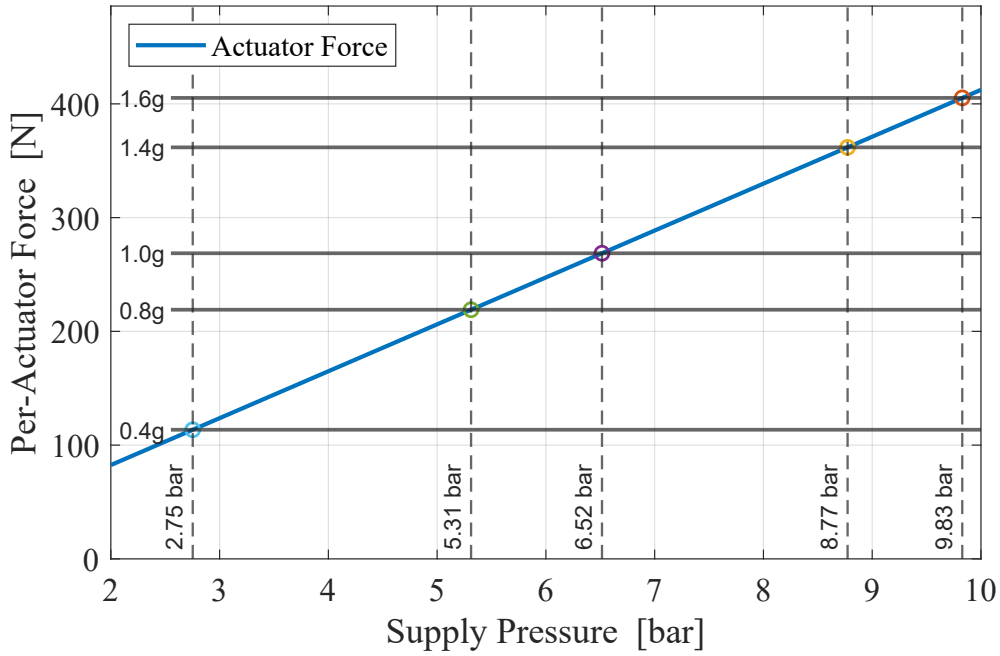

Figure 3.20: Actuator operating range, required forces for different deceleration cases and corresponding needed supply pressure.

All in all, the EBS chosen actuator prove to be able to work in a very wide range depending on the supplied pressure that can easily be adjusted. Thanks to the chosen actuator pedal ratio, the force needed from the actuators is greatly reduced, and thus the dimensions of the actuator have been reduced in comparison to the ones of the SCD25 that acted directly on the master cylinders.

Feature	**Value**
Part number	8076351
Model	ADN-S-25-35-I-PPS-A
Stroke	35 mm
Piston diameter	25 mm
Piston rod thread	M6
Moving mass	38 g
Product weight	175 g
Pneumatic connection	M5

Table 3.6: Specifications for ADN-S-25-35-I-PPS-A [2]

3.4 Pedal

Having already deeply analyzed the braking dynamics when sizing the emergency braking system, based on different road conditions and considering different setups, the baseline for the braking system has been established.

3.4.1 Manual Braking Dynamics

When considering the manual operation with a driver inside the cockpit, the same assumptions can be considered with the main difference being the change in total mass of the vehicle and center of height, the total mass can therefore be considered with a driver of 70 kg, bringing the total mass to 270 kg. On the other hand, the center of gravity is raised to $h_d = 0.252\ m$, and with those newly established parameters the required forces for the front and rear during braking become:

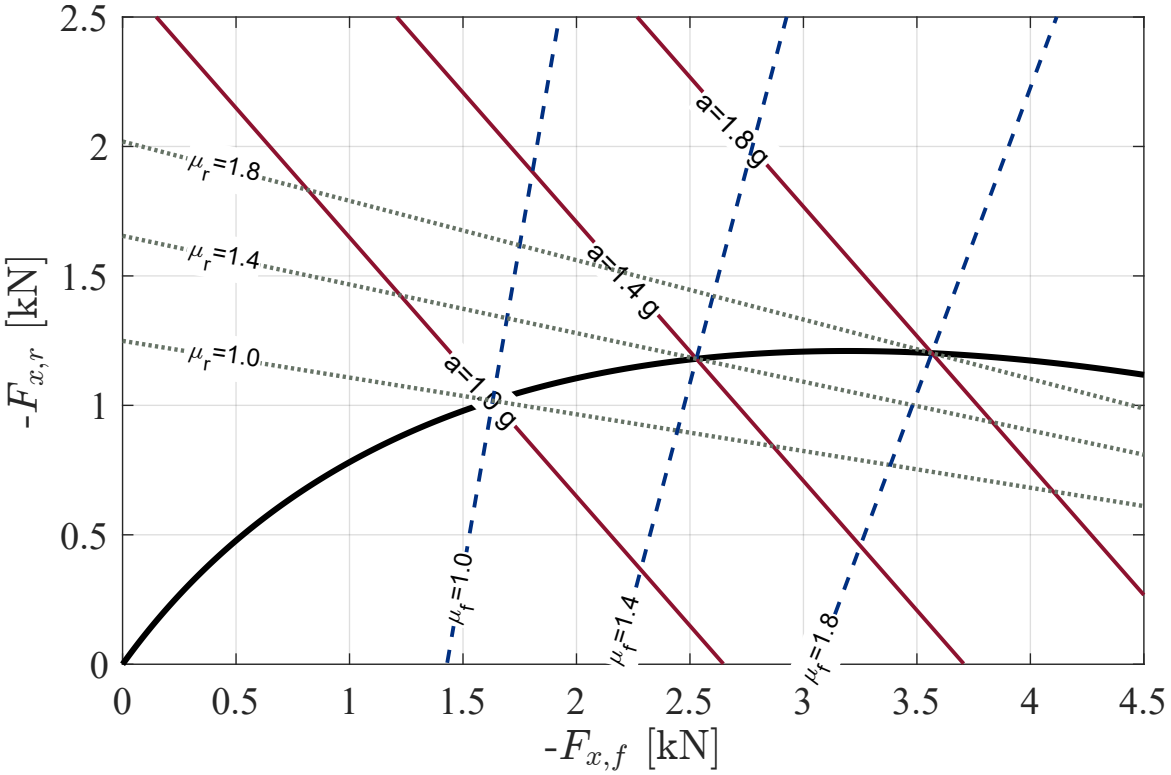

Figure 3.21: Driver ideal braking map

The increase in mass results in an increase in longitudinal braking forces needed to stop the vehicle, considering the brake repartition generally is more subjective when it comes to drivers, due to different braking techniques.

Braking Techniques:

Braking strategy plays a crucial role in both longitudinal deceleration efficiency and corner entry stability. Some of the most adopted techniques include:

- **Threshold braking**, which consists of applying the maximum possible brake force without exceeding the tire's peak friction coefficient, in other words, drivers try to replicate as closely as possible the ideal braking line while avoiding going into lock-up. This can be achieved by reducing brake pedal pressure progressively with the speed decrease.
- **Trail braking,** a more advanced and dynamic approach, where the driver extends the braking phase into the initial portion of corner entry. Instead of completing all deceleration in a straight line, the driver gradually releases brake pressure while simultaneously increasing steering input. This technique intentionally maintains a forward load transfer, increasing the vertical load on the front tires and so increasing front-end grip during turn-in. By doing so, the driver induces a controlled rotation of the vehicle around its vertical axis, improving corner entry.

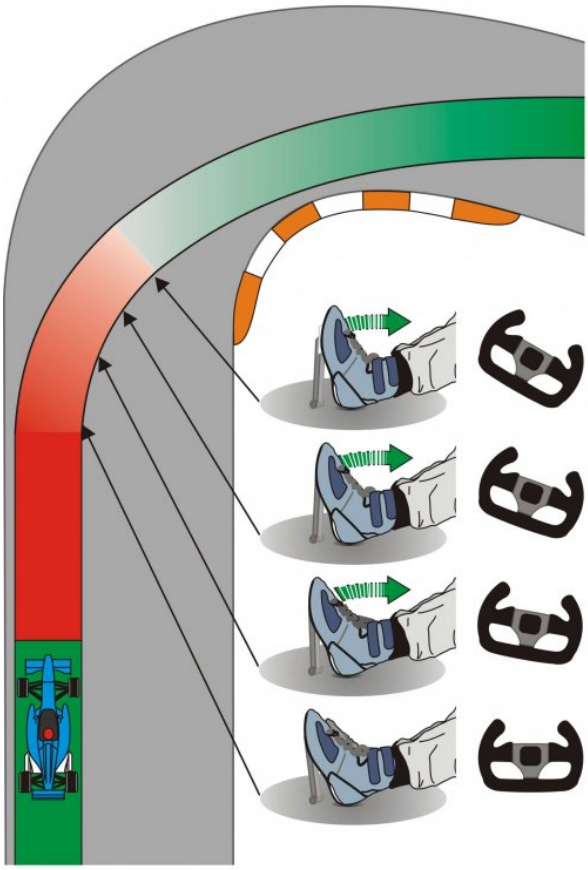

Figure 3.22: Trail Braking

The potential use of different braking techniques, as well as the possibility of adjusting the brake bias directly from inside the cockpit, makes the ideal brake repartition more complex and better adjusted directly on track.

3.4.2 Ergonomics

The main aspect to consider when designing and sizing the pedal is the pedal ratio, which dictates the force and travel of the foot. As already introduced in Section 2.2.4,

a trade-off has to be considered when choosing either a high or low pedal ratio with the general range for Formula Student prototypes being between 3 and 6. To better define the possible design ranges, the pedal box must be able to fulfill two basic requirements:

- Verify that the pedal allows the driver to generate the maximum braking force needed in all possible conditions.
- Allow the driver to operate the brakes for extended periods of time without sustaining fatigue.

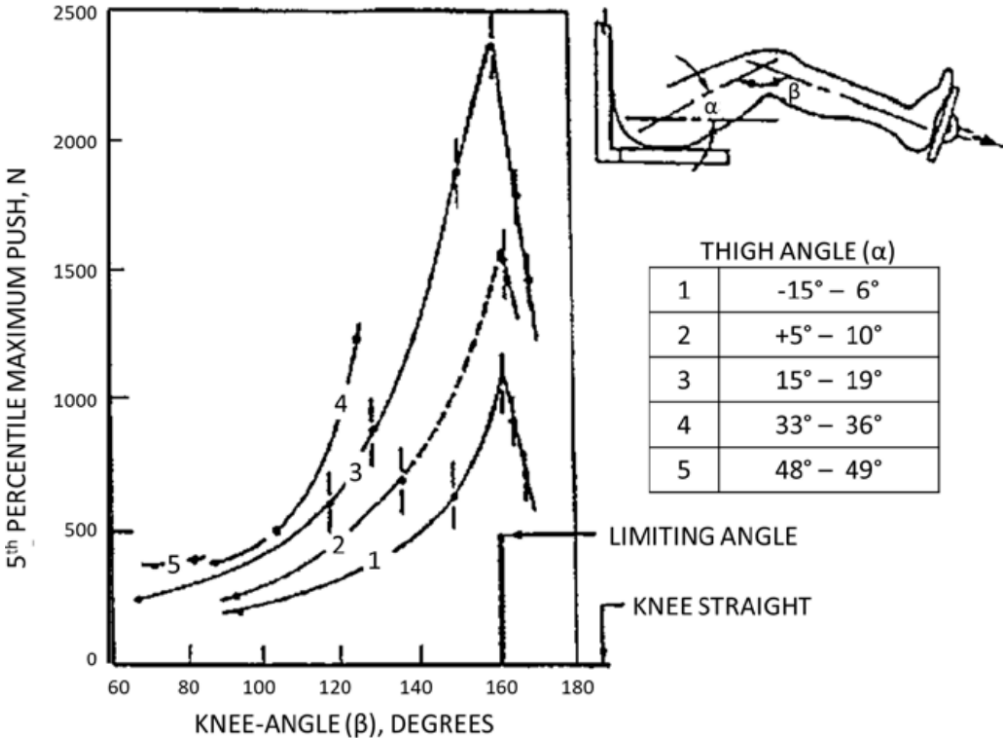

Figure 3.23: Leg strength at various knee and thigh angles (5th percentile male) [11]

Regarding the first point, the driver must be capable of locking all wheels as specified in IN11.2.3. To guarantee this, we can refer to MIL-STD-1472G [11], the design criteria standard which give an approximate leg strength at various knee and thigh angles considering the 5th percentile male, ensuring that all drivers are able to operate the brakes, including drivers with lower physical capabilities. Taking again as reference the SCD25, data found throughout the seasons showed typical values for most driver angles are about $\alpha = 25°$ for the thigh angle and $\beta = 146°$ for the knee angle. As the thigh angle falls between the 3rd and 4th curve, a linear interpolation is conducted to get the maximum push force:

$$F(\alpha, \beta) = F_3(\beta) + \frac{(\alpha - \alpha_3)}{(\alpha_4 - \alpha_3)} \left[F_4(\beta) - F_3(\beta)\right] \tag{3.17}$$

Taking the midpoint values for curves 3 and 4, respectively: $\alpha_3 \approx 17°$ and $\alpha_4 \approx 34.5°$. From the chart at $\beta = 146°$, the 5th-percentile push is approximately:

$$F_3(\beta{=}146°) \approx 1500 \text{ N}, \qquad F_4(\beta{=}146°) \approx 2100 \text{ N}. \tag{3.18}$$

and thus the maximum push force inside the SCD25 monocoque can be considered to be around:

$$F_{leg,max} \approx 1774 \text{ N}. \tag{3.19}$$

Having established the maximum push force the weakest driver is able to generate on the pedal inside the monocoque, the second step is to determine the maximum braking force needed at the master cylinders under high deceleration requirements, taking as reference a deceleration of $a_x = 2.2\ g$ and by using the Figure 3.21, the front and rear longitudinal braking loads are obtained:

$$F_{x,f,\max} = 4743.5 \text{ N} \quad \text{and} \quad F_{x,r,\max} = 1083.7 \text{ N} \tag{3.20}$$

and by following the exact steps from equations (3.11) to (3.14), the maximum force at the master cylinders is identified as:

$$\boxed{F_{\text{MC},\max} = 3088.7 \text{ N}}$$

Having established the maximum push force that can be generated and the maximum required force at the master cylinder, the pedal ratio bounds can be defined by considering the second requirement to be met for the pedal box design. Designing a pedal box that requires high forces for each brake actuation may result in fatigue, especially in long testing sessions or the endurance event, where cars have to compete over a distance of 22 kilometers, a long distance for typical Formula SAE prototypes.

In order to keep the drivers comfortable, in reference to ergonomics literature, human strength should not be utilized at its limit for control operations (such as braking actuation) as repetitive action close to the maximum voluntary contraction (MVC) may cause fatigue or loss of precision [30]. Law and Avin [30] demonstrate that endurance time decreases exponentially with increasing %MVC, with continuous efforts sustainable only up to approximately 15–20% of MVC. Similarly, Potvin [31] provides a quantitative relationship between duty cycle and maximum acceptable effort, confirming that acceptable intermittent exertions generally lie between 30–50% of the individual's maximum capacity.

Using these criteria for the pedal design, it is possible to distinguish two typical braking conditions that dictate the required pedal effort:

- **Low deceleration levels:** Below 1 g, braking occurs over a longer duration and involves maintaining a steady pedal pressure to stabilize vehicle speed or control entry into a corner. In these cases, the driver holds the pedal in more or less a continuous manner, keeping a sustained muscular contraction for several seconds. Therefore, the pedal force has to stay relatively low to avoid excessive fatigue and preserve precision control for long events, and thus the tolerable pedal effort is defined as 15–20% of the MVC.

- **High deceleration levels:** Above 1 g, the braking action is more dynamic and intermittent. The push force is generally shorter and sharper such as end of straights or emergency stops. The driver actuates with higher instantaneous forces but for a much shorter duration, allowing him to operate in the range of 20–50% of the MVC without experiencing discomfort.

Having defined all the operating ranges based on the required effort, the required force for various deceleration cases are plotted for different pedal ratios.

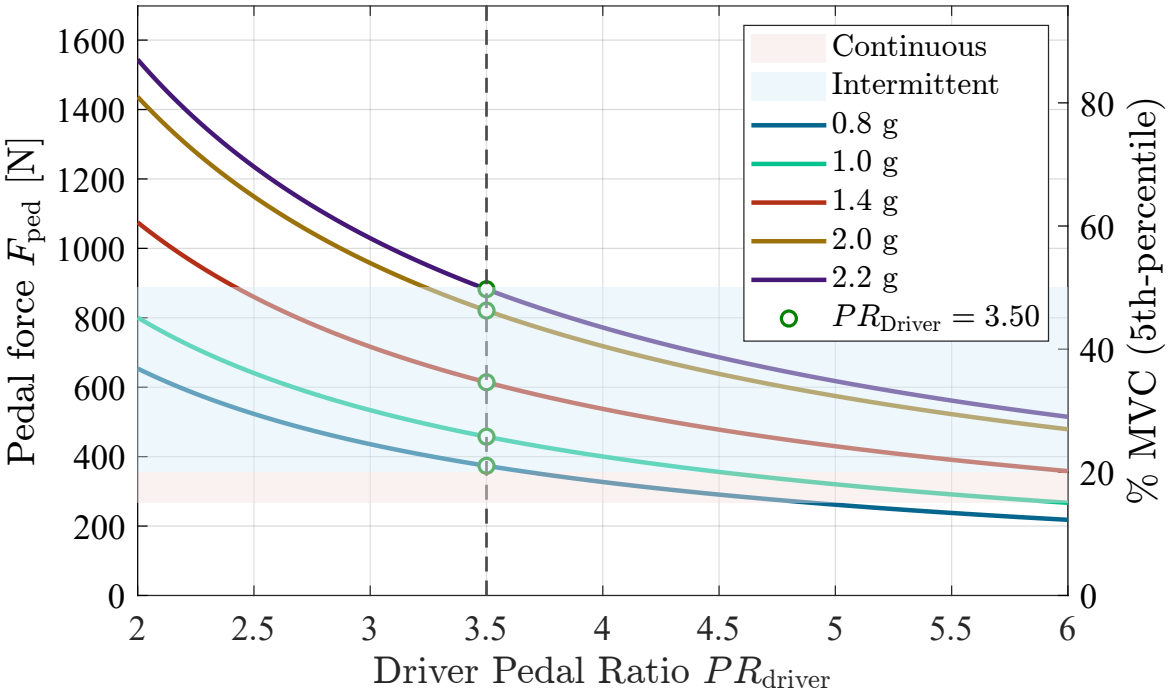

Figure 3.24: Required pedal force for different pedal ratios and decelerations

As shown in Figure 3.24, the minimum selected pedal ratio of $PR_{\text{Driver}} = 3.5$ provides a good trade-off for both performance and comfort across different deceleration cases. By setting the braking demand of 1.0 g slightly above the upper limit of continuous exertion threshold, driver comfort is guaranteed without decreasing too much the force at the pedal allowing drivers to accurately input different loads on the pedal. In the case the pedal ratio becomes too high, it may become too difficult to apply the correct pedal force as a softer pedal makes the feedback and response harder to distinguish. On the other hand, the required forces for higher deceleration demands fall well below the upper limit of intermittent actuation, allowing the drivers to sustain braking action for extended periods of time without experiencing fatigue. In addition, with the selected pedal ratio, it is guaranteed to meet rule IN11.2.3 and lock all four wheels, as the required force of 882 N to decelerate at excessively high values ($a_x = 2.2$ g) is half of the maximum force the weakest driver may be able to generate (about 1774 N).

Chapter 4

Design and Validation

Having established all the necessary parameters, the new system can be designed through an iterative process based on the FEM results.

4.1 Design Constraints and Validation Objectives

4.1.1 Design Constraints

Based on the bench marking already conducted in chapter 2 that allowed us to evaluate performance targets such as the overall weights of the system, in addition to the actuation solution, pedal ratios and actuator choice of chapter 3, the design phase of the pedal box can be conducted. The chassis division of Squadra Corse Driverless was also able to provide an overall volume for the pedal box as a starting point for a new monocoque design adapted to driverless prototype, and with that the design constraints can be divided as follows:

- **Functional Constraints:** The pedal box must allow repeatable and reliable operation of the pedal mechanism under all dynamic conditions. The only allowed movement should be the rotation around the pivot axis, any other motions such as slack or lateral displacements must be eliminated through the use of proper bushing or bearing selection. In addition, the EBS actuator must be able to transfer force linearly without any bending or misalignment from any position. Finally the manual actuation must never be hindered by the autonomous actuators and vice-versa, the system must always guarantee T15.1.4 by ensuring the higher pressure is always applied.

- **Ergonomic Constraints:** The pedal base must allow changes in relative position to accommodate the anthropometric range of different drivers, this can be achieved by different mounting holes or a more complex sliding mechanism. The pedal face must be made of non slip material or covered by such material and provide a comfortable resting surface.

- **Packaging Constraints:** The working volume available for the pedal box is defined by the internal geometry of the monocoque and the surrounding components such as the steering column and accelerator pedal. The envelope provided by the

chassis team constitutes the boundary for the entire assembly, with the length being the most critical parameter, considering the significant additional length required to mount the autonomous actuators behind the pedals with respect to the previous pedal box.

- **Performance Constraints:** Both pedal ratios for the manual operation and the actuators has previously been established, which gives us the target values that have to be respected. In addition, the master cylinders and pneumatic actuators chosen have to be mounted inside the assembly while ensuring proper functioning and mitigating unnecessary loads.

- **Weight Constraints:** The previous braking system was characterized by two separate subsystem, the pedal box that fulfills all manual braking operations and the emergency actuation mechanism. As the new system combines both subsystems, the target weight can be taken from the total weight of the two previous assemblies. An initial weight reduction target, 30% was established relative to the total mass of the former two assemblies subsystems. While this figure is only a preliminary benchmark, the project goal is to exceed this reduction by optimizing the structure through iterative procedures and topology optimization. In addition, material selection will play a critical role for reducing the weight of the new assembly. Most of the components will be manufactured using high-strength ergal aluminum alloy (7075-T6), chosen for excellent strength to weight ratio.

- **Manufacturing and Assembly Constraints:** The design had to be compatible with available manufacturing processes such as CNC machining, laser cutting, and TIG welding. Additionally, ease of assembly and maintenance were taken into consideration, ensuring that the pedal box could be installed and serviced within acceptable time frames.

- **Structural Constraints:** The main requirement for structural strength is dictated by T6.1.9 where the brake pedal and its mounting must be designed to withstand a force of 2 kN. In addition, different load cases based on different operating conditions will be tested on each component to ensure no failure occurs. These load cases will either be conducted on a singular part or on a subassembly depending on the conditions.

With all the constraints defined, the following table establishes concrete numbers based on the different categories.

Category	Parameter	Target Value
Ergonomic	Adjustment range	$\pm$20 mm
Packaging at Base	Volume	180 $\times$ 90 $\times$ 230 mm
Performance	Minimum Manual Pedal Ratio	3.5
	Actuator Pedal Ratio	2.5
Weight	Previous system mass	4259 g
	Target mass (30% reduction)	2981 g

Table 4.1: Summary of main design constraints and target values

4.1.2 Integration and Validation Objectives

Once the design constraints were established, the overall design strategy began with defining the main geometric references by including the pivot axis location and the pedal pad position. by selecting appropriate master cylinder and autonomous actuator mounting points in a way that the over all ratio is equal to the target ratios, the sketching of the parts was conducted on CAD starting with the pedal base a reference.

The validation process includes multiple load cases representing the most critical operational configurations which will be set either on singular component level or sub assembly levels. The analyses are performed to assess stress levels, stiffness or possible deflections in components. All Primary structural components, including pedal arm, plate are modeled using ergal 7075-T6 aluminum alloys with the following characteristics:

Property	**Value**
Density	2810 kg/m^3
Young's Modulus	71.7 GPa
Yield Strength	505 MPa
Ultimate Tensile Strength	572 MPa
Poisson's Ratio	0.33
Shear Modulus	26.9 GPa
Elongation at Break	11%

Table 4.2: Mechanical roperties of Ergal 7075-T6 Aluminum Alloy

4.2 Base

4.2.1 Pedal Ratio

The previous method used to determine the pedal ratio proved to be flawed, as during the movement the pedal ratio is not a constant value but a function of the instantaneous geometry of the system. In particular, the earlier method approximated the pedal travel only with the vertical component, which ignores the arc motion of the pedal pad and does not take into account the changing lever arm or direction of the push rod relative to the master cylinder axis. As a result, the static moment method produces a pedal ratio that has no physical meaning and does not represent the true load transfer through the mechanism.

To obtain a correct pedal ratio, the actual pedal travel has to be evaluated against the compression of the master cylinder for every step.

By modeling the pedal as a rigid body rotating about its pivot, the motion of all relevant points must be described explicitly. For each pedal angle, a rotation matrix

$$R(\theta) = \begin{bmatrix} \cos\theta & -\sin\theta \\ \sin\theta & \cos\theta \end{bmatrix}$$

is applied to the vector from the pivot to the master-cylinder clevis and to the foot pad. This produces the updated positions at each rotation step.

The master-cylinder compression is computed by projecting the change in clevis position onto the master-cylinder axis:

$$\Delta x_{\mathrm{MC}}(i) = \left(\mathbf{x}_0 - \mathbf{x}_i\right) \cdot \hat{\mathbf{u}}_{\mathrm{MC}},$$

where $\mathbf{x}_0$ is the initial clevis position, $\mathbf{x}_i$ is the rotated position, and $\hat{\mathbf{u}}_{\mathrm{MC}}$ is the unit vector along the MC axis.

Similarly, the pedal input displacement is obtained from the vertical displacement of the foot pad:

$$\Delta y_{\mathrm{foot}}(i) = y_{\mathrm{foot},0} - y_{\mathrm{foot},i}.$$

The instantaneous pedal ratio is therefore expressed as

$$\mathrm{PR}(i) = \frac{\Delta y_{\mathrm{foot}}(i)}{\Delta x_{\mathrm{MC}}(i)}.$$

This method captures the nonlinear evolution of the geometry during the rotation, the angle change between MC and the horizontal as well as maps for every displacement the correct pedal ratio.

With the method chosen, using the geometry points established for design, it is possible to obtain the initial and final position of the pedal as well as the respective pedal ratios considering the maximum stroke calculated in section 3.3.2.

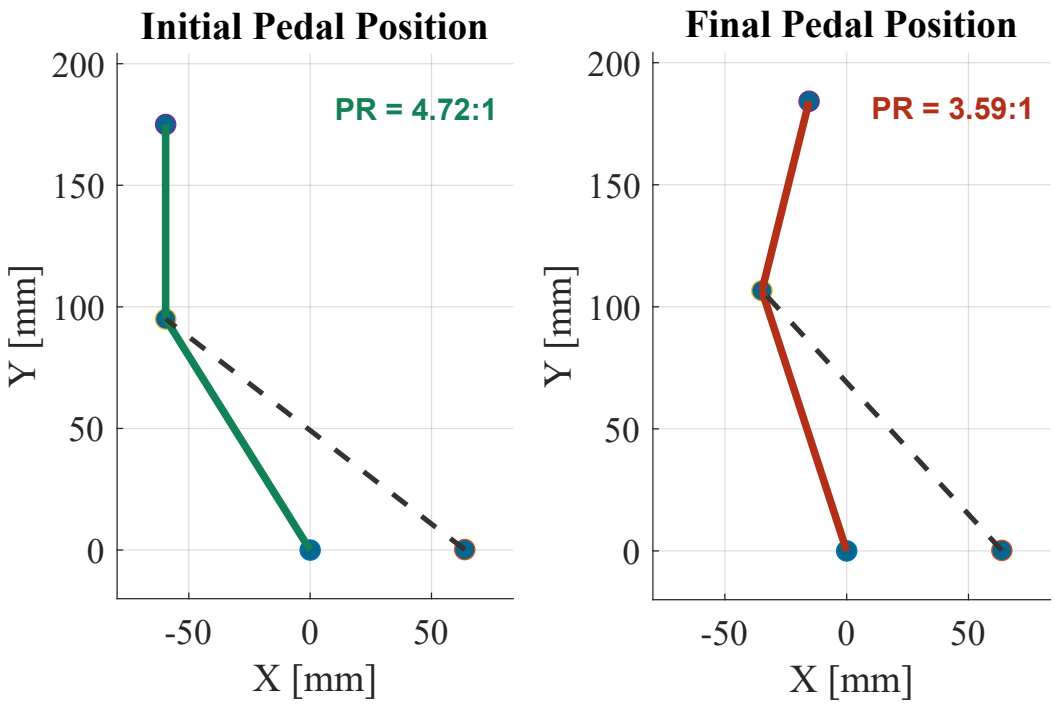

Figure 4.1: Initial and final pedal ratios

The main issue of the previous method of the team can clearly be seen from the big discrepancy between the pedal ratio at the initial and final positions. In fact, relying only on the first number would underestimate the effort the driver has to input by a generous margin, since the effective pedal ratio decreases as the pedal rotates, meaning a higher foot force is required near the end of travel to achieve the same master cylinder force. This would make the driver experience fatigue earlier than expected.

In addition, when analyzing the components from a structural point of view, using the initial, higher pedal ratio also leads to an overestimation of the actual load the supporting parts have to endure. Throughout most of the stroke, the master cylinder behaves as a compliant hydraulic element and does not act as a rigid reaction point. Only when it reaches its maximum usable compression does it constrain the pedal and transmit the full reaction forces into the structure. Therefore, the correct point for evaluating the reaction loads is the instantaneous pedal ratio at maximum master-cylinder compression, which is lower than the initial value. As a result, the forces transmitted through the parts at this condition are lower than previously assumed, allowing better dimensioning and weight reduction.

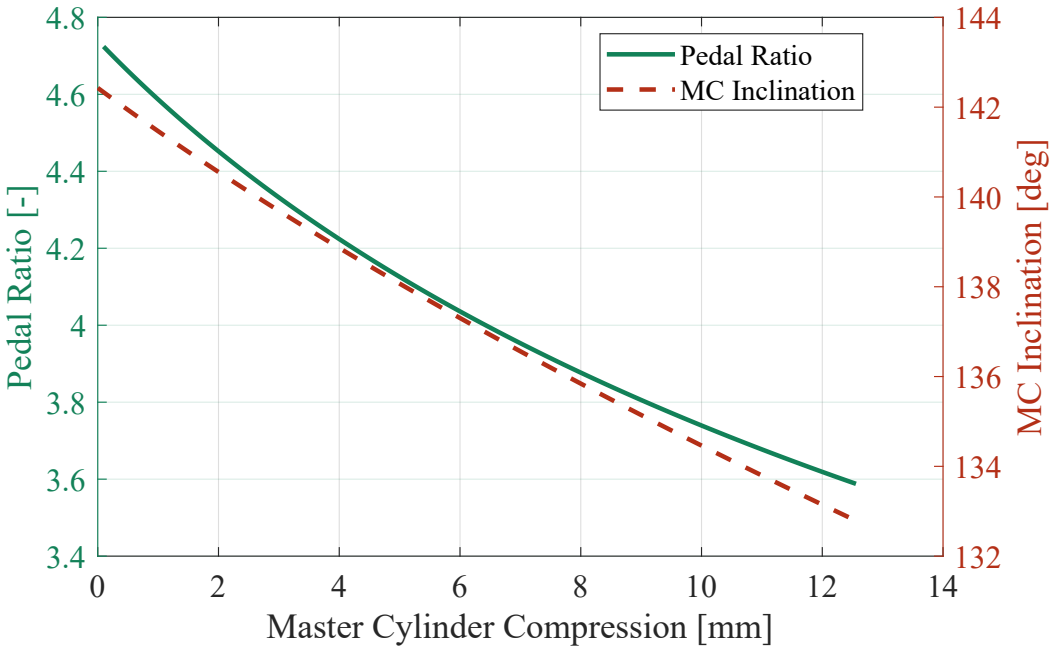

Figure 4.2: PR & MC Inclination vs Compression

Figure 4.2, confirms the nonlinearity of the pedal ratio throughout the travel, with a mean value for the pedal ratio being around **4.1**. Considering the lowest pedal ratio reached at maximum compression of the master cylinder is **3.59**, the target established in section 3.4.1 is clearly met, guaranteeing no early fatigue from the drivers perspective.

4.2.2 Design

The base mounts to the monocoque and helps support all of the components. Figure 4.3 shows the mounting holes on the extremities with different spacing which allow the ergonomic constraint to be verified as each hole, being spaced 10 mm from the next one allow for adjustments accommodating the drivers. the support for the pedal and actuators are all integrated in the base, allowing the numbers of parts and the total weight to be reduced compared to using different supports for the pneumatic actuators.

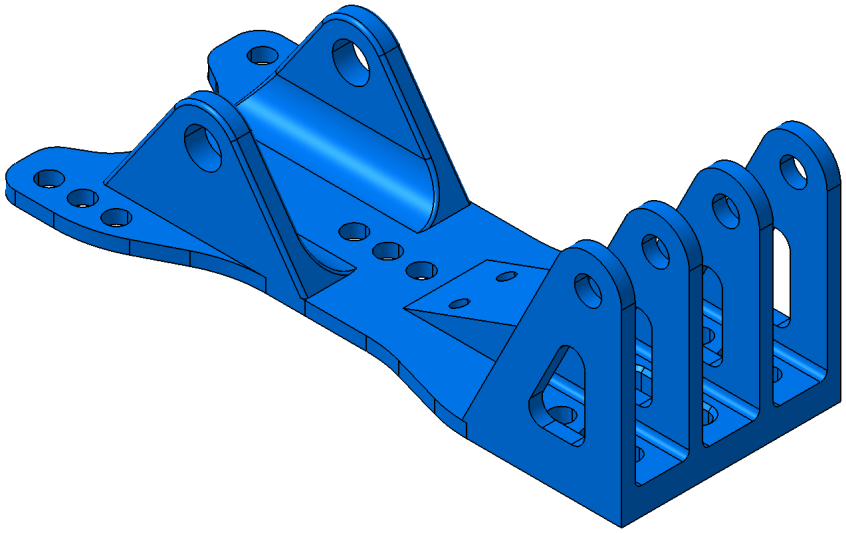

Figure 4.3: Base isometric view

The pedal pivot of figure 4.4 follows a simple design based on the previous pedal box that incorporates the use of both bronze bushings and nylon spacers. As the pedal rotates around the shoulder screw (Type of precise screw used in applications that require a mounting pin, joint, pivot with high shear resistance [32].) the outer bronze bushings help preserve the base surface and hole from wear while providing low friction between screw and base without the need of lubrication. On the inner side of the assembly, a nylon washer is positioned between the pedal arm and the supporting structure. Similar to the outer bushing, low friction sliding is creating between the two surfaces while absorbing any minor misalignment. Nylon also provides small vibration damping which reduces perceived noises. The use of such components help adhere to the functional constraint as the only permitted motion will be around the pivot axis, eliminating any lateral play or resistance from friction.

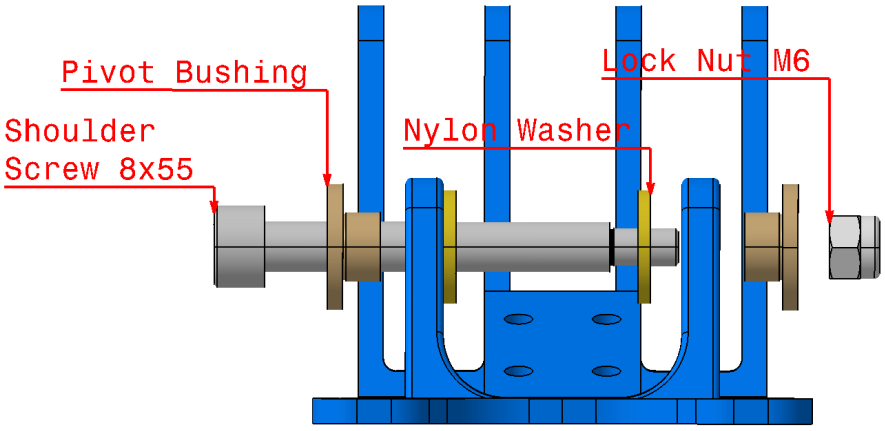

Figure 4.4: Pivot axis components

The second critical aspect of the base is the mounting of the balance bar that, as recommended from the manufacturer must form a perpendicular angle with the master cylinder axis under full compression. While this is not strictly achieved due to the complexity of machining the base and the tight space available for the overall base,

the found solution involves inclining the surface at the steepest possible angle from the horizontal surface, which constitutes an improvement in comparison to the previous pedal box which sits flat. As also set by the manufacturer, the bottom is attached by button head screws EN ISO 7380-1 M4x10. The use of a button head instead of the generic socket cap head allows a shorter head width that would sit inside the base.

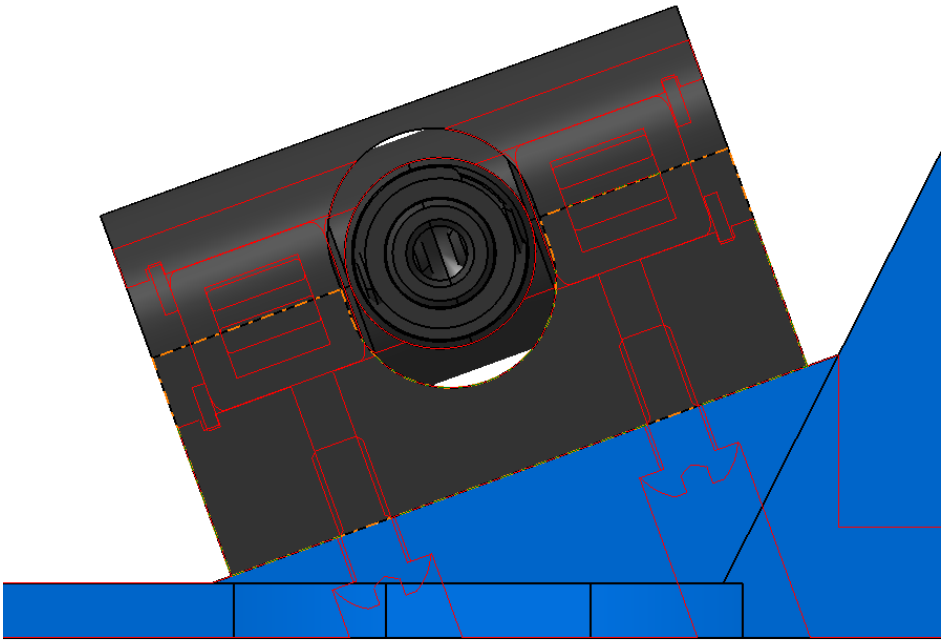

Figure 4.5: Balance bar mounting

4.2.3 Validation

For what concerns the loads experienced on the base during manual operation, the most effective model that can be considered is achieved conducting a static analysis at maximum compression by applying a force of 2000 N as specified in T6.1.9 at the pedal and calculating the reaction experienced at the pivot. Instead for the autonomous operation, the force estimate is much simpler as the reaction is directly obtained on the actuator attachment based on the maximum force generated from the pneumatic cylinders.

Before starting with the numerical evaluation of the pedal base, the CAD geometry was imported into Altair Hypermesh, where the meshing was conducted followed by material and properties application. The next step involved defining proper boundary conditions and loads: rigid elements (RBE3) were used. These multi-point constraint elements help distribute the applied load to a set of dependent nodes. The base is mounted to the chassis via the bolts that are simulated using the rigid connections previously mentioned and a single point constraint at the master node. by restricting the correct degrees of freedom at each bolt, the load transfer will allow for a correct local deformation while avoiding over-constraining the model, ensuring the correct stresses and displacements are captured during the finite element analysis.

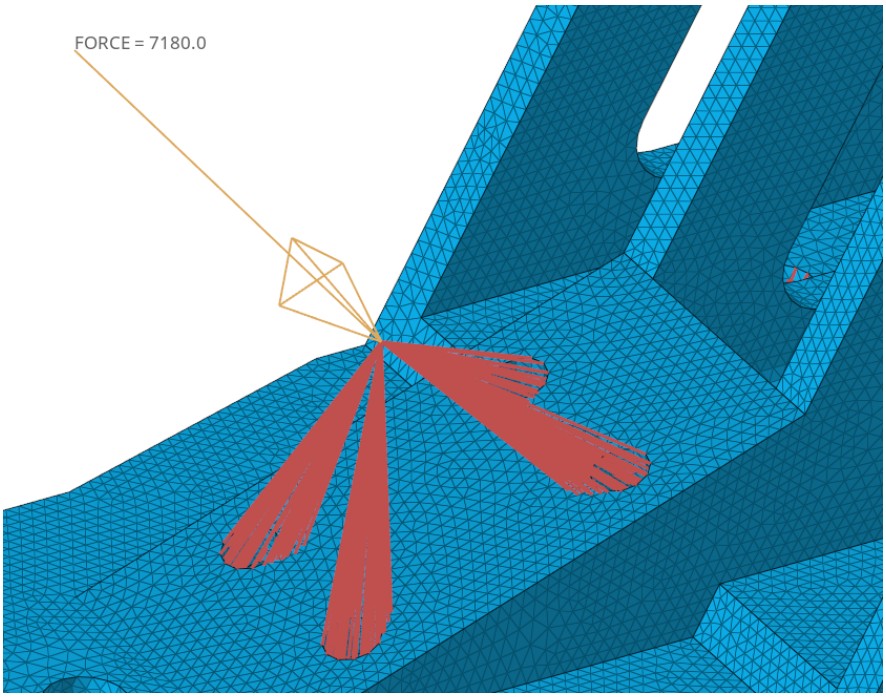

Figure 4.6: Reaction force applied on rigid connection

The next step involves defining the different loads for the two subcases:

- For the manual braking condition, starting from the force of 2000 N at the pedal, and the pedal ratio of 3.59 at maximum compression, the reaction forces at the pivot rotational point and balance bar can be obtained. For the pivot point, the reaction force is 5180 N applied at the center of the pivot point using the rigid connections. Meanwhile the force of 7180 N (the pedal maximum force multiplied by the pedal ratio at maximum compression) is applied at a node coinciding with the center of the balance bar and then rigidly connected to the mounting holes of the balance bar to base (Figure 4.6), approximating a worst case scenario. It is worth noting that the forces direction coincides with the inclination of the MC at the maximum compression.

- For the autonomous braking condition, the same constraints are used, meanwhile two loads of 500 N are applied at the center of the two mounting flanges for the autonomous actuators. The load chosen is slightly higher than what each actuator is able to generate even at maximum operating pressure, rendering our calculated safety factors even more conservative.

With all the necessary setup done, and the boundary conditions defined, the two load steps created using the loads with their respective load collectors can be solved. The table below summarizes the two load cases considered.

Type	Magnitude	Description
Case 1: Manual Operation		
Constraint	—	Base rigidly fixed with 5 bolts
Force 1 (Pivot)	5180 N	Reaction at pivot
Force 2 (Balance Bar)	7180 N	Reaction at balance bar mounting
Case 2: Autonomous Operation		
Constraint	—	Base rigidly fixed with 5 bolts
Force 1 (Actuator 1)	500 N	Applied at actuator mounting 1
Force 2 (Actuator 2)	500 N	Applied at actuator mounting 2

Table 4.3: Pedal base load cases

Stress

With the results in hand, for what concerns the stress, using the vonMises criterion, the element stress is plotted for both subcases below:

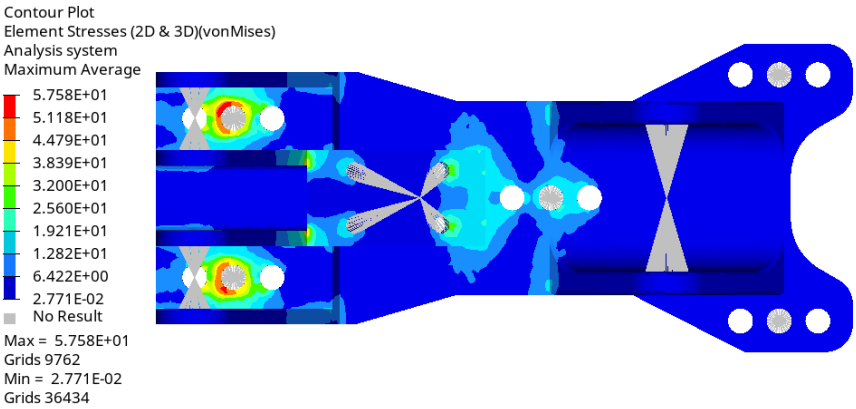

Figure 4.7: Stress distribution in autonomous braking

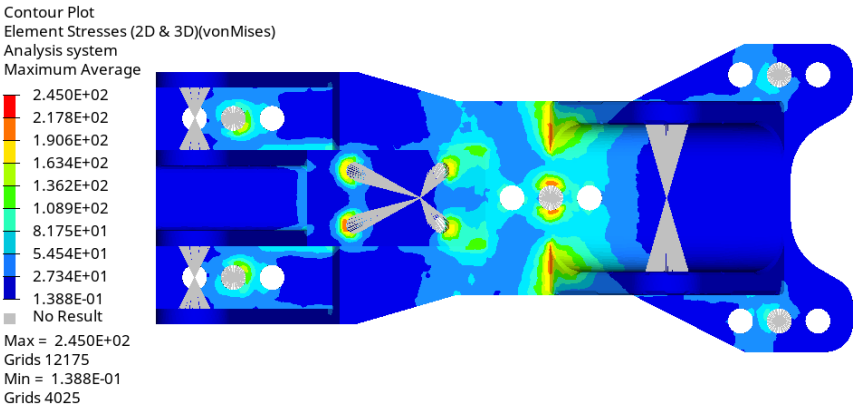

Figure 4.8: Stress distribution in manual braking

From the plots above, it is clear that the manual braking case is severely more critical (more than 4 times more stressed) than the autonomous case. Nonetheless, the stress distribution is still acceptable with the most critical stress in the central bolt and on the edges of the pivot bracket.

The safety factor for the base can therefore be define:

$$SF = \frac{505 \text{ MPa}}{245 \text{ MPa}} \approx 2.06$$

Being above the minimum 1.5, the design of the base plate guarantees safe operation even during the brake test extreme load.

Displacement

Considering the worst case out of the two operating modes, the displacement can be plotted:

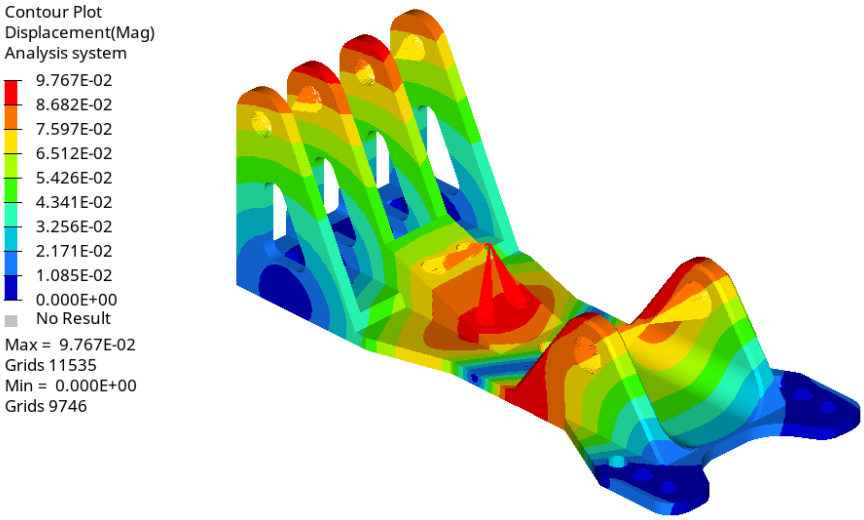

Figure 4.9: Displacement distribution in manual braking

with the maximum experienced displacement being 0.097 mm at the tips of the base, and considering the system employs spherical bearings for the mounting of the critical components, such a deflection is acceptable and will not damage any component or block their motions.

4.3 Master Cylinders & Actuators Mounting

4.3.1 Design

Having fixed the base with the balance bar, the master cylinders can be mounted on both ends. To ensure no bending loads occur on the master cylinders, the piston end is fitted with a custom rod end with a radial spherical plain bearing from SKF [33]. the selected bearing is identical to the one currently mounted on the master cylinders, these bearings help in accommodating radial and combined radial and axial loads, and also misalignment, making them ideal for our application. On the upper end, a rod will be inserted into the pedal, facilitating mounting and maintenance and reducing wear on the component. Similarly to the pivot axis, a pair of bronze bushings on each side allow to reduce any potential friction caused from the metal contacts.

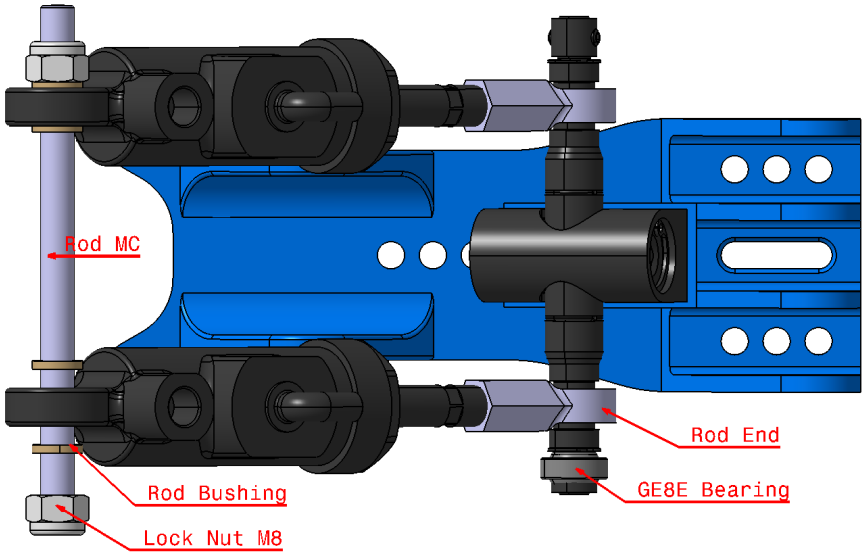

Figure 4.10: Master Cylinders Mounting

For what concerns the pneumatic actuators, the best option found was using already made parts from Festo such as the clevis flange SNCL-25 [34], reducing manufacturing cost with acceptable weight values. On the other hand, the mounting bar from the clevis foot LBN-20-25 [35] will be borrowed with the retaining clips as the product matches perfectly with the flange chosen. the bar and the flange can directly be coupled to the base as seen below, allowing easy mounting dismounting for maintenance.

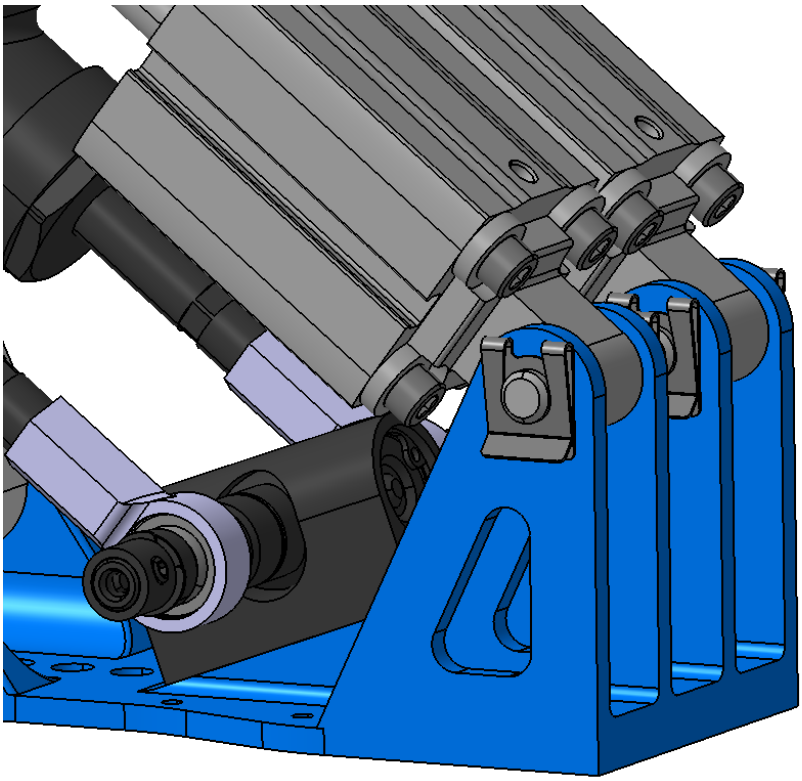

Figure 4.11: Pneumatic actuators mounting

4.3.2 Validation

For what concerns the validation of the mounting components, the parts used for attaching the pneumatic actuators are bought directly from the same supplier, and are already designed to work even under maximum conditions, in that case no analysis is needed. On the other hand, the rod that supports the master cylinders experiences very high levels of stress considering the reaction force it is subjected to. Being a rod subjected to a radial load of $F = 3590$ N, the analysis can be conducted analytically, considering the radial offset of $e = 6$ mm from the bearing edge. the resultant bending moment

$$M = F\,e = 21.54 \text{ N·m}. \tag{4.1}$$

The circular rod of diameter $d = 8$ mm is already dictated by the master cylinder hole, making the bending stress equal to:

$$\sigma_b = \frac{Md}{2I} = 4.29 \times 10^8 \text{ Pa} = 429 \text{ MPa}. \tag{4.2}$$

with I being the second moment of area.

The transverse shear stress for a circular rod is approximated as

$$\tau_{\max} = \frac{4F}{3A} = 95.2 \text{ MPa}, \tag{4.3}$$

where $A = \pi d^2/4$ is the cross-sectional area.

The resulting von Mises equivalent stress is

$$\sigma_{vm} = \sqrt{\sigma_b^2 + 3\tau_{\max}^2} = 460 \text{ MPa}. \tag{4.4}$$

With the use of ergal aluminum, the safety factor is:

$$SF = 1.1, \tag{4.5}$$

Rendering the material unsafe for our application. Instead, using AISI 4340 in the quenched and tempered condition with a yield strength of $\sigma_y \approx 1080$ MPa, the factor of safety against yielding is

$$SF = \frac{\sigma_y}{\sigma_{vm}} = 2.34, \tag{4.6}$$

Allowing the rod to sustain the maximum load safely without any possible failure. Aside from the increase of weight due to the use of steel, the weight increases from 16 g to 47 g, but as decreasing the loads leads to a decrease of the bottom ratio below desired values, the weight increase has to be accepted. Other issues arise when coupling steel to aluminum such as galvanic corrosion, but considering the short span of the Formula student season and the possibility to replace the rod due to the cheaper cost, the corrosion can easily be avoided.

4.4 Pedal & Pedal Face

4.4.1 Design

With all the mounting points established, the pedal holes were extruded and the bar itself was subjected to weight reduction in all non stressed areas through trial and error. the overall length was considered in order to stay within the envelope limits.

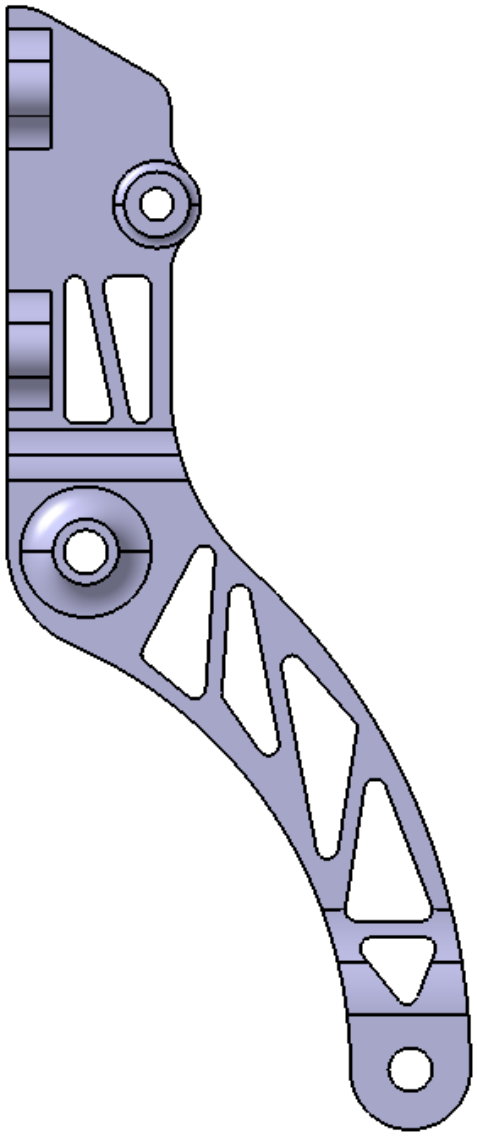

Figure 4.12: Pedal

with the overall weight coming in at 309 g, compared to 287 g and considering the addition of a support for the EBS actuation, the overall weight increase is acceptable. In regards to the pedal face, the team previously employed a carbon fiber pedal face, successfully cutting the weight by about half. Consider the rule T6.1.10 which specifies that the pedal and the face must be fabricated from steel or aluminum or titanium, rendering the carbon fiber face not fully rule compliant anymore. In order to remain within the compliance, the pedal face will be made out of ergal aluminum.

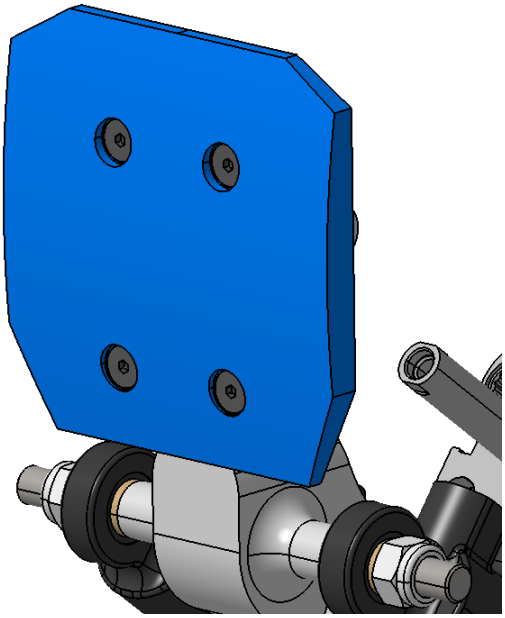

Figure 4.13: Pedal face

4.4.2 Validation

for the validation of the pedal, the setup is straightforward as the load applied is directly 2000 N on the pedal. The pivot point is fully constrained while the master cylinder attachment is constrained in translation and rotation around the movement direction.

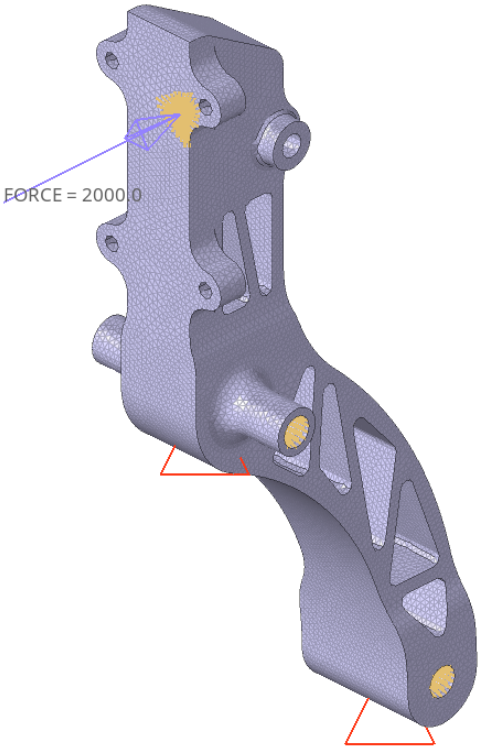

Figure 4.14: Pedal simulation setup

Overall, the most stressed part surges above the master cylinder attachment as expected, with the stress points occurring around the weight reduction slots. Through the use of fillets, the maximum stresses have been severely reduced even at those critical areas, with peaks arriving at 103 MPa making the safety factor of the pedal:

$$SF = \frac{505 \text{ MPa}}{103 \text{ MPa}} \approx 4.9$$

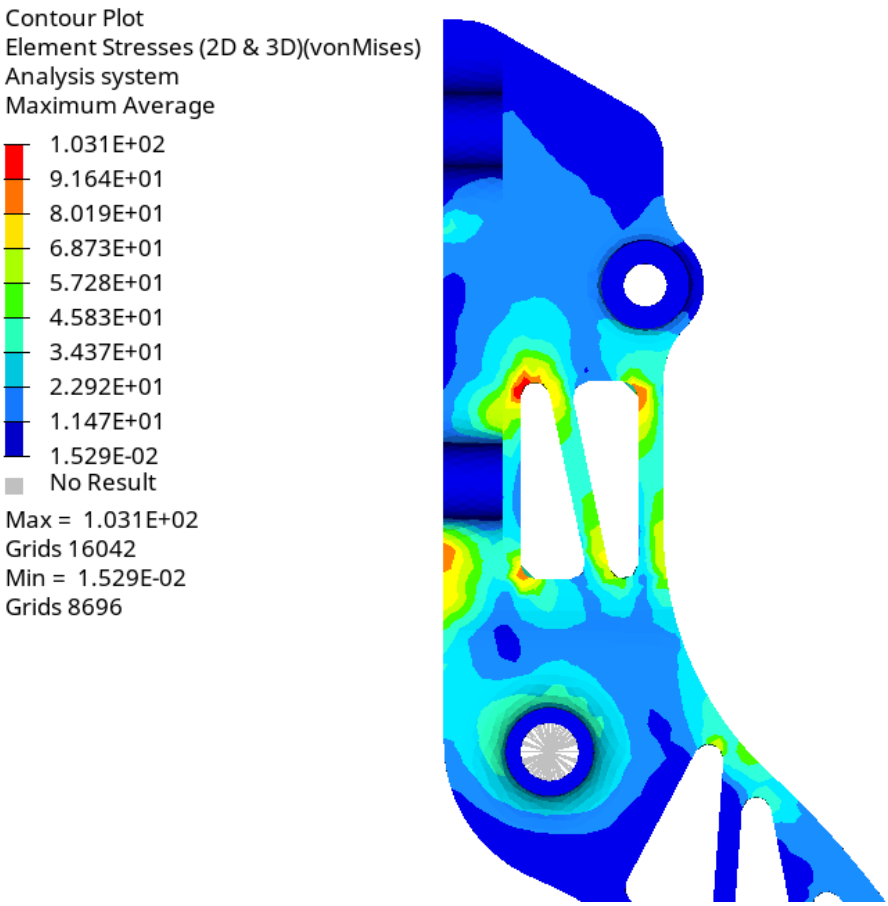

Figure 4.15: Pedal stress distribution

while the pedal safety factor is higher than what is needed, another important aspect to analyze here is the displacement, especially at the tip of the pedal as the previous model suffered a very large displacement which caused unfavorable results as found in the documentations (displacement of 1.72 mm at the tip) making the new goal to stay below 1 mm.

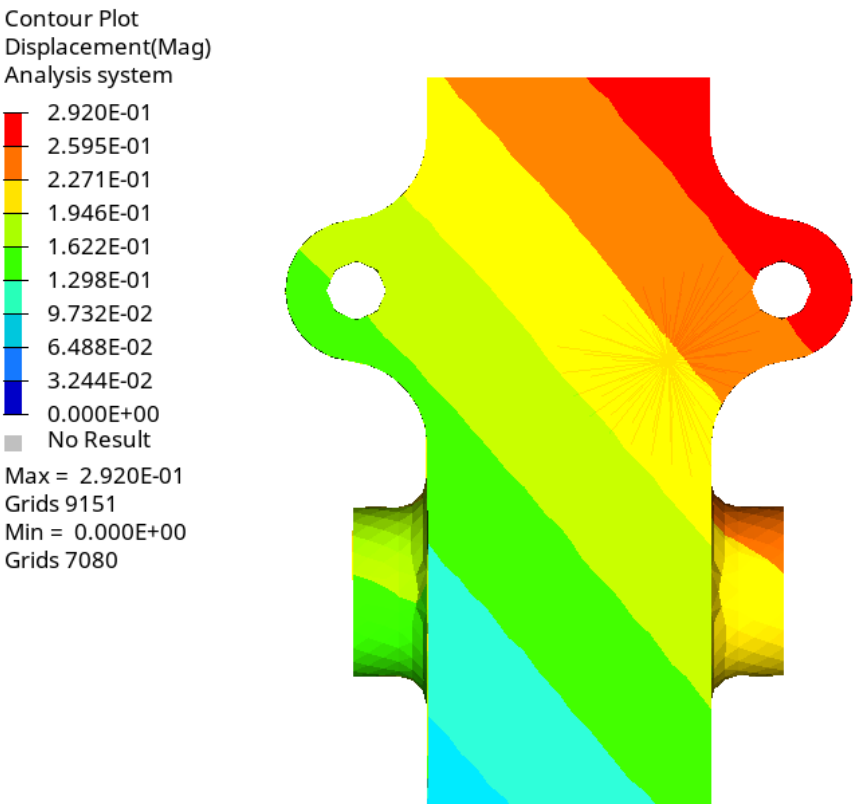

Figure 4.16: Pedal displacement at the tip

The established goal in this configuration is clearly met as the maximum displacement is 0.292 mm, vastly improving on the previous iteration.

4.5 Decoupling Mechanism

All the components of the manual and autonomous braking systems have been defined and mounted, the final link missing is the coupling the pedal and the pneumatic actuators, which should guarantee:

- Actuation of the emergency system from any position, even with manual operation active.
- Manual operation must not be subjected to any interference from the autonomous system, as not to disrupt the drivers input.

To achieve these requirements, the use of tight manufacturing tolerances will allow to eliminate any play, while accommodating the radial load that may occur. The yoke and yoke shaft follow a very similar design to the EBS mounting, with retaining rings.

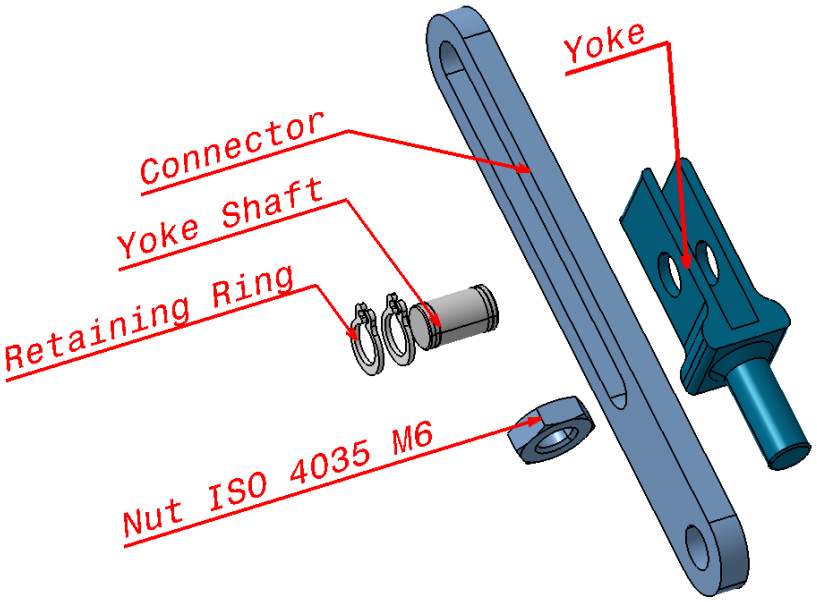

Figure 4.17: Decoupling mechanism components

Considering the low forces in play when activating the EBS, the overall stress and displacement values are very small compared to the parts involved in manual braking. As most components are already small and weight reduction is not possible, and with the use of ergal aluminum, the safety factors for all components results in values above 10. To reduce the cost of production, aluminum 6061 alloy, a very common and readily available alloy for machining may be used. Even with a tensile strength of 276 MPa, slightly less than half of that of 7075 ergal aluminum used (505 MPa), decoupling mechanism components still achieve a very high safety factor, taking as an example the Connector, where peak stresses reach about 58 MPa (Figure 4.18), the safety factor with 6061 aluminum would then be:

$$SF = \frac{276 \text{ MPa}}{58 \text{ MPa}} \approx 4.75$$

Again, the displacement trend for this component and all others of this sub-assembly are negligible.

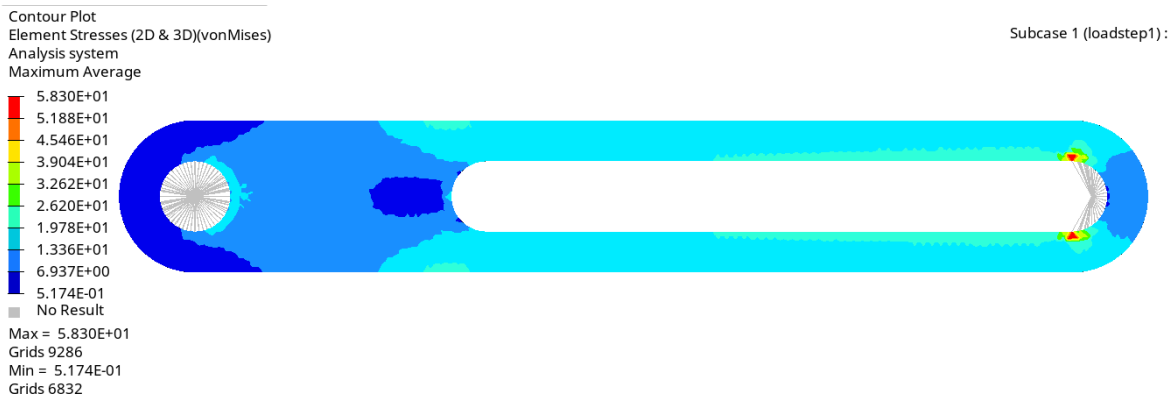

Figure 4.18: Connector stress distribution

4.6 Brake Over Travel Switch & Actuator Support

The Brake Over-Travel Switch (BOTS) has already been Introduced in Section 2.3.2, with the most relevant rules being found in section T6.2 of the rule book. The best configuration involves mounting a normally-closed push-rotate switch directly behind the pedal such that any loss of pressure in the system will cause the pedal to overcome the maximum compression travel and collide with the switch, satisfying both T6.2.1 and T6.2.3.

Under normal braking, hydraulic pressure limits pedal travel. In the event of brake system failure, the pedal experiences increased travel due to loss of pressure. The pedal then reaches a mechanical stop and surpasses the threshold distance configured for BOTS activation. The latching NC switch, can be borrowed from the previous BOTS system by using the Omron A165E-S-01, easily integrable with the rest of the circuit without any modifications. The actuation sequence can therefore be defined as:

1. During normal braking, the pedal does not contact the switch.
2. When over-travel occurs, the pedal contacts the switch.
3. The switch actuates, transitioning from NC to open.
4. The internal latch engages, keeping the switch open.
5. The SDC opens, shutting down the vehicle.
6. Reset requires flipping the switch, inaccessible to the driver from the cockpit.

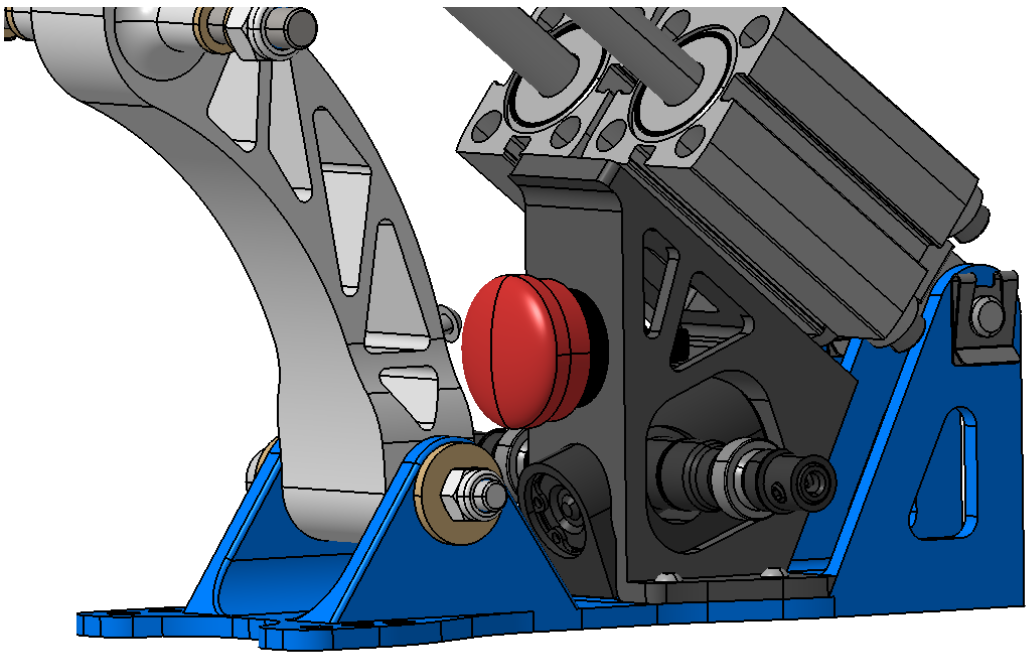

Figure 4.19: BOTS

As the button is mounted on a custom 3D printed support, we can ensure no interference occurring with any balance bar adjustment settings. In addition, the support fulfills a secondary function necessary during manual activation:

- As the manual braking is activated, the pneumatic actuator linkage will tend to rotate downwards due to the decoupling mechanism.
- Activation of the pneumatic actuators will cause the stem to retract, pulling upwards the two actuators.

As it is critical that no interference occurs between the actuators and any other braking component during manual operation, the downward motion has to be blocked. By supporting the face with a simple support, the motion can limited for the top half only. It is worth noting that no loads will be transferred into the support, as its only function is to hold some of the weight of the actuators, allowing the use of non structural materials, making 3D printing ideal, by also reducing unnecessary weight. In order to better adjust and customize the necessary travel of the pedal to activate the BOTS, a small screw has been added to the back of the pedal.

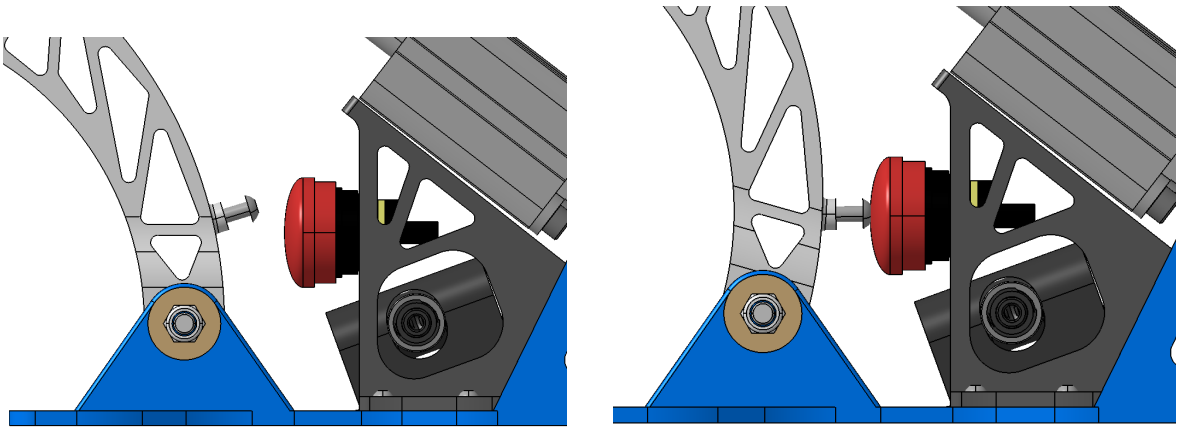

Figure 4.20: Normal operation and BOTS activation

Chapter 5

System Assembly

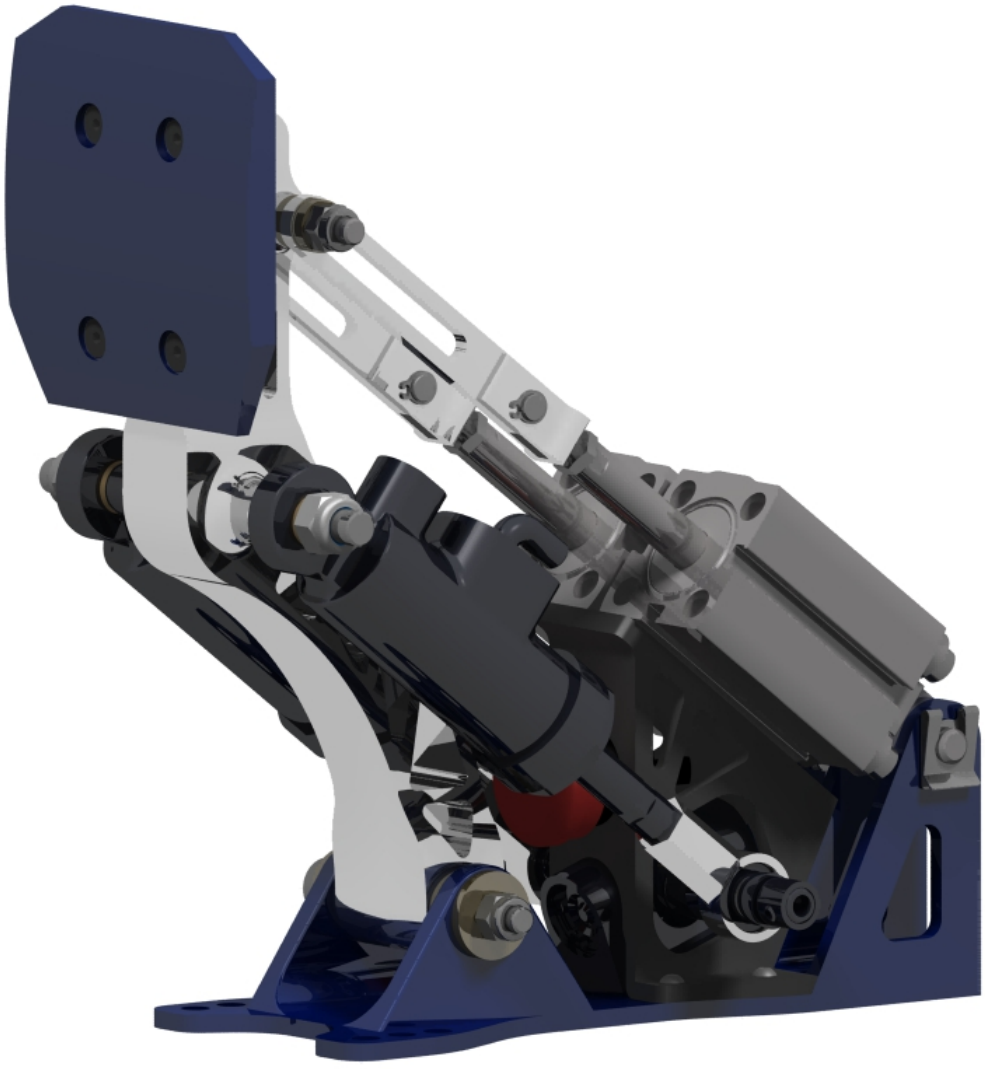

Figure 5.1: Assembly render

5.1 Weight Analysis

With the assembly completed, the first parameter to evaluate is the weight decrease in order to understand if the initial weight reduction was met. by following a similar procedure done for both the previous pedal box and EBS.

Component	**Qty**	**Material**	**Mass [g]**
ADN-S-25-35-I-P-A	2	–	350.0
Master Cylinder	2	–	320.0
Pedal	1	Al 7075-T6	310.0
Base	1	Al 7075-T6	260.0
Balance bar	1	–	225.0
Pedal Face	1	Al 7075-T6	121.0
Clevis Flange	2	Steel	82.0
Rod MC	1	4340 Steel	45.0
BOTS support	1	PLA	42.0
Shoulder screw	1	Steel	28.0
Shaft	2	Steel	24.0
DIN-912 SHCS M5×20	8	Steel	24.0
Rod End	2	Al 7075-T6	20.0
Pivot Bushing	2	Bronze	18.0
Rod EBS	1	Steel	17.0
Connector	2	Al 2024	16.0
Radial bearing GE8E	2	–	13.2
Yoke	2	Al 2024	10.0
Spacer MC	4	Bronze	8.0
Spacer EBS	4	Bronze	8.0
BHS M4×10 (ISO 7380)	5	Steel	5.8
Locknut M8 (ISO 7040)	2	Steel	5.2
Locknut M6 (ISO 7040)	3	Steel	4.5
Yoke Shaft	2	Al 2024	4.0
CSK screw M4×10	4	Steel	3.2
ISO 4035 M6 Nut	2	Steel	3.2
Nylon Washer M8	2	Nylon	2.0
BHS M3×8 (ISO 7380)	4	Steel	1.6
Total System			**1970.7**

Table 5.1: New system bill of materials

The final weight comes in at 1970.7 g, greatly improving the initial weight and surpassing by far the set target of 2981 g in table 4.1.

To better understand where the weight saving comes from, it is worth showing a clustered chart with the relevant components modified from the old to the new configuration. The aim is not to compare every component but rather the essential ones relative to the functioning of the pedal box and emergency braking system.

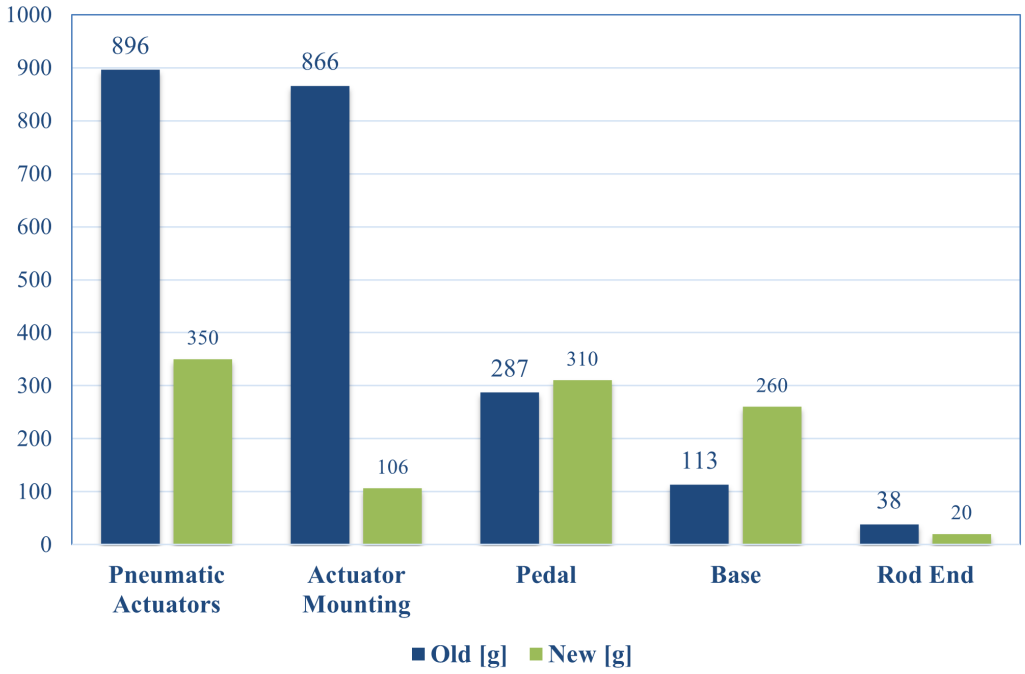

Figure 5.2: Weight comparison

It is evident by the chart above, that the main improvement was achieved on the emergency system, where both the pneumatic actuators and especially their mountings were reduced by more than a kilogram. The main benefit for the actuator reduction was not only in weight saving, but as well in functionality as shown in the previous chapters where the system has been optimized to avoid tire locks and over dimensioning. the main consideration was the performance with the weight saving naturally following. Instead, the actuator mounting which showed the greatest reduction, is mostly due to the reduction in actuator force mentioned as well as the use of aluminum instead of steel. In the previous configuration, the system had to be support from both the bottom and top ends whereas in the current configuration, the pedal and the base that are already reinforced create the support for the actuators and thus reducing unnecessary material. The additional weight seen on the pedal of about 20 g was mainly due to the addition of an anchoring point for the decoupling mechanism. Although the safety factor proved to be higher than other components indicating potential more weight saving, the main goal is reliability over weight reduction as an initial step, leaving further refinement for the next iteration. The base experiences the highest weight increase, almost doubling that of the previous assembly. As mentioned, the EBS is not supported by the base, and that weight increase can be explained by the supports found at the back of the base, responsible for supporting the entire system of the emergency braking. This increase in weight is the main factor responsible for the large decrease of the second column, justifying doubling the weight of the base.

5.2 Compressed Gas System

In Section 2.4.2, the compressed gas system was introduced briefly. In order to operate the developed system, the energy storage system must be fully rule compliant and guarantee a safe operation to protect the driver and safely stop the vehicle. The release of the energy should occur only under specific conditions:

- Shutdown circuit is opened (RES,BOTS or other...).
- Electric power loss.
- Safe state or non-ready state is active.

To guarantee meeting these conditions, as well as the deactivation points of T15.1.7, a series of mechanical and electro-mechanical valves must be added. Before setting the circuit, an analysis of the storage and its capacity must be conducted.

5.2.1 High Pressure Delivery System

The onboard storage of the compressed air is critical, as handling very high compression pressures requires strict safety measures. T9.1.3 limits the pressure of the circuit to 10 bar but that limit may only be exceeded in the cylinders or tanks through the use of a pressure regulator mounted directly onto them. The most widespread solution involves the use of paintball style canisters which operate at high pressure, reducing the overall size needed for storage. Another critical aspect is the number of actuations necessary before refilling the tanks. While the rule book does not specify the actual number of actuation needed, we can take a look at the necessary number needed for one single mission:

- Two actuations for the initial EBS check-up sequence:
  - One actuation to test both redundant pneumatic circuits together.
  - One actuation to test each circuit individually and verify correct pressure build-up.
- One actuation to transition the vehicle into *Ready-to-Drive* mode.
- One actuation to terminate the mission and bring the vehicle to a stop.
- One additional actuation caused by pressure loss when arming the EBS while the ASMS is initially open.

The time to replace the canister highly depends on the ease of access of the canisters on the vehicle as well as the possibility of keeping several canisters ready for swapping instead of waiting for the refill. The number of actuations a canister can deliver can be determined with a simple iterative procedure considering:

- **Mass of air required per actuation**
- **Total air mass contained in the high-pressure tank**

Using the ideal gas law under isothermal conditions, the mass of air contained in the tank is calculated as:

$$m_{\text{tank}} = \frac{P_{\text{tank,initial}}\, V_{\text{tank}}}{R\,T} \tag{5.1}$$

where $P_{\text{tank,initial}}$ is the absolute initial pressure of the tank, V_{tank} the tank volume, R the specific gas constant for air, and T the operating temperature. After extensive research for different Paintball HPA canisters, The smallest volume found was the 13 ci standard (0.21 L). The lightest bottle found was the PowAir TACTICAL Line CC 0.21L / 13ci Paintball HP Bottle 300 bar with a net weight of **227 g**.

Similarly, the mass of air required to fill the actuator, tubing, and additional components is given by:

$$m_{\text{act}} = \frac{P_{\text{act}}\, V_{\text{load}}}{R\,T}\lambda_{\text{loss}} \tag{5.2}$$

where the load volume V_{load} is defined as the sum of the cylinder stroke volume, the cylinder dead volume, and the internal volume of the pneumatic tubing:

$$V_{\text{load}} = V_{\text{stroke}} + V_{\text{dead}} + V_{\text{tube}}.$$

The loss factor accounts λ_{loss} for regulator inefficiencies, pressure drops in the tubing, and valve internal volumes.

Once m_{tank} and m_{act} are known, the **maximum number of actuations** before the tank reaches its minimum allowable pressure $P_{\text{tank,min}}$ can be computed iteratively. In MATLAB, this is implemented as a loop that reduces the tank mass by m_{act} at each iteration and recalculates the tank pressure. By testing different values for initial pressure, it was found that for $P_{\text{tank,initial}} = 150\ bar$, at least 24 actuations can be successfully achieved. While the pressure set to be used is about half of the rated pressure of the tank, it is important to select appropriate regulators in order to remain in line with T9.1.3. General Paintball regulators can only output down to around $32 - 60\ bar$, nowhere near enough the required 10 *bar*, forcing the use of 2 regulators in series creating a two step regulation.

High Pressure Regulator

For the first step between the HPA canister and the low pressure regulator, several pressure regulators are offered by a variety of brands, with the lightest model found being offered by Ninja Paintball at weighting at **107 g**:

Parameter	**Pressure (bar)**
Maximum input (tank) pressure	300
Regulated output pressure range	31 – 58.6

Table 5.2: Pressure specifications of the Ninja Ultralite 300 bar HP Regulator

Low Pressure Regulator

Regarding the low pressure regulation, the possibilities were slightly more limited, where the best regulator found was the Micro Reg™ GEN2 weighting **130 g**, which fully aligns with the necessary pressure regulation.

Parameter	Pressure (bar)	Pressure (psi)
Maximum input pressure	62.1	900
Maximum regulated output pressure	9.0	130
Minimum regulated output pressure	2.8	40
Optional high-pressure output	13.8	200

Table 5.3: Pressure specifications of the Micro Reg™ GEN2 (PolarStar Airsoft)

The minimum regulated output pressure of 2.8 bar is slightly higher than the minimum one set in section 3.3.3. The small sacrifice in operating range is quite acceptable especially considering the team would almost never operate the EBS in pressures below 4 bar. In addition, the input is withing the output of the first regulator at 58.6 bar.

System Selection

By considering the Maximum input pressure of the regulator as $P_{\text{tank,initial}} = 150\ bar$ the calculation can be remade to obtain about **8 actuations**, three times less than the first case and that would suffice for completing 1 driving mission only which would be unfavorable.

Building on to the idea of removing the high pressure regulator and increase the first tank size to 0.5 L with the best weight for such canister being around **500 g**, the system would be able to deliver 20 actuations equal to 4 complete missions at max operating pressure of the low pressure regulator.

Option	Weight	Advantages
Small Tank + 2 Regulators	464 g	More than 100 actuations possible at maximum rated pressure. Lower weight compared to the single big tank option. Smaller total packaged volume
Big Tank + 1 Regulator	630 g	Reduced system complexity. Lower Price

Table 5.4: Comparison of HPA delivery system options

The benefits of using a smaller tank with the 2 step regulation is the better choice with numerous advantages both in weight and much bigger possible number of actuations.

5.2.2 Deactivation Points

Under T15.1.7 and T15.1.8 of the rulebook, the ASB must feature at the maximum two deactivation points with several characteristics, of which the most relevant:

- Work without the aid of electrical power
- be operable by maximum two simple push/pull and/or turning actions

In addition, the deactivation point must be able to withstand the maximum operating pressure set as 10 bar. The most reliable way to achieve this is by using mechanical selector valves offered by Festo, such as the VHEF-EST-B32-G18. The manual valves can therefore be able to arm the system by allowing the flow to pass in the lines or empty the air lines such as during manual operation. Another important aspect is preserving the pressure inside the canisters when disengaging the system which can be done with the 3/2 system with three ports (inlet P, Outlet A and exhaust R) and 2 positions. In the first position, P and A are directly connected while A is closed in order to supply the compressed air directly to the actuator. In the second position, A and R are connected while the P inlet is shut, venting the downstream circuit while preserving the canister air.

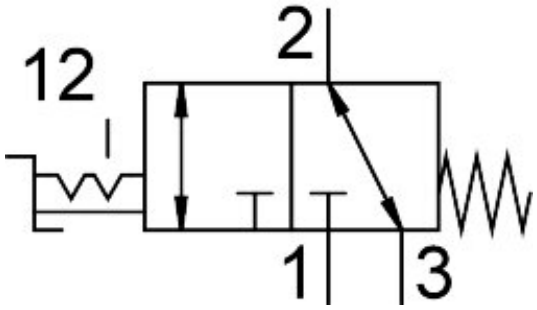

Figure 5.3: VHEF-EST-B32-G18 schematic

5.2.3 Solenoid Valves

The final component before reaching the actuator is the solenoid valves, very similar to the 3/2 mechanical valves. The selected valves are of normally open (NO) electro valve. While an electric current is provided, the valve is closed and the pressure canister is cut off from the pneumatic actuators, on the other hand under any loss of current or under shut down circuit opening, the electro valve returns to its normally opened state, where the pneumatic actuators get actuated by the high pressure air. The use of a normally open solution is the safest option considering the system will always end up in engaged mode in case any malfunction occurs on the electric side.

The first option to be evaluated was the solenoid valve offered by Festo, but the most suitable model has a maximum operating range of 8 *bar*, and by following T9.1.4, this would limit all the rest of the circuit to this lower pressure, effectively lowering our maximum generated force by the EBS. The other suitable solution is the current one employed by the team from AirComp. the EV8 1/4" 22 3 SL PM NO M is already fully compatible with the low voltage side of the vehicle, reducing the necessary changes needed from the electrical division. In addition, the valve is very lightweight at **120 g**.

The final compressed gas system, with the necessary fittings can be schematized below:

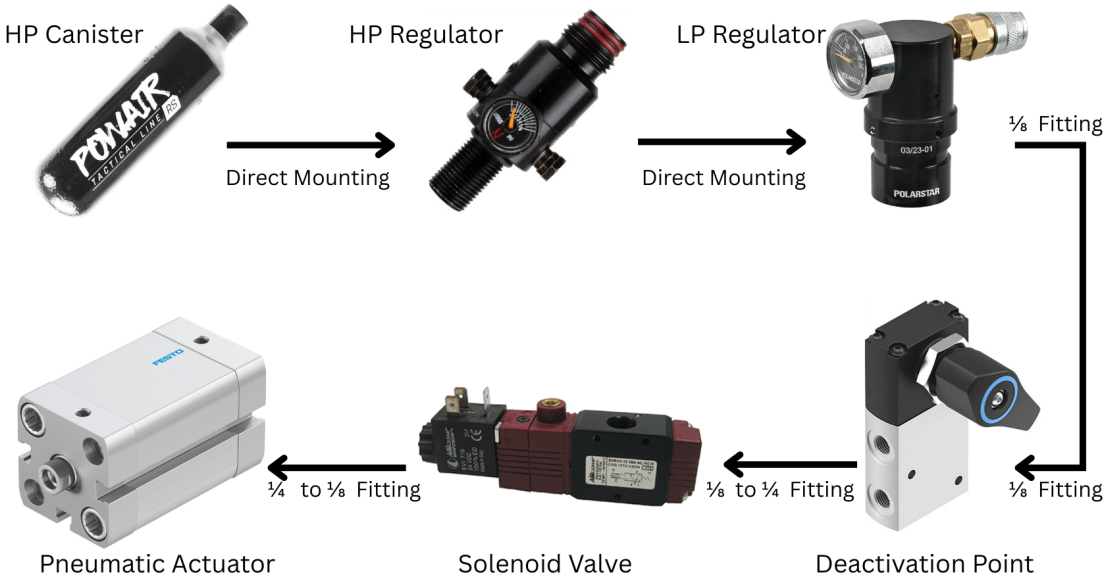

Figure 5.4: Compressed gas system schematic

5.3 Kinematic Analysis

With the assembly completed, using CATIA DMU Kinematics, the constraints established are transformed into a mechanism with the joints of the entire assembly:

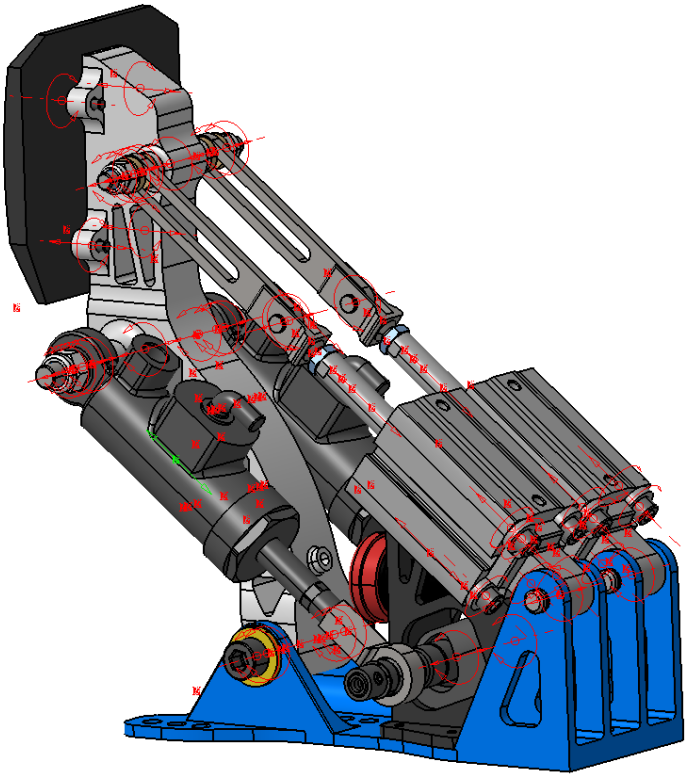

Figure 5.5: Joints of assembly

The main aim of the kinematic analysis is identifying the inputs and corresponding outputs over the entire range. By setting the input as the master cylinder stroke, different cases can be analyzed, obtaining values already calculated such as the pneumatic actuator compression and Pedal ratio. In addition, clashes during movement can be detected, especially in very tight fit areas such as near the decoupling mechanism in manual operation. While other parameters such as velocity and acceleration of the components or the overall occupied volume can be obtained, regarding a mechanism such as the pedal box, such parameters do not provide any significant performance.

5.3.1 EBS Activation

The first essential check conducted from a kinematical point of view was simulating the activation of the EBS, from the uncompressed master cylinder up until the maximum compression previously calculated.

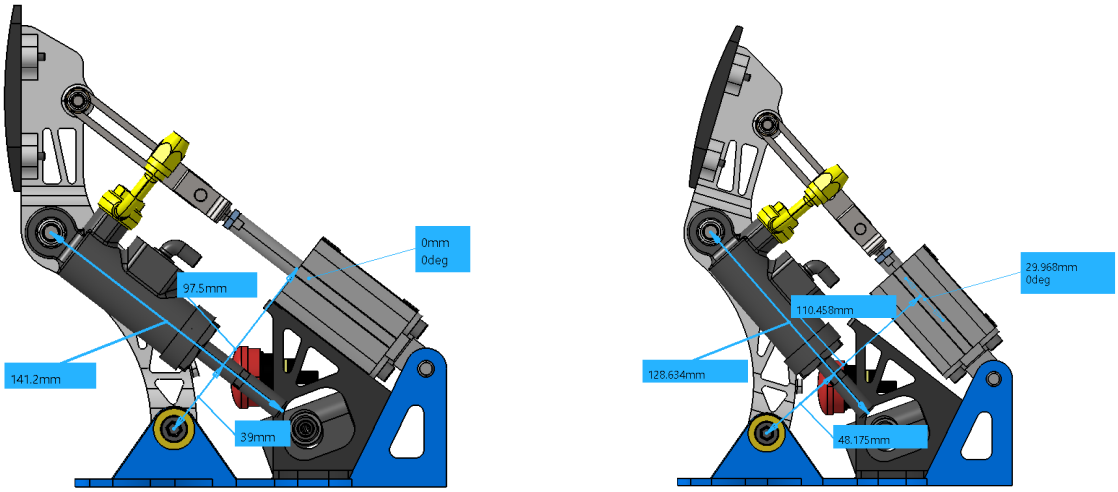

Figure 5.6: Comparison of initial (left) and final (right) positions of EBS activation.

To make the analysis more realistic, especially for what concerns the clashes, the banjo bolt and brake line head have been added to the assembly, ensure no contact occurs in any operation. for the initial position, the values confirm what was already stated:

- Actuator pedal ratio 2.5.
- Uncompressed MC and pneumatic actuators.

At maximum compression of 12.566 mm, the actual perceived actuator ratio is slightly lower than the initial one, as the pedal ratio is now 2.29, explaining the maximum compression of the pneumatic actuators as being 29.968 mm instead of the expected 31.5 mm covered in section 3.3.3. This phenomena was already covered for the pedal ratio (section 4.2.1) where the non-linearity of the geometry evolution arises during rotation. The main difference here is that with the two components being parallel, the overall change is much smaller leading to less discrepancy between the expected and actual stroke of the pneumatic actuator. The value being almost equal to 30 mm confirms the necessity of using the model with a 35 mm stroke for our assembly.

5.3.2 Manual Braking

The second kinematic check to be conducted is during manual braking, where the linkage system must not interfere with the driver in any way or form. The most important aspect is the clashes that may occur, especially at maximum compression. By simulating this condition, two critical locations have been identified:

- Between Connector of the linkage, and the banjo fitting of the brake line.
- Between the tip of the connector, and the bolts holding the pedal face.

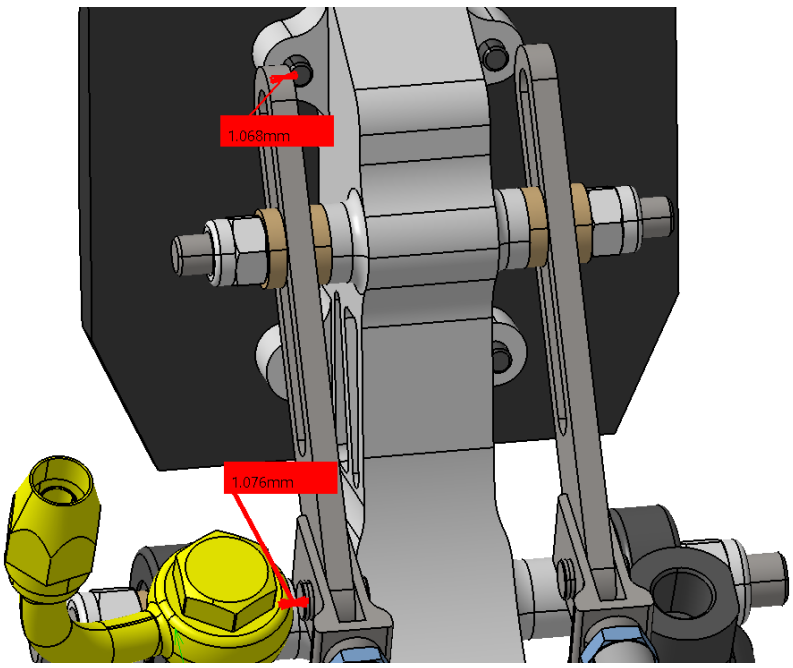

Figure 5.7: Potential clashes

With both values being around 1 mm, the risk of clash is relatively low. In addition, the top part can be reduced by using shorter bolts as the pedal will be threaded. For what concerns the bottom value, this analysis was done on the absolute maximum compression, where generally the compression of the master cylinder would be even lower, and considering the fact that using the bearings, the master cylinders can be directed outwards, increasing the gap, the minimum value can be considered safe.

Chapter 6

Conclusion

Throughout this thesis, several points were introduced with regards to the development of the pedal-box-integrated emergency brake system which can be addressed in this final chapter. With regards to the previous iteration of the EBS, which was characterized by problems related to air bleeding and increased complexity due to the presence of multiple master cylinders connected through OR valves, the new iteration was greatly simplified and eliminated the need for an additional pair of master cylinders through the actuation directly on the pedal. This architectural change not only reduced the number of hydraulic components, but also improved the robustness of the system by removing connections that were prone to leakage and difficult to bleed.

The second notable issue of tyre lock-up during braking manoeuvres was addressed by the thorough longitudinal braking dynamics analysis conducted for different driving conditions, which allowed to identify ideal front bias brake repartitions for both wet and dry conditions under different deceleration targets. As the new system makes use of the balance bar of the pedal box, the working range may be adjusted to several different deceleration targets depending on track and tyre conditions by tuning the pressure release value and thus the force exerted on the system. In this way, the same hardware can be configured for conservative wet setups or more aggressive dry setups without compromising stability. As shown in the previous chapters, the system is able to achieve about 94.1% braking efficiency with respect to ideal conditions at 1.4 g of deceleration, while meeting the required stopping distance of 8.5 m for the brake test.

Another issue resolved by this system is the excessive force generated by the large pneumatic actuators that were needed in the past, as they were directly connected to the master cylinders. Both the dimensions of the actuators and the force required for actuation were reduced through the introduction of the pedal ratio between the actuators and the master cylinders, allowing the pneumatic system to operate with smaller cylinders.

As all notable issues were addressed with this iteration, the overall weight of the assembly was significantly reduced from 4259 g to 1970.7 g, a reduction of about 54% much greater than the initial target of 30%. The main factors that contributed to the significant weight reduction are due to the adoption of more compact actuators, aluminium mounting structures instead of heavy steel brackets and additional master cylinders.

The next step was conducting the FEM analysis, which confirmed that the new components satisfy the structural requirements under the worst-case loading scenarios. The

base plate, pedal, actuator mounts and decoupling elements were all analysed under both manual and autonomous braking loads, verifying most importantly the load exerted by the judge during technical inspections. The obtained results validated that elastic deformations remain within acceptable limits. Following the structural validation, a detailed kinematic study of the assembly was carried out in order to ensure that both operating conditions (manual and autonomous) function properly through the decoupling mechanism and without any potential clashes.

The second topic of discussion was the improvements conducted on the manual side. Notably, the introduction of proper measure and definition of the pedal ratio, taking into account the geometric evolution of the linkage over the pedal stroke rather than a constant value. By analysing the variation of the effective lever arms as a function of pedal travel, it was possible to obtain a more realistic estimation of the force transmitted to the master cylinders. Subsequently, through an ergonomic analysis for both short and long braking actions, driver comfort and feel was guaranteed even for the smallest percentiles.

Despite these improvements, some limitations of the system must be acknowledged. Even though the packaging was greatly optimized compared to the previous iteration, the confined space available in the front bulkhead still imposed constraints on the layout of the components. Certain clearances remain tight and may complicate assembly and maintenance operations. Furthermore, although the mechanism was validated from a structural and kinematic point of view, driver feel may still be affected due to the decoupling mechanism which should be evaluated through testing and driver feedback.

Future work should focus on the development of a prototype for test bench analysis, where the behaviour can be assessed in a controlled environment before installation on the vehicle. Such a hardware in the loop procedure would allow to evaluate generated pressures, decoupling mechanism and potential failure scenarios without risk to the driver. In addition, the concept of adaptive brake bias could be explored further by automating the balance bar adjustment, enabling the system to modify the front-rear repartition during an event based on tyre wear, temperature or friction estimates. Finally, although the chosen solution based on pedal actuation offered an excellent compromise between complexity, mass and reliability, the more advanced concept previously referred to as pressure transducer remains an interesting long-term direction. Despite being more complex, it could potentially lead to further weight reductions and an even more compact integration of the autonomous braking hardware.

Bibliography

[1] Brembo S.p.A., *Brembo Racing — Auto Catalogue*. Brembo Racing, n.d. Official Brembo Racing auto catalogue; master cylinder selection guidance and caliper families.

[2] Festo SE & Co. KG, *Compact Cylinders ADN-S, to ISO 21287*, July 2025. Catalogue document.

[3] Intelpoint Insights, "China accounted for nearly one-third of the world's vehicle production in 2023," 2023.

[4] SAE International, "Taxonomy and definitions for terms related to driving automation systems for on-road motor vehicles (j3016)." SAE Standard J3016_202104, 2021.

[5] Formula Student Germany (FSG), "Formula student rules 2025, version 1.1," 2025.

[6] FS Team Tallinn, "Fs team tallinn—official website," n.d. Team website for the Estonian Formula Student team (TalTech/TTK).

[7] AP Racing Limited, *Race Brake Actuation System Set Up: Balance Bar Systems*. AP Racing Limited, Coventry, UK, n.d. Technical bulletin PDF.

[8] M. Stollberger, M. Gebhardt, N. Velz, A. Wischnewski, and M. Hörsch, *Autonomous System Beginners Guide 2021/22*. Formula Student Germany (Driverless Working Group), May 2021.

[9] Gross-Funk GmbH, "Fsg 2017 remote emergency system (res) specification v20170126." Formula Student Germany, Jan. 2017.

[10] Hitec RCD, *HS-1005SGT General Specification (v2.1)*, 2022.

[11] "Mil-std-1472g: Human engineering," 2012.

[12] International Organization of Motor Vehicle Manufacturers (OICA), "World motor vehicle production 2023," 2023.

[13] World Health Organization, "Global status report on road safety 2023," 2023.

[14] R. Nader, *Unsafe at Any Speed: The Designed-In Dangers of the American Automobile*. Grossman Publishers, 1965.

[15] United Nations, "Decade of action for road safety 2011–2020," 2011.

[16] National Highway Traffic Safety Administration (NHTSA), "Critical reasons for crashes investigated in the national motor vehicle crash causation survey," tech. rep., U.S. Department of Transportation, 2015.

[17] D. Pomerleau and T. Jochem, "No hands across america: The navlab 5 cross-country autonomous drive." Carnegie Mellon University, Robotics Institute, 1995. Navlab 5 steered autonomously for 98.2% of the 2,849-mile journey from Pittsburgh, PA to San Diego, CA; throttle and brake manually controlled.

[18] Society of Automotive Engineers, "Formula sae/student competition history," 1981.

[19] Squadra Corse Driverless, Politecnico di Torino, "Squadra corse driverless," 2025. Official website.

[20] Squadra Corse PoliTO, "Squadra corse polito—official formula sae team of politecnico di torino," 2025. Official website.

[21] B. Swonger, "Optimizing brake bias in formula sae: A framework for new and existing members," Independent Study Final Report MEMS 500, Paper 281, Washington University in St. Louis, McKelvey School of Engineering, Mechanical Engineering and Materials Science, St. Louis, MO, Dec. 2024.

[22] G. Genta, *Motor Vehicle Dynamics: Modeling and Simulation*. Singapore: World Scientific, 1997.

[23] W. F. Milliken and D. L. Milliken, *Race Car Vehicle Dynamics*. Warrendale, PA: SAE International, 1995.

[24] S. Fox, "Cockpit control forces—or: How robust do driver controls really need to be?." FSAEonline (SAE Collegiate Design Series), July 2010.

[25] Festo SE & Co. KG, *Compact Cylinders ADN/AEN, to ISO 21287*, Aug. 2025. Catalogue document.

[26] Bosch Rexroth Oil Control S.p.A., "Shuttle valve (re 18309-98)," May 2022. Edition 05.2022.

[27] MathWorks, *Isothermal Liquid Properties (IL)*, 2025. Gives the constant/pressure-dependent bulk-modulus model and entrained-air/dissolution formulation.

[28] "49 cfr 571.106—standard no. 106; brake hoses." Code of Federal Regulations, 2025. Specifies test method and limits for hydraulic brake hose volumetric expansion (cc/ft) at specified pressures.

[29] Power & Motion, "A checklist for matching pneumatic cylinders to load requirements," Mar. 2019.

[30] L. A. F. Law and K. G. Avin, "Endurance time is joint-specific: A modelling and meta-analysis investigation," *Ergonomics*, vol. 53, no. 1, pp. 109–129, 2010. Reviews/derives static endurance curves (Rohmert relationship) linking %MVC to endurance.

[31] J. R. Potvin, “Predicting maximum acceptable efforts for repetitive tasks: An equation based on duty cycle,” *Human Factors*, vol. 54, no. 2, pp. 175–188, 2012.

[32] UC Components, Inc., “What are shoulder screws and what are they used for?,” 2023.

[33] SKF Group, “Ge 8 e—radial spherical plain bearing,” 2025.

[34] Festo SE & Co. KG, “Swivel flange sncl-25 (part no. 537793).” Data sheet, Oct. 2025. Size 25, based on standard ISO 21287, corrosion resistance class CRC2.

[35] Festo SE & Co. KG, “Clevis foot lbn-20/25 (order code 6059).” Data sheet, Oct. 2025. Size 20/25, corrosion resistance class CRC1, ambient temperature –40 °C... 150 °C.